DISSERTATION

A DATA-DRIVEN APPROACH FOR MAXIMIZING AVAILABLE WIND ENERGY THROUGH A DEDICATED PRICING MECHANISM FOR CHARGING RESIDENTIAL PLUG-IN ELECTRIC VEHICLES

Submitted by

Fathalla Eldali

Department of Electrical and Computer Engineering

In partial fulfillment of the requirements

For the Degree of Doctor of Philosophy

Colorado State University

Fort Collins, Colorado

Summer 2019

Doctoral Committee:

Advisor: Siddharth Suryanarayanan

George J Collins
Dan Zimmerle
Salah Abdel-Ghany

ABSTRACT

A DATA-DRIVEN APPROACH FOR MAXIMIZING AVAILABLE WIND ENERGY THROUGH A DEDICATED PRICING MECHANISM FOR CHARGING RESIDENTIAL PLUG-IN ELECTRIC VEHICLES

Wind energy generation is growing significantly because of its favorable attributes such as cost-effectiveness and environment-friendliness. Electricity is the most perishable commodity as it must be consumed almost instantaneously as it is produced. Because of that, the variable nature of wind power generation and the challenges in forecasting the output power of wind impose problems of curtailment (excess of available wind energy than forecast) and deployment of reserves (deficit of available wind energy than forecast). Energy storage for wind power installations is a potential solution; however, storing large amounts of energy over long time periods is an expensive and inefficient solution. Plug-in electric vehicles (PEVs) are recognized as one of the assets to integrate energy storage on the distribution side of the electricity grid. Thus, PEVs charging presents an alternative solution for managing this excess energy in wind energy-rich grids.

An accurate wind power forecasting (WPF) in the day-ahead market leads to a more predictable dispatch and unit-commitment (UC) of generators, thus reducing the need for reserves and storage. Typically, reserves to match the imbalance in supply and demand of electricity are provided by generators that are more expensive than the ones engaged in primary services. Markets in different regions of the world have specific designs, operation policies, and regulations when it comes to variable sources (e.g., wind, and solar). Independent system operators (ISOs), tasked with handling electricity markets in the US, must meet regulating reserve as directed by the North America Electric Reliability Council (NERC). One of these requirements is that the sufficient reserve must be available to cover the generation deficit. This deficit can be due to under-forecasting. There is also a case when ISOs need to curtail wind energy generation because of over-forecasting. In the first part of this dissertation, wind power data from the Electric Reliability

Council of Texas (ERCOT) market is used to improve WPF as Texas has the highest installed wind energy capacity in the North American electricity grid. Autoregressive integrated moving average (ARIMA) model is used for WPF improvement.

There is also a need to develop a coherent metric to quantify the improvements to WPF because different studies use different metrics. Also, using the statistical representation of the reduction in error does not necessarily reflect the overall benefit, especially the economic benefit, for ISOs. In the second part of this dissertation work, modifications of on risk-adjusted metrics used in investments assessments are developed and applied to the operation cost (OC). OC is the result of running the economic dispatch (ED) on realistic synthetic models of the actual Texas grid to evaluate the impact of the WPF improvement on the cost of operation. The modifications of the above-mentioned risk-adjusted metrics are also applied to deferring the capital investment on the distribution systems. Then, the metrics are used to assess the combination of photovoltaic (PV) and battery energy storage system (BESS) at the residential section of the distribution grid as explained in appendix A.

The third part of this dissertation uses a data-driven approach to investigate existing pricing mechanisms for a Texan city (i.e., Austin) located in a wind energy-rich grid such as ERCOT with an increased adoption rate of PEVs. The study performed indicates the need for an alternative dynamic pricing mechanism dedicated to PEVs than the existing choices for maximizing the utility of available energy from wind in the absence of grid-level energy storage.

Dynamic pricing produces an opportunity to avoid high costs for the power provider and benefits the consumers if they respond to the change of the price. However, achieving these benefits needs smart rate design and real data. After justifying the need for fair pricing mechanisms to benefit the utility and the customers for the coordination of wind energy and PEVs charging in wind energy-rich grid, this dissertation designs a time-varying pricing mechanism. This dissertation employs a data decomposition technique to design a dedicated pricing mechanism for PEVs. We use real data of a city with high projections of PEVs (Austin, Texas) located in a wind-rich electricity grid (ERCOT) to demonstrate this design of a dynamic pricing method.

ACKNOWLEDGMENTS

I am very grateful to my advisor, Prof. Siddharth Suryanarayanan for his guidance, contribution and support. I would also like to thank my committee members, Prof. George J Collins, Mr. Dan Zimmerle, and Dr. Salah Abdel-Ghany for their time and effort to serve in my PhD committee. Additionally, I acknowledge the efforts and the contributions of the following professors and researchers: a) Prof. Edwin Chong, and Prof. Timothy Hansen for their contribution to the wind power forecasting modelling, b) Dr. Mauricio Samper for his contribution to the metric development of wind power forecasting improvement, and c) Dr. Prassanna Vadana. D for her help with the dynamic pricing mechanism design. I also appreciate the feedback and suggestions from Prof. H. J. Siegel. Finally, I would like to thank my Advanced Power Engineering Laboratory (APEL) colleagues for their help and support.

I value and appreciate the scholarship support from The Ministry of Higher Education and Scientific Research, Libya to pursue the PhD degree at Colorado State University. Also, part of this research was supported by the US National Science Foundation (NSF) under the award ECCS-1608898 and the School of Global Environmental Sustainability (SoGES) at Colorado State University.

I am also very thankful to my family members and friends for their support and encouragement. Without their support and help, it would not have been possible to complete this work.

TABLE OF CONTENTS

LIST OF TABLES

LIST OF FIGURES

NOMENCLATURES

AIC	Akaike's Information Criterion
AR	Autoregressive
ARIMA	Autoregressive Integrated Moving Average
BESS	Battery Energy Storage Systems
CIP	Customer Incentive Pricing
COD	Coefficient of Determination
CPP	Critical peak pricing
DAM	Day-ahead Market
d-EMS	Decentralized Energy Management System
DER	Distributed Energy Resources
DMD	Dynamic mode decomposition
DRUC	Day-ahead Reliability Unit Commitment
ED	Economic Dispatch
EENS	Expected Energy not Served
EF	Enhanced Forecast
EIA	U.S Energy Information Administration
ERCOT	Electric Reliability Council of Texas
ESS	Energy Storage Systems
f-ARIMA	Fractional Autoregressive Integrated Moving Average
GARCH	Generalized Autoregressive conditional Heteroskedastic
GHG	Green House Gases
HEVs	Hybrid Electric Vehicles
ISO	Independent System Operator
LMP	Locational Marginal Pricing

LOLP	Loss of Load Probability
MA	Moving Average
MAE	Mean Average Error
MAPE	Mean Absolute Percentage Error
MAR	Minimum Acceptable Return
MM	Method of Multipliers
MSOR	Modified Sortino Ratio
MSR	Modified Sharpe Ratio
MRE	Mean Relative Error
NERC	North America Electric Reliability Council
NHTS	National Household Travel Survey
OC	Operation Cost
OCA	Operation Cost associated with the actual value of wind power
OCOF	Operation Cost associated with the original forecast
OCEF	Operation Cost associated with the enhanced forecast
OF	Original Forecast
OPF	Optimal Power Flow
ORDC	Operating Reserve Demand Curve
PEV	Plug-in Electric Vehicle
PHEVS	Plug-in Hybrid Electric Vehicle
PMF	Probability Mass Function
PTR	Peak time rebate
PV	Photovoltaics
RACR	Risk-Adjusted Cost Ratios
RAR	Risk-Adjusted Ratios
RE	Relative Error

RMS	Root-Mean Square
RMSE	Root-Mean Square Error
RRI	Return per Risk Index
RTM	Real-time Market
RTO	Regional Transmission Organization
RTP	Real time Pricing
SOC	State of Charge
SOR	Sortino Ratio
SR	Sharpe Ratio
STWPF	Short-term Wind Power Forecasting
SVD	Singular value decomposition
TDD	Target Downside Deviation
TOU	Time of Use pricing
TSS	Time Step Simulation
UC	Unit-Commitment
V2G	Vehicle-to-Grid
VOLL	Value of Lost Load
WPF	Wind Power Forecasting
Ai	The fuel dependent cost in MBTU/hr
a^k	The step size of the ADMM problem
B	The backward operator of ARIMA model
B, C, D	The cost curve parameters
b	The right hand side column of the constraints
C_i	The operating cost of the unit i in \$/hr
$C(t)$	The hourly cost of purchasing wind power

d	The order of differencing of ARIMA model
$E[R]$	The expected return
$E_r(t)$	The error of WPF with time *t*
$Ex_{wind}\,(t)$	The hourly excess of wind power
F_c	The fuel cost
$IL_j(t)$	The current of line *j* at time *t*
$\log L$	The maximum log-likelihood
$L(t)$	The hourly load in MW
LB	The monthly base load
L_p	The vector norm
N	The number of returns, or the number of EVs
n	The n^{th} EV
P	The number of parameters in ARIMA model
$P(t)$	The hourly actual wind power at hour *t*
$P'(t)$	The hourly forecasted wind power at hour *t*
P_{BG}	The total base generation power
P_{EV}	The PEV power
P_{gi}	The power produced by unit *i*
$P_{L\,T}$	The total load
$P_w(t)$	The time series of the power generated by wind farm *w*
$P_{WC}\,(t)$	The curtailed wind power in MW
$P_{w-capacity}$	The installed capacity of wind farm *w*
$P_{w-total\,capacity}$	The total wind installed capacity in the system
$P_{w\text{-}total}\,(t)$	The hourly total wind generation
$PEV_{dispatch}(t)$	Hourly PEVs dispatch

$PEV_{profile}(t)$ Hourly PEVs expected power profile

p The order of AR of ARIMA model

q The order of MA of ARIMA model

$R(t)$ The hourly revenue of the utility obtained from dispatching PEVs

Rev_{lost} The total lost revenue due to wind power curtailment

r_f The risk-free interest rate

$s(t)$ The hourly spot market price in $/MWh

T The target return, Time Horizon

T_0 The desired target

$u(t)$ The hourly utility price of electricity

V_i The voltage of the transmission or distribution i^{th} node

V_{om} The variable operation and maintenance cost

$Var_{load}\ (t)$ The hourly variable load of the system in MW

X_i The i^{th} return

x^* The optimal value of the primal optimization problem

Y_t Time series

α_{OC} The difference between OCA and OCOF

β_{OC} The difference between OCA and OCEF

ϕ, θ The polynomials of B

ϵ_t Independently and identically distributed white noise

σ The slandered deviation

λ_{WS} The wholesale electricity price in $/MWh

ΔQ The change of quantity (electricity) in MW

ΔP The change of utility price in $

ε The price elasticity of demand

CHAPTER 1

INTRODUCTION AND OVERVIEW

The increase in integrating renewable generation resources in the electricity grid to displace part of the conventional fossil fuel generators poses multiple challenges [1], [2]. Although wind energy can reduce dependence on foreign oil and greenhouse gases (GHG) emissions, its inherent variability imposes the need for low errors in forecasting techniques. This is a paramount requirement to deploy any generation source so that the delicate balance between supply and demand can be met without deviations to the nominal grid frequency. Decreasing the errors in wind power forecasts (WPF) is important for efficient dispatch and unit-commitment (UC), thus helping widespread penetration of wind energy resources in the electricity grid. Accurate WPFs are important for committing, scheduling, and dispatching wind energy resources in the day-ahead bulk power markets. Beside the need to improve WPF, there is also need to develop realistic metrics to quantify the improvement to WPF and the impact on the power system.

There is a growing interest to integrate energy storage systems (ESS) for buffering the wind power output as well as for using it at a time that the grid can use it. However, storing the excess of energy from wind is yet economically infeasible. An alternative to manage the excess of wind energy is to charge the available plug-in electric vehicles (PEVs). Thus, there is a need to design a dynamic pricing mechanism for scheduling the available PEVs to maximize the utility of available wind energy in the absence of grid-level energy storage.

1.1 Motivation

There is a significant global growth of wind energy installations and an increasing penetration and acceptance of PEVs in the transportation sector. In wind energy-rich grids, the wind energy generation is usually high at night (i.e., off-peak times for grid electric demand). At the same time, most of the PEVs are not in use and thus available for charging. Other than using them for transportation purposes, PEVs can help reduce the curtailment of wind energy by presenting themselves as a load at the off-peak times when the wind generation is high. Bulk energy storage at the grid level is yet an expensive and inefficient

proposition [3]; thus, using an alternative solution such as distributed energy storage through PEVs in the end-user realm may lead to an efficient use of the wind energy resource.

1.2 Objectives

The primary challenge in WPF is the reduction of forecast error. This error potentially leads to wind power curtailment or increased cost of expensive reserves; the former scenario represents an inefficiency in the system while the latter may correspond to an inefficiency in the electricity market. Hence, there is a dire need to develop methods to improve WPF with reduced forecast errors for use by independent system operator (ISO). Further, such improvements must be quantified using a relevant metric.

Using grid-level bulk energy storage assets with the potential for storing the excess electric energy generated from wind are yet cost-prohibitive and prone to inefficiencies. An alternative for managing this excess energy is charging available PEVs. The challenge of highly dispersed resources (e.g., PEVs) needs coordination, control, and communication for buffering wind energy. There is also a need for an alternative dynamic pricing mechanism dedicated to PEVs than the existing choices for maximizing the utility of available energy from wind in the absence of grid-level energy storage. The objectives of this dissertation research include the following:

1. The development of a method to improve WPF

The highly stochastic nature of wind energy due to the intermittent nature of wind speed makes it difficult to dispatch. Hence, it becomes more difficult to maintain the delicate balance of supply and demand. The first part of this dissertation, also published in [4], focuses on the uncertainty in dispatch. WPFs are important for efficient dispatch and UC. WPF improvement techniques include aerodynamic atmospheric models and time-series based model. This research presents improvements to WPF using a time-series autoregressive integrated moving average (ARIMA) model on available historical data of hourly wind power data—forecast and actual—from the Electric Reliability Council of Texas (ERCOT). The results show WPF improvements as vector norms of the relative error and how the error is reduced in all the cases. The details of the study and the results are published in [4] and presented in chapter 2.

2. The development of metrics to quantify the improvement of WPF

There are multiple metrics to quantify the reduction in error in renewable sources forecasting. However, most of these metrics do not necessarily reflect the system cost reduction. The paper [5], the second part of this dissertation, develops a set of metrics to quantify the reduction in the cost of reserve and other costs associated with the uncertainty of wind energy generation. The contribution of this part of the work includes modifications applied to financial metrics to evaluate the impact of improved WPF on the operation of the electricity grid. Sharpe and Sortino ratios are modified for quantifying the impacts of WPF improvements on power system operations using the operation cost (OC) resulting from performing economic dispatch (ED). The modifications were carried out for the application of distribution system investment deferral in the case of high penetration solar photovoltaic and distributed battery energy storage systems as in [6] and presented in appendix A.

3. Providing a data-driven justification for dedicated dynamic pricing for residence-based PEVs

In a wind energy-rich grid, the wind power curtailment is a challenge due to the negatively high correlation between the avaibilities of the load and wind power. PEVs are possible alternative of the economically infeasible large-scale energy storage when their charging is coordinated with the availability of wind power. The third part of this research, presented in chapter 4 and [7], employs real data from a wind energy-rich grid (i.e., ERCOT) to investigate the need of dedicated time-varying pricing for PEVs charging in coordination with the availability of excess of wind energy. The results of the case study indicated the important need for a pricing mechanism dedicated for PEVs.

4. Designing dedicated dynamic pricing mechanism for PEVs in the wind energy-rich grid

After justifying the need of a dedicated pricing mechanism of charging PEVs based on the availability of excess of wind energy, this dissertation used a data-decomposition technique to design a time-varying pricing for residence-based PEVs. We employ real data for a city (Austin, TX), located in a wind energy-rich grid (ERCOT).

1.3 Scope

This dissertation proposes a framework that provides technical solutions of the intermittence of wind energy resources. These include WPF improvement, quantification metrics of WPF, and designing a dedicated dynamic pricing for PEVs when there is excess of wind energy. This dissertation employs real data from ERCOT and a Texan utility. It also uses a synthetic model of the Texas grid as it has the highest installed capacity of wind energy resources.

A time-series methodology (i.e., ARIMA) was used for improving WPF. This dissertation focuses on improving WPF in a stage prior to the dispatch stage and deploying the real data from ERCOT to examine the performance of the used model. This work differs from previous research that considers the use of the wind speed data to provide improvement to WPF. This part of the dissertation is presented in chapter 2 and published in [4].

Developing the WPF quantification metrics to better quantify the impact of WPF improvement on the electricity grid operation is important because the statistical representation of the forecasting errors might not best represent the actual impact of the improvement. This dissertation modifies and employs well-known risk-adjusted financial metrics (i.e., Sharpe and Sortino ratios) to study the impact of the WPF improvements on the operation cost of the system under consideration (i.e., Texas grid). This research involves running time step simulation economic dispatch (ED) to find the hourly operation cost of the system when considering the actual wind power, the original power forecast and enhanced power forecast. These results are then used to calculate the modified financial metrics and study their implications. This part of the dissertation is presented in chapter 3 and accepted for publication as in [5].

The last part of this dissertation aims to justify the need of dynamic pricing dedicated only for PEVs charging when there is a forecast of excess wind energy (chapter 4) [7]. It also uses data decomposition method to design the time-varying pricing based on the time when there is access of wind energy (chapter 5). Both chapters employ data-driven approaches where real and relevant datasets are used.

1.4 Tools

Several tools have been used in this dissertation work. Python® and MATLAB® were used for data manipulation and visualization, especially in the WPF modeling as this part had a high demand of data sorting and manipulation. R® and Python® were used for statistical modeling and analysis of the autoregressive model (i.e., ARIMA). PowerWorld® and MATPOWER® were used for power flow studies. The OCs result from running a time step simulation of ED in the synthetic Texas grid. The OCs are then used to determine the risk-adjusted metrics. The dynamic pricing design involves data analysis and data decomposition using MATLAB®.

1.5 Literature Search

The topic of wind energy resources coordination with PEVs appears in the literature. A literature search is conducted to review several research papers that have been published on the topic of wind energy with PEV coordination on multiple different aspects. References [8], [9] discuss that Wind energy resources with storage coordination, which can smooth the wind variation, reduce the cost and make the wind power more reliable. The study [10] attempts to examine that the integration of the PEVs on large scale can lead to an optimal operation of the security-constraint power system and reduce the operational cost. The coordination of the wind energy with PEVs are studies as probabilistic constrained load flow in [10]. Reference [12] studies how the PEVs can be practically integrated to the power systems deploying the V2G technique in order to reduce both emission and cost and maximize the use of renewable energy resources. The above-mentioned references had different objectives of the optimization problems to find the optimal when and where (Spatio-temporal) PEVs should be charged/discharged [13]-[16]. This dissertation attempts to solve multiple aspects of the topic of wind energy coordination with PEVs by providing solution to different parts of the problem. These include WPF improvement and improvement quantification. Also, most of the studies conducted in this topic focuses on identifying the PEVs schedule (i.e., dispatch) without paying much attention to what could lead to such dispatch (i.e., incentive pricing design). It is worth

mentioning that the introduction sections of each of the subsequent chapters (i.e., 2-5) cover the literature search of each of the related studies.

1.6 The Specific Contributions of this Dissertation

The specific contribution of this dissertation includes the following

1. Modeling the aggregate error between the forecast and actual wind power prior to dispatching, thereby allowing improved dispatch and significant financial savings from utilizing reduced spinning reserves. This work also performed the forecasting process of wind power for a one-year period using open source software packages R® and Python®, which facilitates quantifying the reduction in the reserve need.
2. Developing two modified risk-adjusted cost ratios (RACR) metrics to evaluate the impact of improved WPF on the operation of the electricity grid. Specifically, the traditional financial metrics. This work modifies Sharpe and Sortino ratios [17] for quantifying the impacts of WPF improvements on power system operations using the OC resulting from performing ED.
3. Justifying the need of dedicated PEVs charging price based on the avaibilities of excess of wind energy and used a data-driven technique, dynamic mode decomposition (DMD), to design the time-varying pricing mechanism.

1.7 Organization of the Dissertation

The rest of the dissertation is organized as follows: chapter 2 explains the contribution of the WPF improvements and is taken directly from [4]. Chapter 3 explains the risk-adjusted financial metrics and how they can be used to quantify the WPF improvement. Chapter 3 is also taken directly from an accepted manuscript [5]. Appendix A explains how the previously mentioned financial metrics can be further modified and used in another important application, namely capital investment deferral by employing PV with BESS which is also taken from the manuscript [6]. Chapter 4 provides justification for the dire need of fair pricing pertaining the coordination of excess of wind energy with PEVs charging. Chapter 4 is also taken directly from an under-review manuscript [6]. Chapter 5 uses data-decomposition technique that

extract the dynamic features of time series data to design dynamic pricing for PEVs charging. Chapter 6 concludes the dissertation and discusses the future work. The chapters 2-5 are verbatim reproduced from published/under review manuscript of [4], [5], [7].

CHAPTER 2

EMPLOYING ARIMA MODELS TO IMPROVE WIND POWER FORECASTS: A CASE STUDY IN ERCOT[1]

2.1 Introduction

Increasing the integration of renewable generation resources to displace conventional generation imposes multiple challenges. Although wind energy can significantly reduce CO2 and oil dependency, it is stochastic in nature and needs accurate forecasting techniques to maximize utilization. Decreasing the unpredictability of wind is important for efficient dispatch and unit-commitment (UC), thus aiding widespread penetration of wind energy resources in the electricity grid. Accurate WPFs are important for committing, scheduling, and dispatching wind energy resources in the day-ahead bulk power markets. WPF improvement techniques include aerodynamic atmospheric models and time-series-based models. Improving short-term WPF (STWPF) using numerical weather prediction models has significant economic benefits. The economic benefits of the wind forecasting improvement project include production cost reduction due to a more efficient commitment, wind curtailment reduction, and energy balance cost reduction [18]. Our work improves STWPF using time-series models.

Statistical time-series-based models are commonly used in econometrics and business, price forecasting, and scientific applications [19]. Autoregressive (AR) models help capture the small range correlations in data, which are suitable for forecasting processes. In the literature, researchers have used statistical time-series models in multiple forecasting applications. Generalized autoregressive conditional heteroskedastic (GARCH) models are able to predict day-ahead electricity prices, as presented in [20]. The paper uses GARCH methodology to forecast for the day-ahead electricity prices with high variability

[1] This chapter is a verbatim reproduction of the work accepted and published to a peer reviewed conference proceedings in [4]. The required permissions for re-use of the material have been obtained from the copyright holders and are included in the Appendix B. The numbering of the figures and tables has been modified to satisfy the formatting requirements of the dissertation.

periods. Their method provides the next-day market clearing price based on historical data from mainland Spain and California markets.

Electricity from solar photovoltaics (PV) when aggregated at the system level tends to be less variable than at the panel level due the inherent smoothing of outputs resulting from geographical distribution. Reference [21] investigates multiple forecasting techniques for solar PVs including neural networks, least-squares support vector machines, and ARIMA forecasting models. According to [21], ARIMA and neural network models perform better when the daily power difference is significant. Reference [22] employs ARIMA to estimate the future load of New South Wales in Australia. The paper further improves the technique using the weighted mean.

Wind speed forecasting errors depend on the prediction methods, the forecast period, and the forecast location. Reference [23] uses GARCH to predict long term (daily average) wind speed in the Zhangye area in China. The procedure described in [23] eliminates the seasonal effect and then uses GARCH to predict for a daily average wind speed. The paper also shows that the elimination of the seasonal effect improves GARCH models.

Fractional autoregressive integrated moving average (f-ARIMA) models have been also used to predict hourly wind speed. Due to the ability of the f-ARIMA model to capture short-term correlations, the authors used the model to forecast for the day-ahead wind speed at the wind farm level [24]. Reference [25] developed a Markov chain-based wind power forecast model that considers the spatial and temporal dynamics of wind power output of individual wind turbines.

In this chapter, we employ the ARIMA technique to improve WPFs. Unlike the effort in [24], which uses only actual wind speed data, we consider using available historical data of hourly wind power—forecast and actual—from ERCOT to improve the day-ahead wind power dispatch. In [24], wind speed is forecasted, thus imposing the limitation of the cut-in and cut-out wind speeds. An advantage of using ARIMA over ARMA is that the former is more general and allows the time series to be non-stationary. The contributions of this paper are as follows: (i) we model the aggregate error between the forecast and actual wind power *prior* to dispatching, thereby allowing improved dispatch and significant financial savings from

utilizing reduced spinning reserves, and (ii) we performed the forecasting process of wind power for a one-year period using open source software packages R® and Python®, which allows us to quantify the reduction in the reserve need and the cost of reserve. Section 2.2 explains the importance of improving the forecast and its impact on the electricity market. The ARIMA model and its salient elements are presented in Section 2.3. In Section 2.4, the case study we used is described and the results are presented. Section 2.5 summarizes the findings and concludes the paper.

2.2 The Impact of WPF on Electricity Market

From a market perspective, there are four main challenges of integrating wind energy: (i) intermittency of input; (ii) different patterns of wind generation and load; (iii) limitations in transmission systems; and (iv) forecasting. The last challenge is the focus of our work in this paper. The accuracy of WPF affects the quality of UC. An accurate STWPF in the day-ahead market leads to a more predictable dispatch and UC, thus reducing the need for reserves. The market in different regions in the US, operated by ISOs, has had clearer operation policies and regulations when it comes to variable source. ISOs are required to meet enough regulating reserve imposed by the North America Reliability Council (NERC). One of these requirement is that sufficient reserve must be available to cover the loss of generation capacity. This loss can be due to under forecasting. In this paper, we consider and use STWPF data from the ERCOT market [26].

The forecasting system in ERCOT produces the most statistically probable estimate. This is derived from the wind generation with the highest probability of wind production for each wind generation resource for the next 48 hours. The forecasts are then posted on the market information system to find the regional forecast wind production. Based on ERCOT operation information, the day-ahead operation occurs between 6:00 a.m. and 6:00 pm. Day-ahead operations include two major functions: day-ahead market (DAM) and day-ahead reliability unit commitment (DRUC). DAM is a voluntary financial market for energy transaction, and it allows qualified scheduling entities to sell energy ahead of real-time to secure more price certainty. It evaluates and defines the bids based on the prices and system constraints. DRUC ensures adequacy of the generation capacity for the next operating day [27].

We employ our model to improve the forecast of the system-wide (aggregated) wind power in MW. As shown in Fig. 2.1, an important observation is that the aggregated error is always less than the error of each region. The figure quantifies how the relative error (%) reduces when we consider aggregated data. This is due to the canceling effect of under-forecast and over-forecasts of different regions. This improvement will contribute to the financial benefit of reserve cost reduction. As the ancillary service and hourly point-to-point obligations of reserve in ERCOT are defined in DAM, improving the WPF will lead to a reduction of the reserve need.

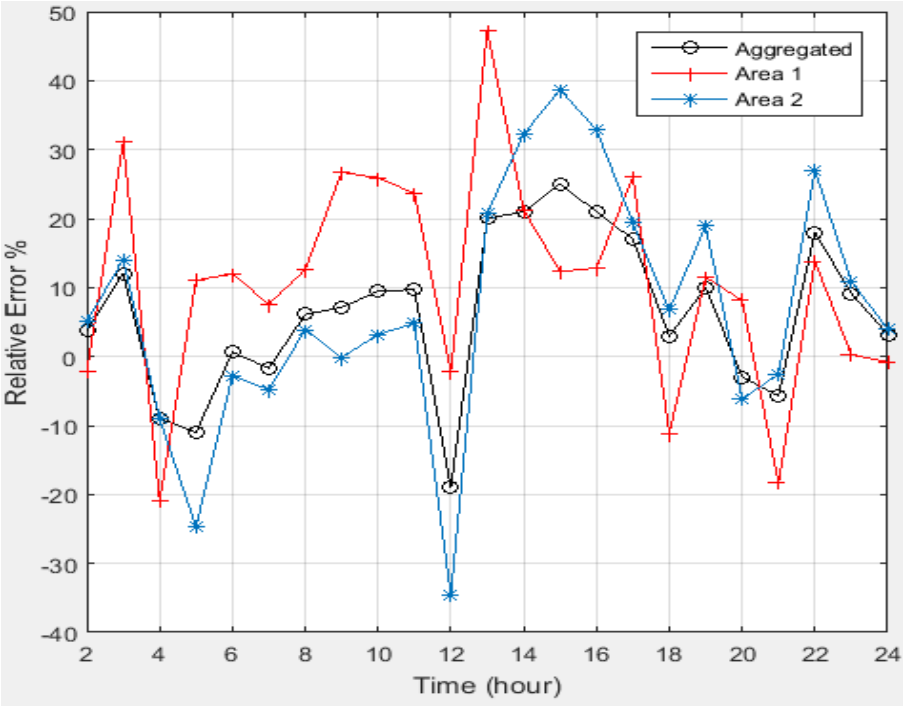

Fig. 2.1 The effect of aggregation on WPF error

2.3 ARIMA Methodology

A sequence of random variables comprises a stochastic process, which can be considered as a theoretical analog of a time series. Stationary time series with complicated autocorrelations are often modeled by combining AR and MA elements. Though this work fits the difference between the recent (month of data) wind power, both actual and forecast, this does not guarantee stationarity. We introduce the differencing operator to ensure that the model is suitable for stationary or non-stationary time series.

We introduce the ARIMA (p, d, q) model in the following subsection (the symbol d here represents the "order" of differencing).

2.3.1 ARIMA Process Formulation

The construction of an ARIMA model from empirical data, which uses maximum likelihood estimation, and its application to forecasting, consists of the following steps: (i) identifying a suitable model from a class of models; (ii) estimating model parameters; (iii) validating the model; and (iv) obtaining the forecast [20]. Denote by Yt a time series, where t is the time index. The ARIMA (p,d,q) process formulation is

$$\phi(\mathrm{B})(1-\mathrm{B})^{\mathrm{d}}\,\mathrm{Y_t} = \theta\,(\mathrm{B})\epsilon_{\mathrm{t}}, \tag{2.1}$$

where ϵ_t is independently and identically distributed white noise with zero mean and constant variance, d is the degree of differencing needed to ensure stationarity, B is the backward operator (generally defined as $B^k Y_t = Y_{t-k}$), and ϕ and θ are polynomials of B, which are defined below in (2.2) and (2.3), respectively:

$$\phi(\mathrm{B}) = 1 - \phi_1\mathrm{B} - \phi_2\mathrm{B}^2 - \cdots\ \phi_{\mathrm{p}}\mathrm{B}^{\mathrm{p}} \tag{2.2}$$

$$\theta(\mathrm{B}) = 1 - \theta_1\mathrm{B} - \theta_2\mathrm{B}^2 - \cdots\ \theta_{\mathrm{q}}\mathrm{B}^{\mathrm{q}}. \tag{2.3}$$

The autoregressive model orders (previous observations of the AR model) and the moving average of previous observations are given as p and q, respectively [18], [23].

Autocorrelation, also known as serial correlation or cross-autocorrelation, is the correlation of a time-series with itself at different lags in time. Informally, it is the similarity between observations as a function of the time lag between them. An auto-regressive process is defined as a stochastic process used in statistical calculations in which future values are estimated based on a weighted sum of past values. An AR process operates under the premise that past values have an effect on current values. A process denoted AR (1) is a first-order process, meaning that the current value is based on the immediately preceding value. An AR (2) process has the current value based on the previous two values. An AR process that depends on

p past observations is called an AR model of degree p, denoted AR (p). An MA model is used to model a time series that exhibits short-term dependencies between successive observations and is denoted MA (q) [19].

The construction of an ARIMA process consists of two steps: (i) a general ARIMA formulation is selected to model the stationary time series; and (ii) the selected time series is tested for stationarity. If the series is non-stationary, then a d order of differencing is applied to the time series to produce a more stable variance.

2.3.2 Estimating the Parameters

After the underlying process is accepted as being stationary, the next step is to determine the structure of ARIMA (p, d, q) based on autocorrelation and partial-autocorrelation plots. In the proposed method, we make use of a custom-devised technique to determine the order of p and q based on Akaike's Information Criterion (AIC) for the available data. AIC, defined in (2.4) below, is a metric that evaluates the accuracy of the chosen model and achieves a tradeoff between fit and complexity. Minimum AIC is commonly used to find the optimal model:

$$AIC = 2P - 2 \log L, \tag{2.4}$$

where P is the number of parameters in the model and $\log L$ is the maximum log-likelihood. The last step is to test the accuracy of the predicted model using root-mean-square error techniques. The *p,d,q* combination of values that leads to minimum AIC is the most suitable model order [19].

2.3.3 Model Validation

Before using the model in our forecasting process, we must validate the model. In this step, we examine how the model captures the variations in the trend. We can use multiple ways to perform this step. In some cases, we can simply observe how the fitted data follows the actual data. We also can validate the model by checking the statistical significance of the ARIMA model and its residuals (the difference between the actual data and the model output) [20]. The statistical significance test can be performed using a technique called Ljung-Box. R® has a function, called Box.test that can perform this test [19].

2.3.4 Applying the Forecasting Approach

After validating the model, we use it for WPF for 24-hours ahead. This can be performed using the *forecast.Arima* function of the fitted ARIMA model and choosing the "ahead" value to be 24. The mentioned function also provides an upper and lower bound of the forecast [19]. Finally, all steps explained in this section are applied to the obtained data in section 2.4.

2.4 A case Study and Results

2.4.1 Wind Power Forecasting

The workflow of this forecasting process, summarized in Fig. 2.2, is as follows:

1. Calculating the error as $E_r(t) = P(t) - P'(t)$, where $P(t)$ and $P'(t)$ are the actual and the original forecast of wind power, in MW, at an hour *t*, respectively.
2. Performing the tuning process to find the optimal ARIMA model by choosing *p*, *d*, and *q* values with the minimum AIC. The latter step consists of constructing two (10 × 10) matrices of AIC at *d* = 0 and 1 to ensure stationarity when the data series is non-stationary [18]. Among these 200 models, we select the model that has the minimum AIC.
3. Fitting the recent data points (i.e., hourly data of the last 30 days) of the error to the optimal ARIMA model selected in the previous step.
4. Using the fitted model to forecast 24-hours of future values that represent the predicted error.
5. Adding the 24-hour error values to the original forecast data for the same day, representing the improved WPF.

2.4.2 Evaluation of WPF Improvement

We developed a forecasting process for wind power, in MW, and automated the process for the period March 2013–February 2014. The improvement in WPF using this ARIMA technique is expressed by the vector (L_p) norms of the relative error (RE) as shown in (2.5):

$$\|RE\| = \left\| \frac{(P - P')}{P} \right\|^p \times 100, \tag{2.5}$$

where $p = 1, 2$, and ∞ represents the reduction of the sum of the absolute RE, the root-mean-square RE, and the maximum absolute RE, respectively.

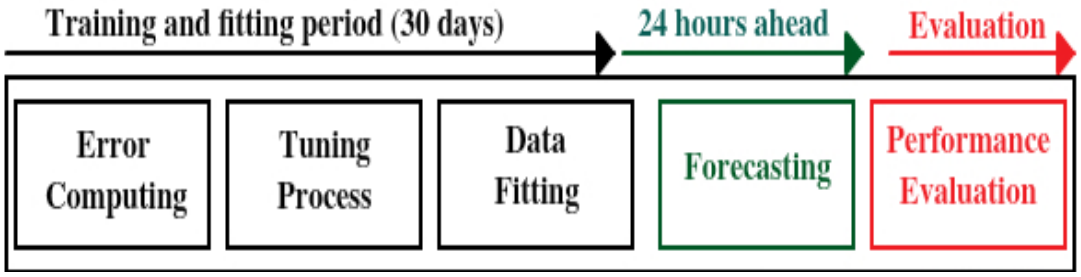

Fig. 2.2 Workflow of wind power forecasting using ARIMA

2.4.3 Empirical Results

The forecasting process was automated to run for one year. The model produces an hourly updated WPF, in MW. Table I shows the mean relative error (MRE) for each month of the tested period (3/1/2013–2/28/2014).

Table 2-1 Comparison between Original and Updated MRE (%) of Each Month

Month	Original forecast MRE (%)	Updated forecast MRE (%)
January	18.5	12.3
February	25.5	17.6
March	35	12.5
April	10	8.5
May	10.5	7
June	16.5	13.3
July	17	12
August	20	13
September	26	15
October	14	11
November	18	13
December	20	15

Figures 2.3–2.5 show examples of the improved forecasted time series in comparison with the original forecast and the actual values. The results of these three days were randomly chosen for different times of the test period to illustrate how the improved forecast using our ARIMA model performed better than the original forecast. As shown in the mentioned figures, the updated forecast closely follows the actual value, which leads to a financial benefit from the avoided cost of the reserve margin needed.

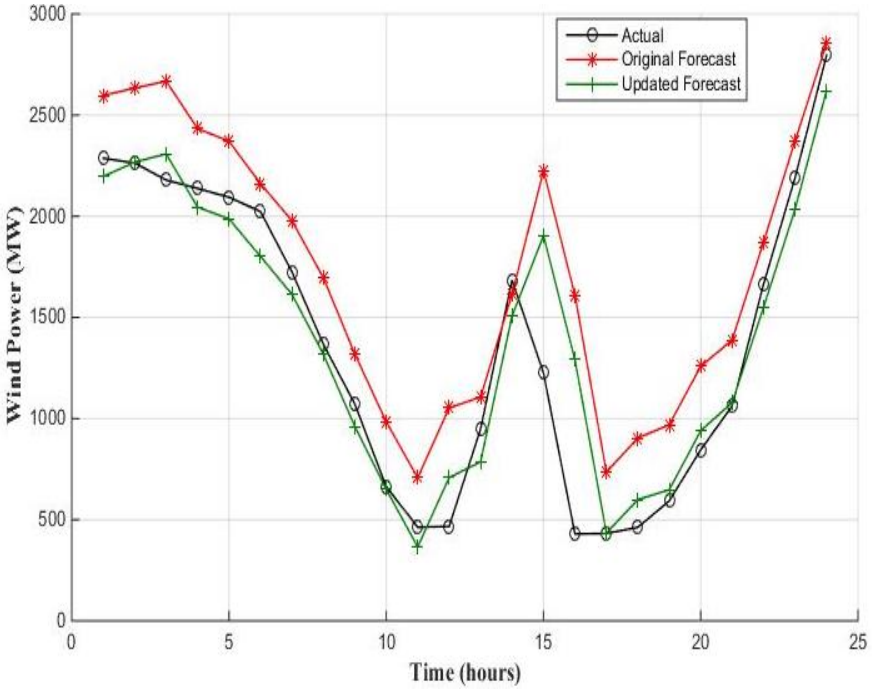

Fig. 2.3 Time series of actual, original forecast and updated forecast (6/29/2013)

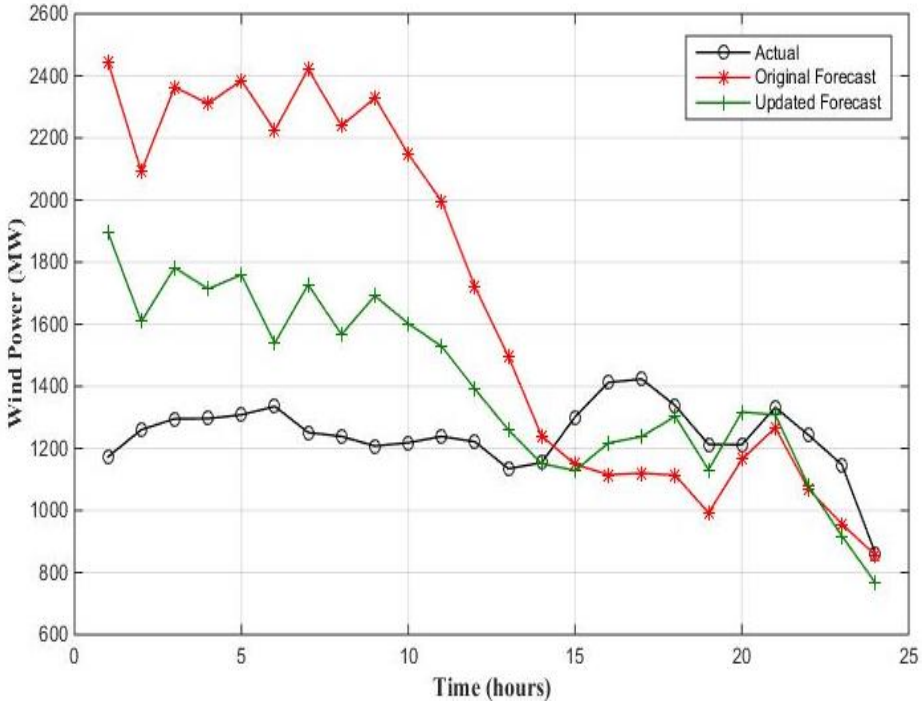

Fig. 2.4 Time series of actual, original forecast, and updated forecast (12/8/ 2013)

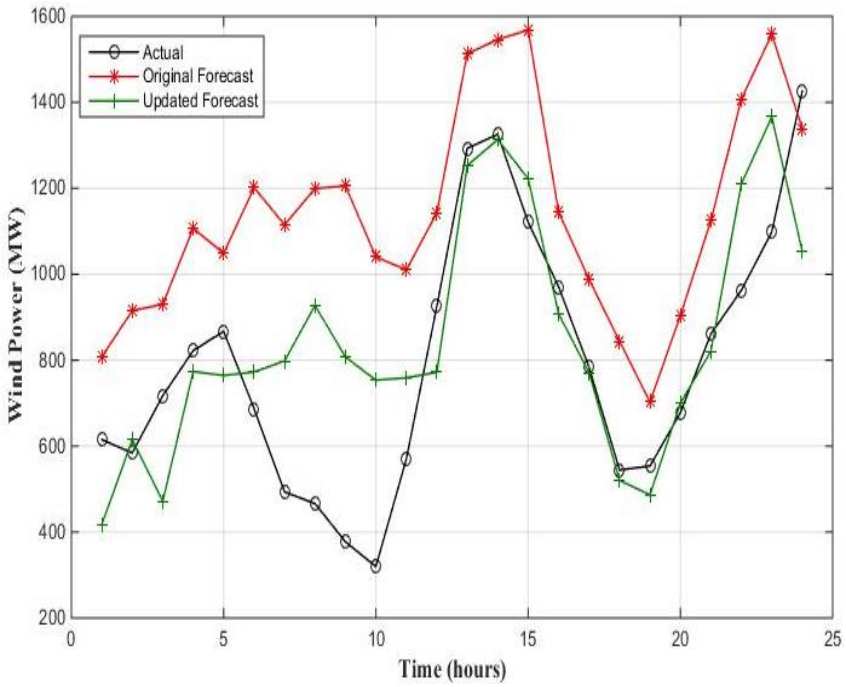

Fig. 2.5 Time series of actual, original forecast, and updated forecast (2/11/2014)

Fig. 2.6-Fig. 2.8 show the improvement achieved in WPF using real data from ERCOT for each season in the period 3/1/2013–2/28/2014. The use of our ARIMA process on the WPF shows improvements for all cases presented. We also calculated the expected energy generated by wind from the original and the improved forecast, and found that the deviation from the actual energy generated was reduced from 311.5 GWh to 112.7 GWh as shown in Table II. Hence, large financial savings are expected due to the reduction in the use of reserves.

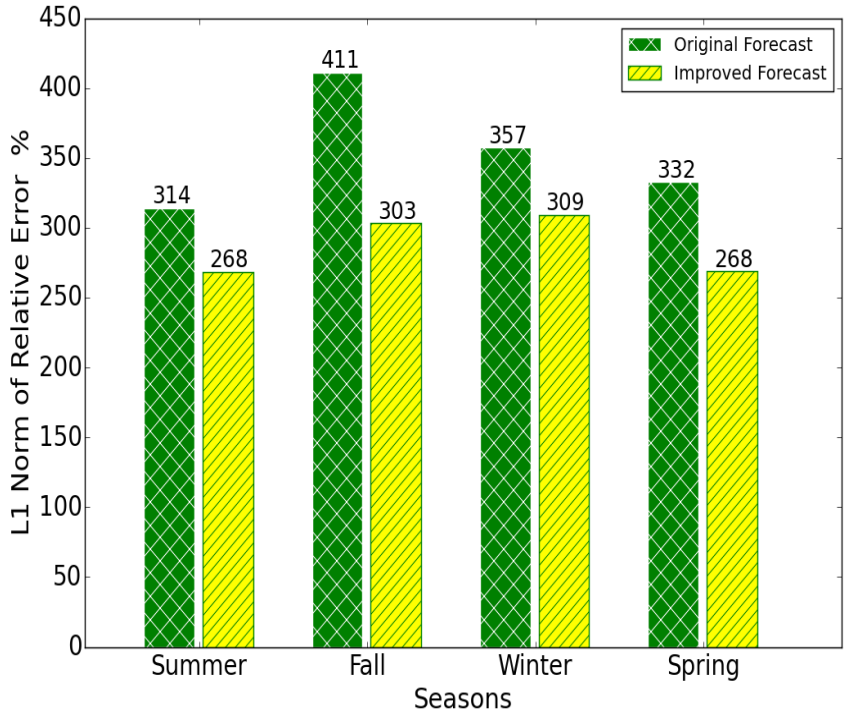

Fig. 2.6 L1 norm of RE for hourly wind power data from ERCOT for 3/1/2013–2/28/2014

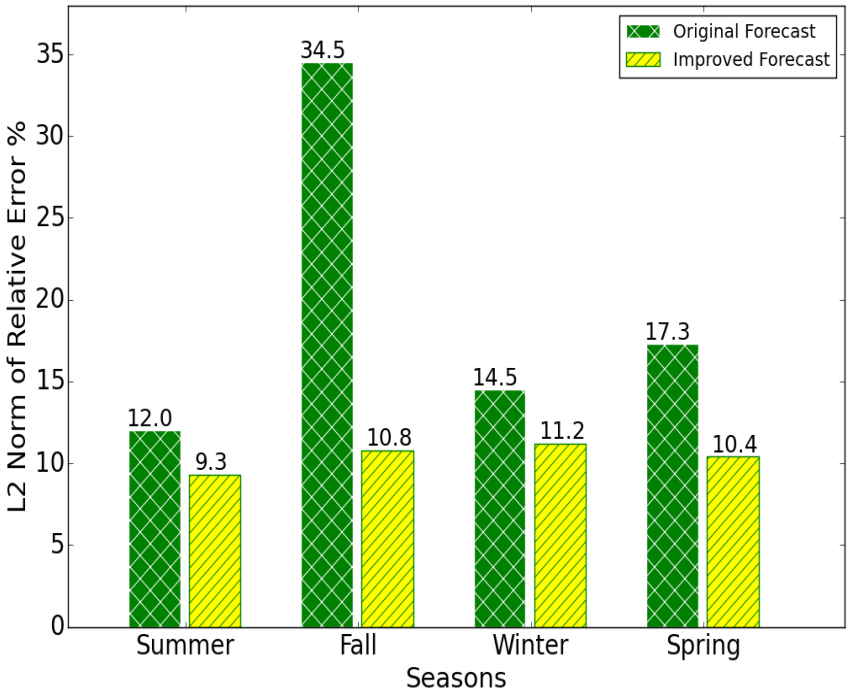

Fig. 2.7 L2 norm of RE for hourly wind power data from ERCOT for 3/1/2013–2/28/2014

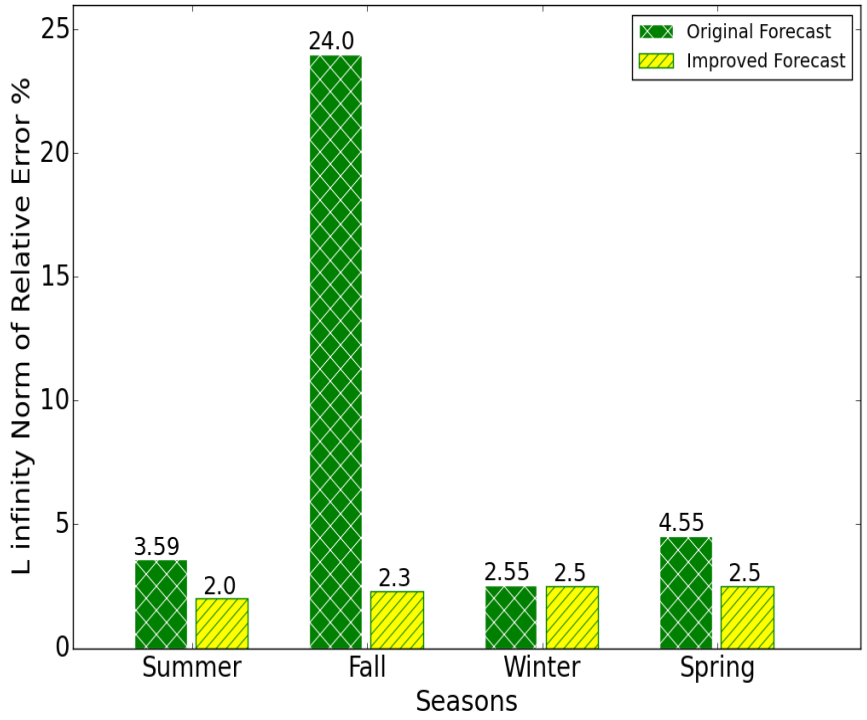

Fig. 2.8 L∞ norm of RE for hourly wind power data from ERCOT for 3/1/2013–2/28/2014

Identifying a rough estimate of the financial savings is important to quantify the efficiency of the improved WPF. In the market report in [27], ERCOT implements an operating reserve demand curve (ORDC) mechanism that can be defined as the multiplication of loss of load probability (LOLP) by the value of lost load (VOLL). ERCOT started to implement ORDC in June 2014. As real-time co-optimization was not implemented before that, ERCOT needs to implement ancillary service imbalance settlement to ensure resource adequacy. The price floor associated with reliability UC is set at 1500 $/MWh.

Using the numbers provided in the report can help estimate the impact of the reserve price and how the DAM forecast improvement can lead to financial savings. As shown in Table II, the difference in wind energy generated between the original forecast and the updated forecast for the full period of study (i.e., one year) is 198.89 GWh. This energy is supplied by reserves in the absence of an improved WPF model. If we multiply this energy by the price floor of reliability UC as stated in [27], which is 1500 $/MWh, we can roughly estimate the avoided cost of reserve as $298.3 Million for that year under consideration in our

studies. This number is an estimate and can vary based on the reserve cost and the ability of the model to improve the forecast.

Table 2-2 Annual Wind Energy Forecasted and Generated for 3/1/2013–2/28/2014

Data	Energy generated (TWh)	Deviation from the actual (GWh)
Actual	33.5285	-
Original Forecast	33.8401	311.59
Improved Forecast	33.6413	112.7

2.5 Conclusion and Future Work

WPF improvements are important to provide more efficient commitment, schedules, and dispatch of wind energy resources. In this paper, we employed an ARIMA model and real data from ERCOT for demonstrating an improved WPF's effectiveness and usability. The results show WPF improvements as vector norms of the relative error and how the error is reduced in all the cases. This paper also illustrates how the WPF improvements reduce the need for reserve, resulting in reduced cost.

In the future, our method can be extended and applied to WPFs in other systems after examining other methodologies to improve the performance of ARIMA. Another future step that might be considered is examining storage solutions and how they can work with WPF models to further improve wind energy integration and increase its penetration.

CHAPTER 3

RISK-ADJUSTED COST RATIOS FOR QUANTIFYING IMPROVEMENTS IN WIND POWER FORECASTING[2]

3.1 Introduction

The accuracy of WPF is paramount for the efficient dispatch and unit-commitment of wind energy resources in the day-ahead bulk electricity markets. WPF improvement techniques include physical models, statistical (i.e., time-series) models, and hybrid models. Reference [28] provides a detailed overview and classifications of WPF techniques in different time horizons and time-scales. It also describes the traditional metrics used in performance evaluation such as mean absolute error (MAE), root mean square error (RMSE), mean absolute percentage error (MAPE), and coefficient of determination (COD). In our previous work [4] we developed an ARIMA model to improve WPFs and demonstrated the effectiveness of the method using available historical data of hourly wind power—forecast and actual— ERCOT. In [4], we used the vector norms L_p of the relative error (RE) as the metric to assess the performance of the WPF improvement. However, it is unclear that the traditional statistical metrics used to evaluate forecasts such as MAE, RMSE, MAPE, COD and L_p adequately represent the impact on power system operations.

Different studies in the literature attempt to develop metrics to evaluate forecasting techniques. The work in [18] discusses the economic benefits of a wind forecasting improvement project. The improved forecast was due to improved quality of metrological measurements and numerical weather prediction models. Reference [18] uses 95th percentile of the error as it is believed to be the main driver for the non-spinning reserve service requirement. The results of the study showed that the amount of savings were relatively small because the aggregated WPF improvements were 1% MAE.

[2] This chapter is a verbatim reproduction of the work accepted to a peer reviewed conference proceedings [5]. The terms and conditions of retaining the permissions for re-use of the material have been obtained from the copyright holders and are included in the Appendix C. The numbering of the figures and tables has been modified to satisfy the formatting requirements of the dissertation.

The objective of the work in [29] is to develop a set of metrics to evaluate the performance of the solar forecasting for different scenarios and perspectives. The paper used the same statistical metrics mentioned in [28] to evaluate the forecasting error. When it comes to the economic metrics, the paper uses the 95th percentile of the forecast error and considers the standard deviation of the WPF error to evaluate the uncertainty.

The work in [30] aims to estimate the spinning reserve requirements considering wind power generation and load forecast errors as well as the possible contingencies that might arise for a given commitment prior to the day-ahead scheduling. It indicates that the benefit of reserve is measured in terms of the reduction of the cost of interruption which can be calculated as the multiplication of the expected energy not served (EENS) by the value of lost load (VOLL). This is similar to the approach that we undertook in our previous work in [4].

Reference [31] analyzes the statistics of the forecast errors of wind power and describes a new approach to determine how much non-spinning reserve that ERCOT needs for reducing the risk associated with resource inadequacy caused by the dramatic net-load ramp up situations or significant increase of the wind power and load forecast errors. This study does not consider an economic evaluation. However, it attempts to establish a methodology to more efficiently calculate the need for reserve. It is worth mentioning that the study only considers the under forecasting as the paper states that the over forecast does not present a significant threat. The 95th percentile and the 98th percentile are commonly used metrics to evaluate the improvement of forecasting error's impact on reserve calculations.

With the increase in attention for improved forecast of the availability of renewable resources, especially wind power, there is a dire need to quantify the improvements and its impact on grid operations. In this paper, we develop metrics, based on RACR, for studying the impact of improved WPF on the operations of the power system. A WPF model from [4] and actual wind power and load data from ERCOT spanning one year are employed with a synthetic simulation model of the Texas electric grid from [32] for demonstrating the application of the modified RACR. The contribution of this paper is the development of two modified RACR metrics to evaluate the impact of improved WPF on the operation of the electricity

grid. Specifically, the traditional financial metrics, Sharpe and Sortino ratios [17] are modified for quantifying the impacts of WPF improvements on power system operations using the OC resulting from performing ED.

The rest of the chapter is organized as follows. Section 3.2 briefly explains the ARIMA WPF forecasting methodology developed in [4]. Section 3.3 describes the data and the system used to perform the case study. Section 3.4 introduces the original Sharpe and Sortino metrics, reviews the applications of the metrics in the field of power systems, and modifies the metrics to quantify the WPF improvements. Section 3.5 presents the results. Section 3.6 concludes the chapter.

3.2 WPF Improvements using ARIMA

ARIMA is a class of stochastic process that is well suited to capture the complex auto-correlation behavior in a stationary time series [19]. There are also other autoregressive models used in forecasting techniques such as f-ARIMA and GARCH [20], [23], [24].

An ARIMA (*p,d,q*) process formulation shown in (3.1) and real wind power data from ERCOT were used to demonstrate improvements to WPFs. For completeness, we present the model and its components from equation (2.1) here.

$$\phi(B)(1-B)^d Y_t = \theta(B)\epsilon_t, \tag{3.1}$$

where ϵ_t is independently and identically distributed white noise with zero mean and constant variance, d is the degree of differencing needed to ensure stationarity, B is the backward operator (generally defined as $B^k Y_t = Y_{t-k}$), and ϕ and θ are polynomials of B.

The sequential forecasting process includes: (i) determining an optimal model from a group of models; (ii) finding the model parameters; (iii) validating the model; and, (iv) enhancing the forecast. The improvement in WPF using the ARIMA technique is expressed by the vector L_p norms of RE expressed in (3.2) and shown for each season in the period 3/1/2013–2/28/2014 in Table 1, where OF and EF represent the original and enhanced forecasts, respectively.

$$\|\mathrm{RE}\| = \left\|\frac{(\mathrm{P}-\mathrm{P}')}{\mathrm{P}}\right\|^{\mathrm{p}} \times 100, \tag{3.2}$$

where P is the actual wind power, P' is the forecasted wind power and p = 1, 2, and ∞.

The result of this improvement process is an enhanced forecast. Table 2-2 shows the calculated energy generated by wind for a one-year period. We calculated the energy in the three cases (i.e., using actual wind power, day-ahead original forecast, and day-ahead enhanced forecast) to compare the difference in wind energy generated.

Table 3-1 Quantifying WPF improvement using L_p norms [4]

Seasons	**L_1 %**		**L_2 %**		**L_∞ %**	
	OF	**EF**	**OF**	**EF**	**OF**	**EF**
Summer	314	268	12	9.3	3.6	2
Fall	411	303	34.5	10.8	24	2.3
Winter	357	309	14.5	11.2	2.6	2.5
Spring	332	268	17.3	10.4	4.5	2.5

We believe this shows part of the picture. However, studying the impact of the enhancement of WPF, which can be performed by variety of techniques, on the operations of the power system is more important. The following section explains the data and the test system that we use to run the unconstrained optimal power flow (OPF) time step simulation (TSS), which is equivalent to time step ED.

3.3 Data and Test System

3.3.1 Status of Wind Energy in ERCOT

ERCOT system has the highest installed capacity of wind generation, exceeding 17.6 GW by the end of 2016, in the US. Most of the wind generation is in the western zone of ERCOT. There are plans for ERCOT to reach 28 GW of installed wind capacity by 2020. Although this will contribute to the reduction in GHG and decrease the dependency on fossil fuel to generate electricity, it will add another layer of complexity to the system to be utilized and avoid wind energy curtailments [33].

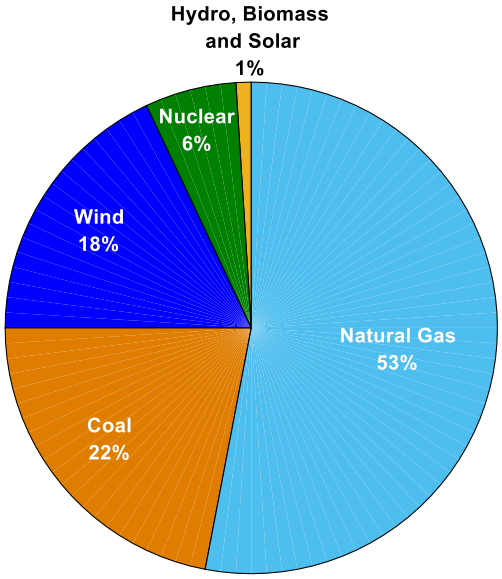

Fig. 3.1 Generation capacity share of ERCOT system with data from [10]

3.3.2 Data

In this paper, we used actual data obtained from ERCOT. The data includes hourly wind power—actual, day ahead forecast—and the enhanced forecast obtained from [4]. The data also includes the hourly demand for all the eight areas in the ERCOT system and the total demand for one year (2013-2014). To perform ED, we utilized the cubic cost curves of generators adopted from [34]. Although ERCOT has more than 15 types of generation sources, this synthetic model considers only the main five types of generation units (i.e., natural gas, coal, wind, nuclear, and hydro) to simplify the system. The data set is mapped onto a synthetic version of the Texas grid from [32].

3.3.3 Test System (Synthetic Model of ERCOT System)

To study the impact of WPF improvement on the power system, we run power flow simulations. Different test systems are used for this purpose. However, having a realistic system that mimics the actual behavior of the real power system of the area under consideration is more valuable and suitable for gaining insight into the operation of the system. The work in [32] introduces a methodology to create synthetic power system models that realistically represent a real power system and makes it available to the public for use in popular power system software packages [35].

This test system is developed by collecting openly available data and statistical analysis of real power systems to determine the size and the location of the power plants and loads, followed by a hierarchical clustering algorithm to group the loads and generations to substations. The synthetic model connects the substations through transmission lines whose parameters are available in datasheets and reference manuals. Table 3-2 has the system description of the synthetic model of ERCOT system.

Table 3-2 ERCOT synthetic model summary

Buses	2092
Wind generators	78
Other generators	204
Load points	1417
Areas	8

3.3.4 Mapping the Data and the Test System

Here we explain the approach to map the data to the test system. The wind power profile for each wind generator in the system is not readily available. We ensemble the aggregated time series wind generation in the three cases (i.e., actual wind power, original forecast wind power, and enhanced forecast wind power) to ensure that the sum of the power of wind generators equal to the total generated wind power as shown in (3.3).

$$P_w(t) = \frac{P_{w-capacity}}{P_{w-total\ capacity}} P_{w-total}(t), \quad (3.3)$$

where $P_w(t)$ is the time series of the electric power from the wind farm w and hour t, $P_{w\text{-}capacity}$ is the installed capacity of the wind farm w, $P_{w\text{-}total\ capacity}$ is the total wind installed capacity in the system, and $P_{w\text{-}total}(t)$ is the hourly wind power generation, which can be the actual, original forecast, or enhanced forecast. We also followed a similar approach to generate the load profiles based on the time series of the load for each area for the period of consideration.

Generator cost models are important to run ED and OPF and include cubic cost model and piecewise linear model. Cubic cost model for the generators adopted from [34] are mapped onto the power

system simulator to perform ED as a TSS. The total generator operating cost cubic model function is presented in (3.4) [34].

$$C_i(P_{gi}) = F_i + (A_i + B_i P_{gi} + C_i P_{gi}^2 + D_i P_{gi}^3) F_c + V_{om} P_{gi} \,, \tag{3.4}$$

where C_i is the operating cost of the unit i in \$/hr, F_i is the independent value of the fuel cost in \$/hr, A_i is the fuel dependent cost in MBTU/hr. B, C, and D are the cost curve parameters. F_c is the fuel cost, V_{om} is the variable operation and maintenance cost, and P_{gi} is the power produced by the unit. After mapping the data to the power system simulator, we perform ED and we find the hourly operating cost of the three cases. Then, we calculate the modified RACR metrics as described in the following section.

3.4 Metrics Using RACR

In economics and finance, risk is defined as the probability that the real return on an investment differs from the expected return. Note that risk includes both downside risk ─ where returns are lower than expected ─ and upside risk. An efficient investment portfolio has the highest expected return for the same level of risk. However, in practice it is difficult to find two assets with similar levels of risk. Hence, it is a common practice to use risk-adjusted returns measures, such as the Sharpe and Sortino ratios [36]-[38]. In general, the goal of these metrics is to find the investment with the higher return per unit risk. In this section, we propose a modification to these metrics to be used as cost metrics.

3.4.1 Overview of the Metrics

The Sharpe ratio (SR) evaluates the excess return per unit of risk. The excess return is calculated by subtracting the risk-free return from the expected return on an investment portfolio. The risk in investment of such a portfolio is represented by the standard deviation, σ [36]. A higher SR value indicates a higher expected return for the same risk level. SR is calculated under the assumption that the returns are normally distributed (i.e., the skewness of the return distribution tends to zero) as shown in (3.5).

$$\mathrm{SR} = \frac{\mathrm{E[R]} - \mathrm{r_f}}{\sigma} \tag{3.5}$$

Where E[R] is the expected return that considers both the incomes due to an investment portfolio and the total costs of such portfolio. r_f is the riskless interest rate. Fig 3.2 shows that SR equally considers the upside and downside volatility.

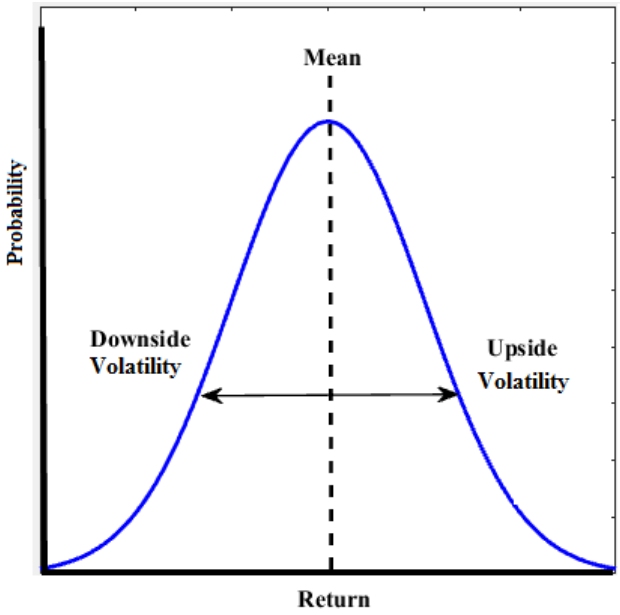

Fig. 3.2 SR considers both upside and downside volatility [38].

When evaluating returns whose distributions experience skewness, using the modification of SR that uses the downside deviation instead of the standard deviation as shown in Fig 3.3. Unlike SR, the SOR considers only those returns falling below a specified targeted value such as the minimum acceptable return (MAR), which may be set to the risk-free rate or zero. The risk in such portfolios is the target semi-deviation or downside (negative) volatility as shown in (3.6).

$$\mathrm{SOR} = \frac{\mathrm{E[R]} - \mathrm{MAR}}{\mathrm{TDD}} \tag{3.6}$$

TDD is the target downside deviation, equal to the square root of the target semi-variance. TDD is the root means square (RMS) of the exhibited underperformance from the target and calculated mathematically as in (3.7).

$$TDD = \sqrt{\frac{1}{N}\sum_{i=1}^{N}\left(\mathrm{Min}(0, X_i - T)\right)^2}, \tag{3.7}$$

where Xi is the i^{th} return, N is the total number of returns, and T is the target return [38].

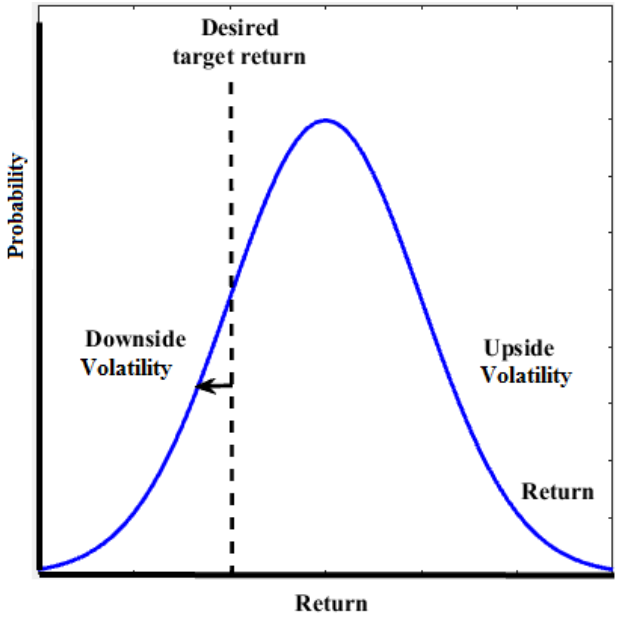

Fig. 3.3 SOR considers either upside or downside volatility

3.4.2 The Applications of the Metrics in the Power Systems Area

In the literature, Sharpe and Sortino ratio have been applied to power system applications, mainly in investment portfolio optimization studies [38]-[42]. These are used especially where the profit per unit risk is maximized to find the optimal power portfolio in the electricity markets or to compare investment strategies in resources planning [43]-[48]. The applications also include investment assessment of renewable energy resources portfolios [42], [43], [48].

In [45], one of the authors of [5] proposed a similar metric to SR. The metric, return per risk index (RRI), was utilized to assess investment network plans for distribution expansion planning. In practice, RRI is an additional measure that complements the information given by the traditional net present value.

In this work, we propose the use of the modified Sharpe and Sortino ratios as metrics to quantify the improvement in WPF. As the original Sharpe and Sortino ratios are applied on the return, we apply the

modified metrics on the deviation in the operation costs (OCs). In the following subsection, we explain the proposed modification to these metrics, and provide examples to better understand the modified metrics.

3.4.3 Application of the RACR Metrics to WPF Improvement Evaluation

We propose metrics based on RACR that relate WPF improvements to OC in an electric power system. In this work, OC is obtained by running ED in three cases using wind power data: actual, OF, and EF. We define the deviation of the actual operation cost (OCA) from the operation costs (OCs) associated with original forecast (OCOF) and enhanced forecast (OCEF) as α_{OC} and β_{OC}, respectively, in (3.8) and (3.9).

$$\alpha_{oc} = OC_A - OC_{OF} \tag{3.8}$$

$$\beta_{oc} = OC_A - OC_{EF}. \tag{3.9}$$

Here, the operation costs based on ED of the ERCOT power market are considered. Then, either neglecting the incomes or assuming them as constant, the EF (resulting from improved WPF) will show a reduced β_{oc}. The ideal values of both α_{oc} and β_{oc} are zero. Based on that, we propose to apply a modified Sortino ratio (MSOR) considering only the cost differences as shown in (3.10).

$$MSOR_{\mu} = \frac{E[\mu] - T_0}{TDD_{\mu}}, \tag{3.10}$$

where $\mu = \alpha$ for OF and $\mu = \beta$ for EF.

Also, when α_{oc} or $\beta_{oc} > 0$, the actual wind power has a higher probability to be less than the forecasted. This represents a need to re-dispatch more expensive generators to supply the demand. The aim is to have a lower MSOR, considering the TDD as the target upside deviation, i.e., the right tail from 0 on the probability distribution of α_{oc} or β_{oc}.

Similarly, a modified Sharpe ratio (MSR), shown in (3.11), for quantifying the performance of the improved WPF on OC is developed. Thus, smaller values of MSR and MSOR are more favorable.

$$MSR_{\mu} = \frac{E[\mu] - T_0}{\sigma_{\mu}}. \tag{3.11}$$

Note that in (3.10) and (3.11), T_0 is the desired target when the actual wind power is exactly equal to the forecasted value (OF or EF).

Next, to explain the application of both the proposed ratios — MSOR and MSR — three examples are presented for two normally distributed probability curves, α and β. Table 3.3 summarizes the input data and the computed ratios for these three examples.

- Case 1: if both α and β have the same expected value (μ), the one with lower deviation (σ), indicating the lower risk, should be chosen. As shown in Table 3.4 and Fig. 3.4, β has a lower deviation than _ and its MSOR is also lower than the MSOR of α, however; its MSR is higher than the MSR of α. In this case, the MSOR leads to choosing β as the better option with lower risk.

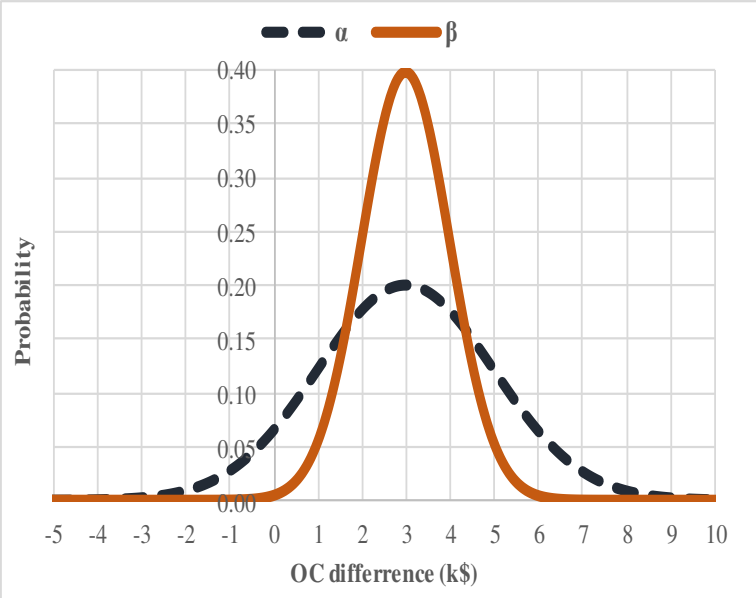

Fig. 3.4 . Case 1 of Table 3.3, both α and β with the same μ but different σ

- Case 2: if both α and β have the same deviation, the one with lower expected value, due to its lower expected cost, should be chosen. As shown in Fig. 3.5 and Table 3.3, β has the lower μ. β also has lower MSOR and MSR.
- Case 3: if α has the lower deviation but the higher expected value and, in contrast, β has the higher σ but the lower μ , the one with lower expected value per unit of deviation should be chosen. Based on the data shown in Table 3.3 and Fig. 3.6, β is the better option with the lower MSOR and MSR.

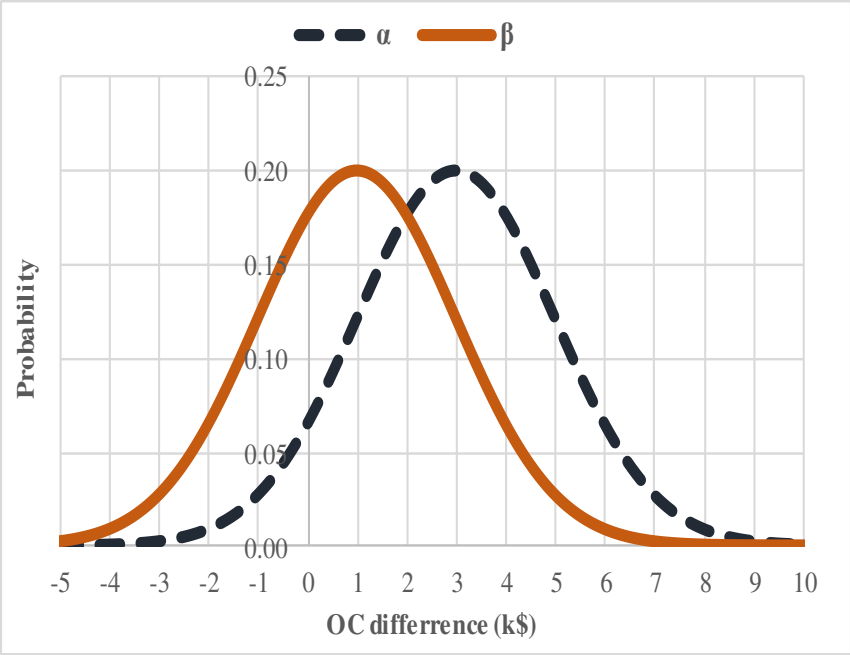

Fig. 3.5 Case 2 of Table 3.3, both α and β with the same σ but different μ

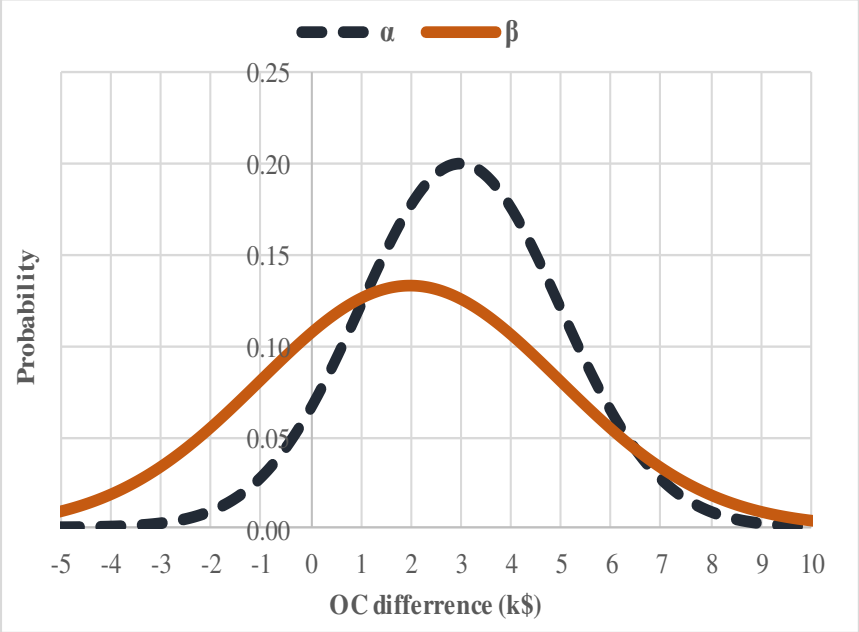

Fig. 3.6 Case 3 of Table 3.3, both α and β with different μ and σ

Referring to the analysis of the examples mentioned above, it can be concluded that the MSOR always leads to taking good decisions by choosing the option with the lowest expected cost per unit of deviation, but the MSR is not always enough to take the right decision, as shown in the first example (Case 1).

Table 3-3 MSOR and MSR analysis considering different normal distribution examples curves of α and β

	Base-Case	Case 1	Case 2	Case 3
	α	β	β	β
Expected value, μ	3	3	1	2
Standard deviation, σ	2	1	2	3
Target semi-variance, TDD	3.937	5.177	1.959	2.762
MSOR	0.762	0.580	0.511	0.724
MSR	1.500	3.000	0.500	0.667

3.5 Results

ED for the three cases of wind power (actual, OF, and EF) [4] for a one-year period (3/1/2013 – 2/28/2014) was performed and their OCs in each case were found. Then, α and β curves of OCs were computed. These results are summarized in Table 3.4 and Fig. 3.7.

Table 3.4 and Fig. 3.7 show the statistics and the probability distributions of α_{OC} and β_{OC}, respectively. From Fig. 3.7, we notice that β_{OC} has a higher probability of zero, indicating that the day ahead forecast UC and the actual unit commitment are equal more frequently when the enhanced forecast is used. We also observe that the absolute value of the mean of $\beta_{OC}$is lesser than that of α_{OC}. This indicates the impact of the smaller forecast error on dispatching the resources. More importantly, β_{OC} has smaller MSR and MSOR values. The skewness values for bothα_{OC} and β_{OC} are close to zero suggesting that both metrics can be used for WPF quantification. However, MSOR is still preferred because one of the sides is riskier than the other. These indicate that the WPF improvements using the ARIMA model from [4], real wind power and load data from ERCOT, and a realistic model of the Texas grid in power flow simulations, have a positive impact on the power system market and OC.

Table 3-4 Statistics and calculated metrics

Statistics and metrics	α_{oc}	β_{oc}
Mean ($)	4213.6	-530.8
Standard Deviation ($)	6164	7264
Kurtosis	4.369	7.651
Skewness	0.2	-0.8
MSOR	1.799	-0.089

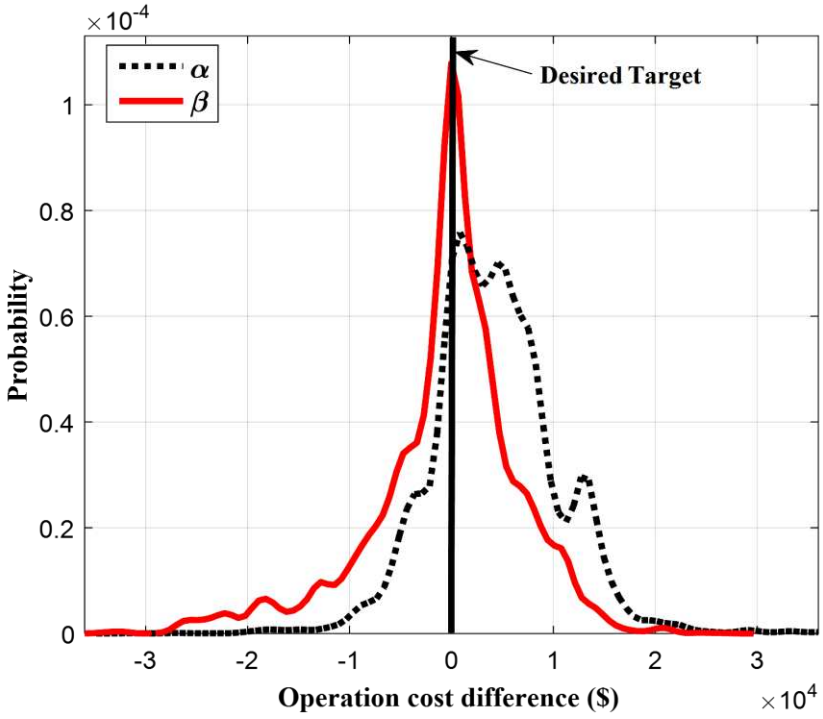

Fig. 3.7 The probability distributions of αoc and βoc computed for the test system under analysis

3.6 Conclusion

Different metrics have been used to evaluate improvements in renewable power forecasting techniques. However, the statistics and the distribution of the forecasting error might not be enough to examine the impact of the improvement in a real power system. In this paper, we propose two ratios ─ the MSOR and MSR ─based on modifications to traditional risk-adjusted financial metrics to evaluate the impacts of the enhancement of WPF in the day-ahead power market. Further, these metrics can be applied to evaluate other forecasting techniques and, specifically, the MSOR allows for better decisions making to choose the option with the lower expected cost per unit of deviation.

CHAPTER 4

A DATA-DRIVEN JUSTIFICATION FOR DEDICATED DYNAMIC PRICING FOR RESIDENCES-BASED PLUG-IN ELECTRIC VEHICLES IN WIND ENERGY-RICH ELECTRICITY GRIDS[3]

4.1 Introduction

Plug-in electric vehicles (PEVs) are gaining more acceptance globally. In addition to avoiding or minimizing the use of fossil fuels powered internal combustion, PEVs can also be charged using electricity generated from renewable sources like wind, thus extending the reach of their contributions to curbing greenhouse gas (GHG) emissions. Individual light duty PEVs consume a few tens of kilowatthours thus limiting their individual impact on the load leveling efforts. However, with projected proliferation of PEVs, the potential of noticeably impacting the electricity demand provides an opportunity for balancing an abundance of wind energy as opposed to curtailing it for lack of demand to avoid frequency deviations. This introduces the primary challenge of how to schedule the charging of available PEVs by increasing the utilization of an intermittent resource like wind energy. Studies indicate that the availability of wind energy is high in the evening and night time when most of the PEVs will likely be available for charging [49]–[51]. Thus, a pricing mechanism may incentive PEV owners to match their charging pattern with the availability of wind energy.

Recently, utilities have focused on two main efforts pertaining to PEVs: a) increasing the adoption of PEVs in their service areas for environmental benefits; and b) designing incentivized pricing mechanisms to encourage PEV owners to charge at the best time for both the utility (i.e., off-peak) and the customer (i.e., availability of cheaper price). However, these efforts attempt to design a general time of use (TOU) or other pricing mechanisms for all the loads at an end user facility, which have different power

[3] This chapter is a verbatim reproduction of the work under review in a peer reviewed journal (The IEEE Power and Energy Technology Systems Journal) [7]. The terms and conditions of retaining the permissions for re-use of the material have been obtained from the copyright holders and are included in the Appendix C. The numbering of the figures and tables has been modified to satisfy the formatting requirements of the dissertation.

requirements, availability times, and duration than PEVs. Some utilities have already started implementing simulation and pilot studies to investigate the benefits of developing dynamic pricing for PEVs only. To help accelerate the adoption of PEVs in California, Pacific Gas and Electric (PG&E) launched its new PEV charge network program in January 2018. PG&E, jointly with business owners and PEV charging companies, is starting to install 7500 PEV charging points at condominiums, apartment buildings, and workplaces across northern and central California [52]. This will provide two main benefits: a) increasing the adoption rate of PEVs thus providing cleaner transportation; and b) increasing the number of charging stations. Currently, PG&E offers two TOU-based pricing plans; the first option is a universal TOU for all loads in the residential premises including the EV and the second option is a dedicated TOU for EVs through a separate meter for EVs. Both options use TOUs with peak, partial-peak, and off-peak hours as detailed in[53].

In a wind energy-rich grid such as ERCOT in Texas, curtailment arises due to under-forecasting and the negative correlation between the availabilities of the electrical load and wind energy. The coordination of wind energy with PEVs has generated research interest recently with solutions considering maximizing renewable sources penetration, cost minimization, GHG emission reduction, and load leveling [9],[54], [15], [54], [56]. These studies do not consider dedicated dynamic/incentive pricing to encourage the customers to charge their PEVs at appropriate times during the day. In 2013, a Dallas-based electricity provider offered a promotion program called “free nights” for charging PEVs at no cost to the owners [57]. The intent of this promotion was to utilize the high wind energy production during nighttime in Texas by incentivizing the PEV owners. However, free electricity may not bode too well for market efficiency.

Here, we investigate the need for a dedicated dynamic/incentive pricing for PEVs (CIP-PEVs) at times when there is an excess of wind energy. We employ real-world data, simulation models of synthetic power grid of ERCOT, and results from our previous study[4]. The datasets include enhanced wind power forecast (WPF) [4] , load for all eight ERCOT areas [58], spot market pricing data (i.e., locational marginal prices) supplied by ERCOT, utility prices for a Texan city (i.e., Austin) [59], and driving characteristics from the 2017 National Household Travel Survey (NHTS) collected by the US Department of

Transportation [60]. It is worth mentioning that this study focuses on residential charging only as it represents more than 80% of the charging points in Austin, TX [50], [51], [61]. Also, we do not consider any vehicle to grid (V2G) operations due to the lack of supporting infrastructure and other technical challenges that lie outside the scope of this study.

The rest of the chapter is organized as follows. Section 4.2 describes the current and projected adoption rates of PEVs and wind energy in Texas. Section 4.3 provides a description of the data used in our case study. Section 4.4 explains details of analysis in our case study. Section 4.5 presents the results of the case study and discusses the need for a dedicated dynamic pricing for PEVs in Austin, TX. Section 4.6 concludes the chapter.

4.2 Current Levels and Projected Trends of Wind Energy and PEVs in Texas, USA

In this section, we present the results of some literature search on the current rate of adoption and the projected trends for PEVs in Texas. We present our analysis of wind energy data obtained from ERCOT and the results from our previous study, in [4], to determine the potential of charging PEVs with the excess of wind energy.

4.2.1 Current Adoption Rate and Future Trends of PEVs in Texas

PEVs help reduce the reliance on fossil fuel which powers around 92% of the transportation sector in 2017 [62]. The US sales of PEVs experienced a 40% annual increase in 2017 [61], [63]. In 2016, there were about 400, 000 PEVs in the US; however, with legislation like climate actions plans calling for reduction in emissions, [64], and the sale price drop of PEVs, the share of PEVs in transportation fleet is expected to increase. In 2016, 8, 397 EVs and 199, 096 electric and gas hybrid electric vehicles (HEVs) were registered in Texas [65]. There is also an expected increase of PEVs to be as high as 835,000 by 2030 [61].

Reference [49] provides the projected increase of PEVs in Texas from a study to identify the services that PEVs could provide for existing markets from the perspective of independent system operators (ISOs) and regional transmission organizations (RTOs). An important finding from [49] is that one million PEVs may be deployed in North America by 2020. It also aimed to find the projected concentration of

PEVs in different ISO/RTO and determine the significant capacity increase in the load. Three levels of growth in the PEVs sales, namely the fast, slow, and targeted growths in all ISOs in the North American markets are available in [49]. Fig. 4.1 shows the growth rates in ERCOT. The annual slow growth and the targeted growth by ERCOT are 33% and 48%, respectively, which would result to 900, 000 and 1.5 million PEVs, respectively by 2025. Also, publicly available information in [66] categorizes vehicles in Texas based on the fuel types and provides information on the number of registered vehicles in in every congressional district of Texas. This information helps determine the number of PEVs currently available in the wind energy-rich areas and what the projected number of PEVs is in the future years.

4.2.2 Wind Power in ERCOT

As of 2018, Texas has the highest installed capacity of wind energy resources of all the states in the US [67]. The ERCOT system has eight areas, namely, coastal, east, west, north, south, far west, north center, and south center. South Houston aggregates south and south center areas while north west aggregates north, north center, west, and far west areas [35]. In the ERCOT system, Austin lies in the south Houston aggregation, which along with the north west aggregation, is considered one of the two wind-rich areas [27]. From our previous study on WPF improvement in [4] and improvement quantification in [5], we found a negative correlation between the average hourly wind power production and the hourly system load in ERCOT. Thus, there is a potential of load leveling approaches using the excess of wind power and PEVs load. Austin, Houston, and Dallas are the top three Texan cities for PEVs adoption rates[50], [68].

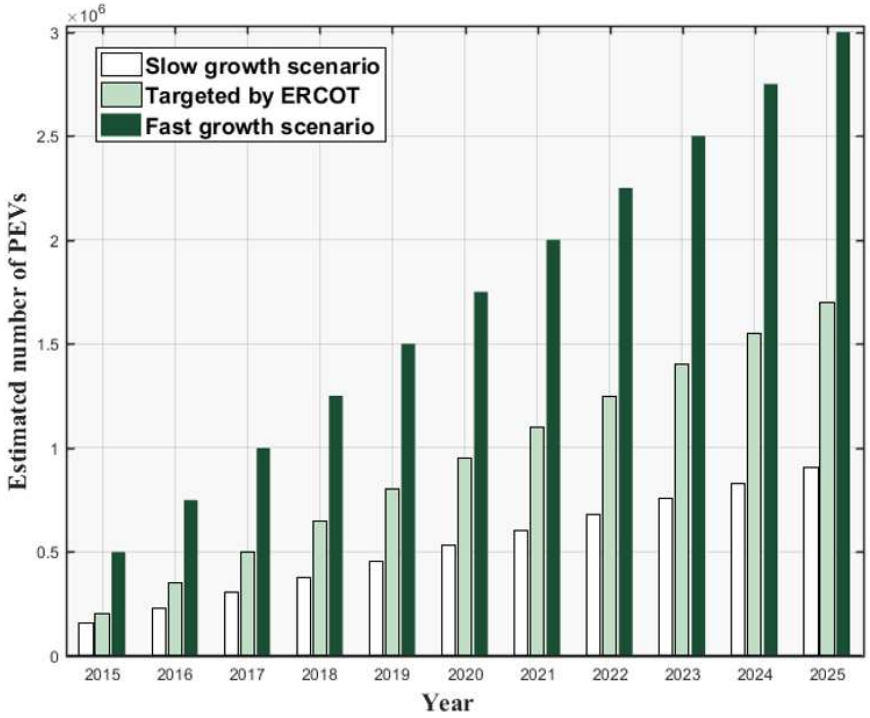

Fig. 4.1 The growth of PEVs in ERCOT system based on three different scenarios

With data on wind power—actual and forecast— obtained from ERCOT, we studied WPF improvements using statistical time series for period March 2013–March 2014 [4]. In [4], we improved the accuracy of WPF by halving the root mean square error using a statistical time series model (i.e., ARIMA). Here, we further analyze this data to find the potential of PEVs to consume the excess of the wind power production. Table 1 shows the excess of wind power due to under-forecasting in the ERCOT system for the period under study (i.e., 03/2013– 03/2014).

Table 4-1 Statistics of excess wind energy in ERCOT regions due to under-forecasting for the period 03/2013–03/2014

Statistics (MW)	North west aggregation	South Houston aggregation	Total
Maximum	5,334	2,277	7,611
Mean	134.5	125	259.5

ERCOT includes the day-ahead market (DAM) and the real-time market (RTM) in the functioning of its market. When the actual wind power (i.e., in the RTM) exceeds the wind power forecast (i.e., from the DAM) in an area with high wind power generation, there is a revenue lost due to wind power curtailment. Some of this lost revenue can be captured by improving WPF (as shown in [4]). But, improved WPFs are also error prone and may lead to under-forecasting. To minimize the curtailments in such cases, we can consider dispatching some flexible resources (e.g., PEVs) to increase the load at times when the clean cheap energy (i.e., wind energy) is available. The wholesale electricity price from U.S Energy Information administration (EIA) is used to calculate the approximate value of lost revenue due to wind power curtailment in (4.1) [69].

$$\mathrm{Rev}_{\mathrm{lost}} = \sum_{t=1}^{8760} P_{WC}\,(t)\,\lambda_{WS}(t) \qquad (4.1)$$

where $P_{WC}\,(t)$ and $\lambda_{WS}\,(t)$ are the curtailed wind power in MW due to forecast error and the wholesale price in \$/MWh, respectively. Rev_{lost} is the total lost revenue in the year under study. Based on this calculation, the total estimated lost revenue based on the original and the enhanced forecast are \$56 million and \$54.7 million, respectively. Thus, even with improvements in WPF, the lost revenue from curtailed wind power is high and warrants additional considerations.

4.2.3 The potential of PEVs Consumption to Match the Excess of Wind Energy

Based on the previously-mentioned reports, the annual rate of PEVs adoption in Texas is projected to increase by 38 − 40% from 2016. Using the information from [49] and [66], we project the annual registered PEVs in the north west, and south Houston aggregations using the slow growth rate as shown in Fig. 4.2. Here, we consider the slow growth of PEV adoption to avoid high expectations when accounting for the number of vehicles in these two aggregations. South Houston aggregation is expected to have around 180,000 PEVs by 2030. Since we use the enhanced WPF data for the year 2013–2014, we use the number of PEVs in Austin in 2014 (i.e., 1,132) in our analysis. However this number has rapidly increased since

2014. So, we will also examine the increase of PEVs adoption by using the number of PEVs as of 2018 (i.e., 20,000) and study the impact on the profitability of the wind energy-PEVs coordination in the results.

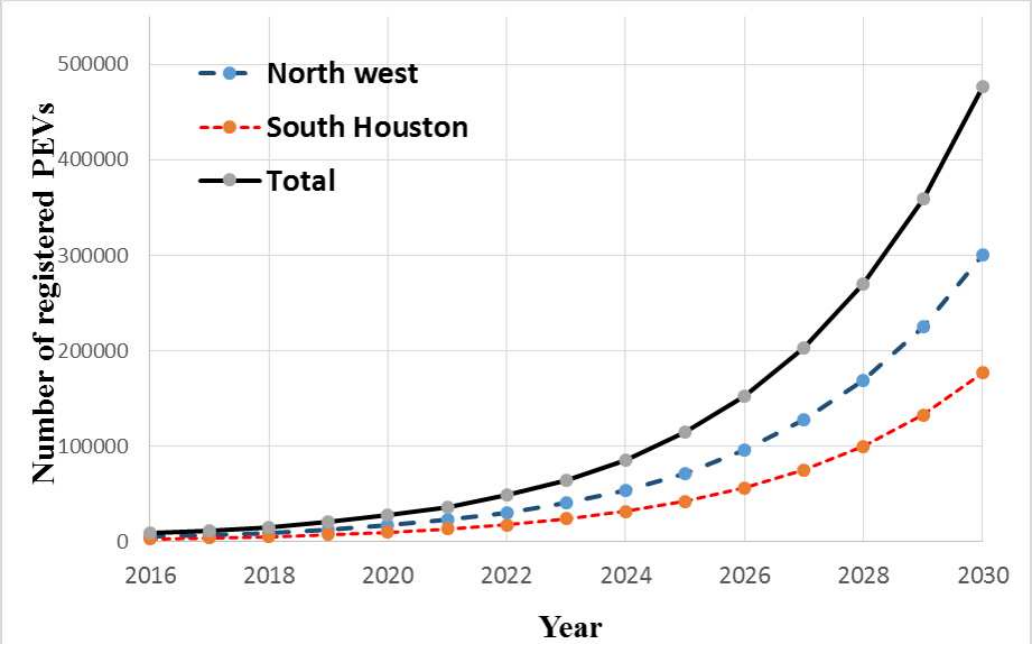

Fig. 4.2 The projected annual sales of PEVs in the north west and south Houston aggregations of ERCOT

4.3 Data and Analysis

In this study, we use multiple datasets to perform case studies to present evidences for dedicated dynamic pricing for PEVs in wind-rich regions of ERCOT. These datasets include the enhanced wind power forecast from our previous work in [4], datasets of electric utility prices for a utility company [59], and spot market provided by ERCOT and load data from ERCOT and is available in [70]. Since most of the wind capacity in Texas is installed in the North-West and South-Houston areas, we collected data corresponding to these two areas. The steps of gathering the needed data include: i) finding the locations of the closest urban or suburban cities in the two wind energy-rich areas and identify its postal (ZIP) code; ii) finding an example of a utility price in these cities; and iii) finding the spot market price as a DAM locational marginal price (LMP) from ERCOT for this location. ERCOT also provides the locational information of buses for the nodal prices [70]. Finally, we used two approaches to create realistic PEV profiles for level-I and level-

II charging using datasets from NHTS and the available meters-validated data from the National Renewable Energy Laboratory (NREL) [60], [71]. Listed below are the details of these datasets.

- **Wind power forecast data:** In our previous work from [4], we used real data obtained from ERCOT. The wind datasets include actual wind power and day-ahead forecast. Our work in [4] resulted in an enhanced forecast with higher accuracy. In this work, we use this enhanced forecast to calculate the profit from the coordinated charging of PEVs.
- **Load data**: The ERCOT load data from its eight areas is available to the public [58]. The base load for ERCOT is determined as the lowest load value of the month. As in our previous study in [5], we have synthetic information of the different substations in the ERCOT system from [35], [32], [72]. We use the information of the rated load of these substations to scale down the load for the specific considered substation.
- **Residential electric utility price**: Although some of the electric utilities operating in the ERCOT system use a flat rate tariff for electricity throughout the day, many utilities in Texas have started implementing dynamic pricing rates such as TOU for the whole year or for the peak months (i.e., summer months). We obtained a utility price data set for a utility in Austin from[59].
- **Driving characteristics**: NHTS publishes household traveling survey data every several years [60]. In this study, we use information from the 2017 NHTS survey to determine some driving characteristics such as probability mass functions (PMFs) of starting trip times and locations of vehicles at different times of the day and to better understand the traveling habits of large number of people in the US. Although this data is not exclusively for the residents of Austin, TX, we believe it is representative of any large city in the US.
- **PEV charging profile based on NHTS data and NREL data**: Using the PMFs of the departure and the arrival times of vehicles, power ratings and duration of the different charging levels and charging behavior models, we created a realistic PEVs demand profiles for each charging level [73], [74]. The

PEVs charging profiles are validated against the general profile in [61], and the profile data from NREL [71].

In the following section, we explain the process of performing the case study and highlight the specific data used in each case.

4.4 Case Study

The case study of coordinating the charging of PEVs in a wind energy-rich grid is described here. This case study shows how a utility's revenue from wind energy-PEVs charging depends on the type of pricing mechanism (e.g., flat rate or TOU) and the rates used. The case study is described as follows:

- **Identifying wind energy-rich service areas and the available resources**: In a wind energy-rich grid, we start by identifying a substation in one of the cities that has a high current or projected adoption rate of PEVs. For this case study, we choose Austin, TX because one of its utilities provides a universal TOU for its residential customers and an optional flat charge pricing for its PEV owners. Here we ensemble the aggregated time series of the enhanced WPF of the south Houston area and scale it down to the farm level similar to our previous work [4], [5]. We use the information from [75] to find the largest wind farm closest to Austin, TX. Similarly, we find the largest substation closest to Austin, TX from the synthetic model from [35], [35] to create the profiles as shown in (4.2), and (4.3).

$$P_{wf}\,(t) = \frac{P_{wfc}}{P_{TWC}}\,P_W\,(t) \tag{4.2}$$

where $P_{w\,f}\,(t)$ is the time series of the electric power output from the wind farm wf at hour t, P_{wfc} is the installed capacity of the wind farm wf, P_{TWC} is the total wind installed capacity in the system, and $P_W(t)$ is the hourly wind power output from the enhanced forecast all in in MW.

$$P_s\,(t) = \frac{P_s}{P_{SC}}\,P_{SC}\,(t) \tag{4.3}$$

where $P_s\,(t)$ is the time series load of the substation s at hour t, P_s is the rated load of the substation s, P_{SC} is the rated load of the south center area, and $P_{SC}\,(t)$ is the hourly load of the south center area

obtained from ERCOT all in MW [58].

- **Using the needed pricing datasets:** For the Austin, TX area, we obtained the hourly DAM LMP data from ERCOT for all the nodes in the system. We use the information of the settlement points and electrical buses mapping available in ERCOT [70]. We also use an example of the utility price of a utility that serves this area. Fig. 4.3 shows a four-tiered TOU for residential energy usage provided by a serving Austin, TX [59]. It is worth mentioning that the same utility provides another option of pricing for PEVs owners that is a flat rate of $30/month for PEV customers that use less than 10 kW and $50/month for customers that use greater than 10 kW. The flat rate is conditional to the PEV owners charging their vehicles only at pre-identified off-peak times.

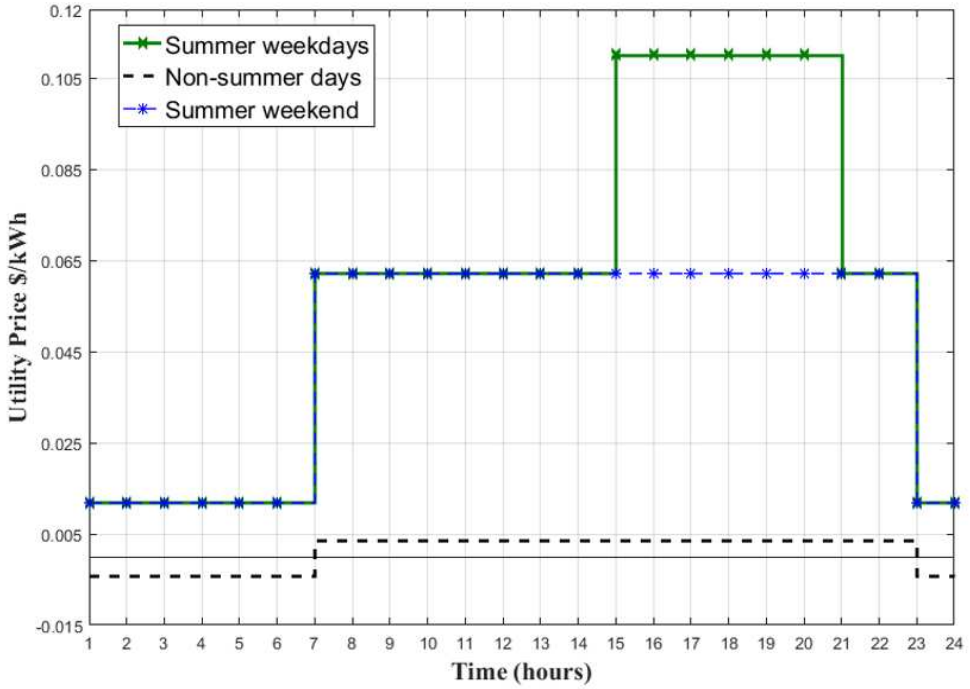

Fig. 4.3 Four-tiered universal TOU pricing for residential customers of a utility in Austin, TX

- **Creating PEVs profiles:** To create a realistic PEV profile, we gathered information of the estimated number of PEVs in Austin, TX, the percentage of each charging type (residential, commercial, or industrial), the percentage of the charging levels, and charging behavior model. Based on recent reports, Austin, TX has approximately more than 20, 000 PEVs in 2018 and approximately 80% of

them are tied to residential charging [50], [61], [65]. Table 4-2 summarizes the information of the different charging levels and their percent- age in the area of study. This study considers residential charging only as it represents most of the charging points; further, we use the residential TOU rates offered by a utility in Austin, TX. We use this information along with the charging behavior model from [74] and the PMF of PEVs arriving home from work from [60] to create two PEV profiles for each charging level. Reference [74] details pilot studies showing PEV owners tend to start charging their vehicles when they arrive home from work; this is supported by analyzing the data obtained from NREL [71]. Reference [74] compared around 100 studies of time-varying pricing and concluded that the ratio of peak to off-peak should be around 8:1 to achieve a 15% reduction in demand. This implies a price elasticity of demand, ε, of -0.04 [74]. In this study, we use these two assumptions, supported by the NHTS data and NREL PEV profile to generate near-realistic PEVs profiles and include the impact of the current TOU shown in Fig. 4.3.

Table 4-2 The information of the residential charging levels and their percentage in Austin [50], [73].

Charging level	**Rated power (kW)**	**Charging duration (hours)**	**Charging points %**
Level-I	1.6–2	8–20	18%
Level-II	3.5–6.5	4–8	82%

Figures 4.4 and 4.5 show the PEV profile created based on NHTS data and a randomly selected day of the hourly PEV profile obtained from [71], respectively. Fig. 4.4 depicts generalized PEVs profiles per a PEV which is generated using the PMF of the NHTS data. We then incorporate the information of the number of PEVs and the percentage of the two residential charging levels (i.e., level-I and level-II) for Austin, TX as shown in Table 2 to create the PEVs load profiles. Figure 5 depicts the normalized load profiles of PEVs for a random day in 2010 data [71]. We used these two generalized profiles to model the number of PEVs and the associated load profiles in Austin TX (circa 2013 and 2018).

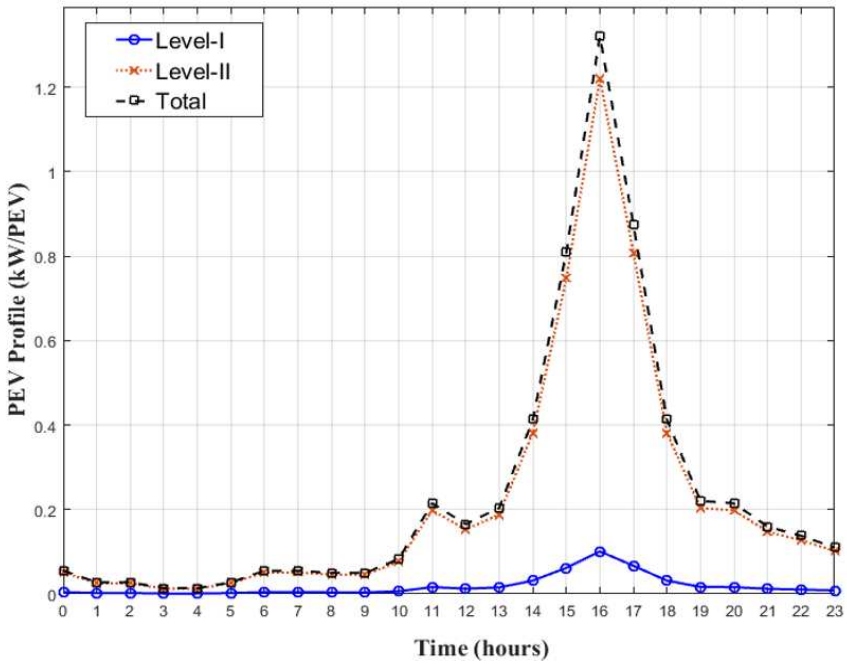

Fig. 4.4 Normalized PEV profiles based on NHTS data

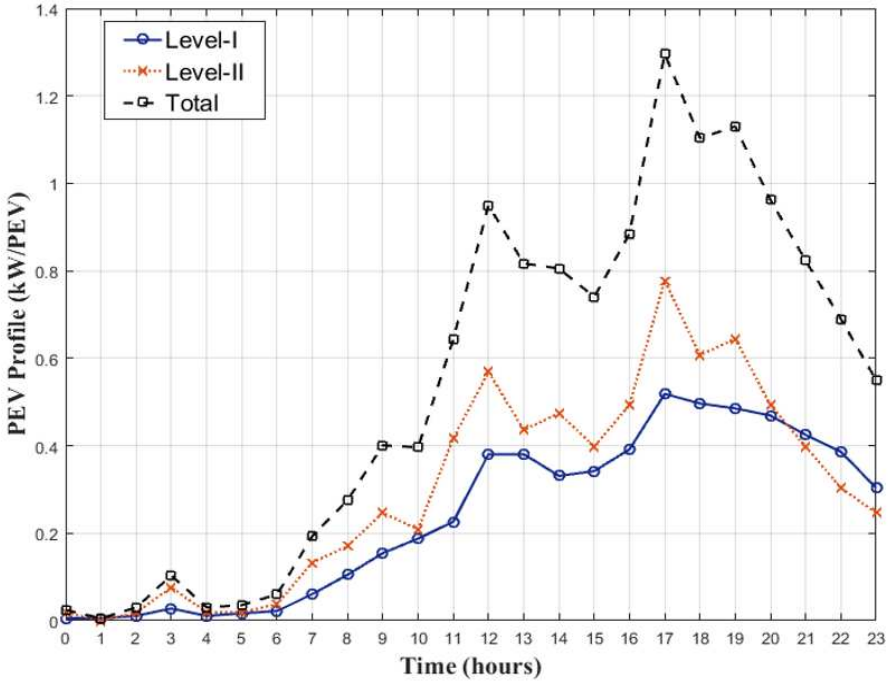

Fig. 4.5 Normalized PEV profiles of a randomly selected day from 2010 [71]

- **Calculating profits:** Using the datasets described above, the forecast profit for the utility from the excess wind energy-PEVs coordination is calculated as follows. We start by creating the wind power

profile and the load profile of the area according to (4.2) and (4.3), respectively. We also use the PEVs profiles as depicted in Figures 4.4 and 4.5. We use (4.4)–(4.9) to calculate the forecast profit of the utility from the excess wind energy-PEVs coordination. The variable load in the system is shown in (4.4),

$$Var_{load}\,(t) \;=\; L(t) \;-\; L_B \tag{4.4}$$

where $Var_{load}\,(t)$ is the hourly variable load in the system, $L(t)$ is the total hourly load, and LB is the monthly base load. The excess of wind energy in the area is computed in (4.5),

$$Exwind\,(t) \;=\; WPF(t) \;-\; Varload\,(t) \tag{4.5}$$

where $Ex_{wind}\,(t)$ is the hourly excess of wind energy and $WPF(t)$ is the DAM enhanced wind power forecast. If the value of $Ex_{wind}\,(t) > 0$, that indicates an excess of wind energy that can be dispatched to charging PEVs. If $Ex_{wind}\,(t) \leq 0$, then there is no access of wind energy and there is not a potential revenue to acquire at that time. When $Exwind\,(t) > 0$, the expected dispatched PEV profile at time t is computed in (4.6). Then, the hourly cost, hourly revenue, and the hourly forecast profit are computed in (4.7)–(4.9) respectively. where $PEVs_{dispatch}(t)$ is the PEVs dispatch at time t and $PEV_{profile}(t)$ is the PEVs expected profile at time *t*.

$$PEVs_{dispatch}(t) = \; min(Exwind\,(t), PEV_{profile}(t)) \tag{4.6}$$

$$C(t) \;=\; Exwind\,(t) \;\times\; s(t) \tag{4.7}$$

$$R(t) \;=\; PEVs_{dispatch}(t) \;\times\; u(t) \tag{4.8}$$

$$P(t) \;=\; R(t) \;-\; C(t) \tag{4.9}$$

$C(t)$ is the hourly cost of purchasing wind power in \$, $s(t)$ is the DAM spot market price from ERCOT in \$/MWh, $R(t)$ is the revenue of the utility obtained by dispatching PEVs based on wind energy resources, and $P(t)$ is the hourly profit.

4.5 Results

After gathering the data and performing the calculations, the monthly excess of wind energy in Austin area and the profit gained are presented here. Fig. 4.6 shows that the excess wind energy is minimum

in the summer months (June-September), which is normal for ERCOT as Texan cities have summer peaks due to weather conditions.

Fig. 4.7 presents the monthly profit of the utility for the year of study (March 2013–March 2014) and using the number of PEVs in Austin, TX for the same year (i.e., 1,132 PEVs). Although, there is an excess of wind energy for all the months, with much higher in the non-summer months, the utility does not make any profit. We calculate the total profit from the wind energy-PEVs charging coordination to be $-\$11.5$ millions (loss). This loss is due to two reasons. Firstly, the residential TOU used by the utility (shown in Fig. 4.3) has negative prices in the off-peak hours of the non-summer months. Secondly, the relatively small number of PEVs makes the impact of the PEVs load in levelling low.

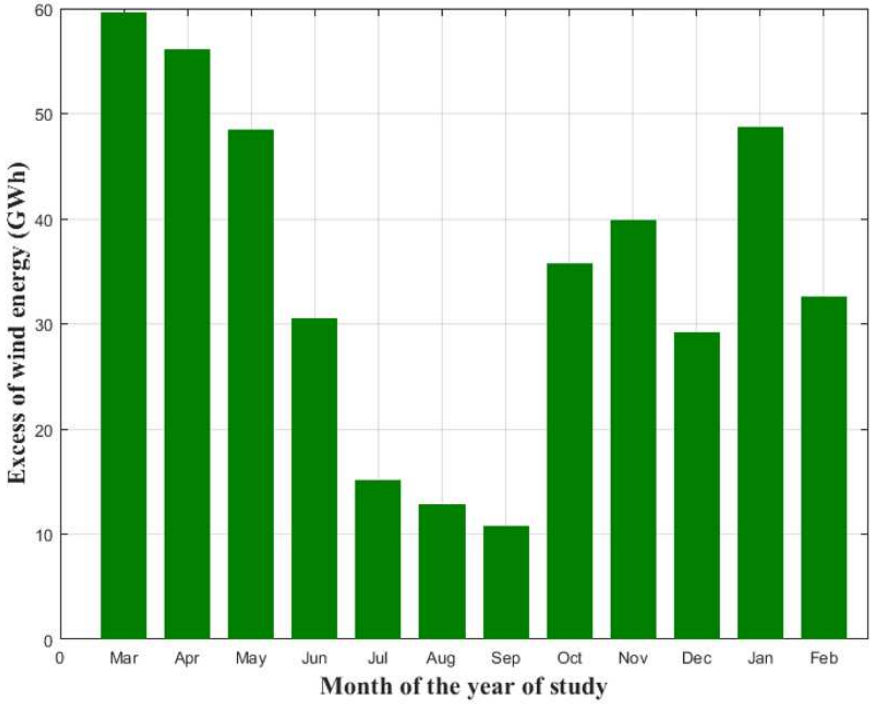

Fig. 4.6 The monthly excess of wind power of the year of study (March 2013–March 2014)

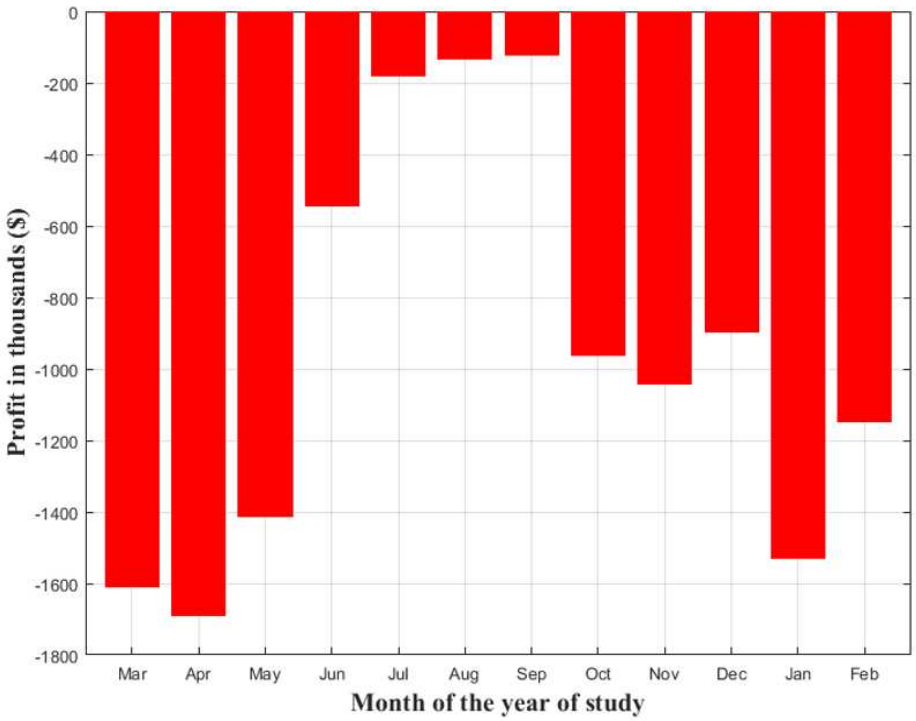

Fig. 4.7 The monthly profit of the utility resulting from the current residential TOU considering the number of PEVs in 2013–2014

We further examine the impact of the rapid increase of PEVs in Austin, TX and calculate the profit using the number of PEVs in Austin in 2018 and assuming the same WPF data (March 2013–March 2014). Fig. 4.8 shows the monthly profit when using the TOU rates. Although the excess of wind energy is higher in the non-summer months, significant profit is attained only in the summer months because of the TOU rate used. In the non-summer months, the utility could potentially be generating a loss (negative profit) from dispatching PEVs. Because we used a higher number of PEVs corresponding to 2018 (20,000), the total annual profit for 2018 increases to $-\$9.6$ millions (loss).

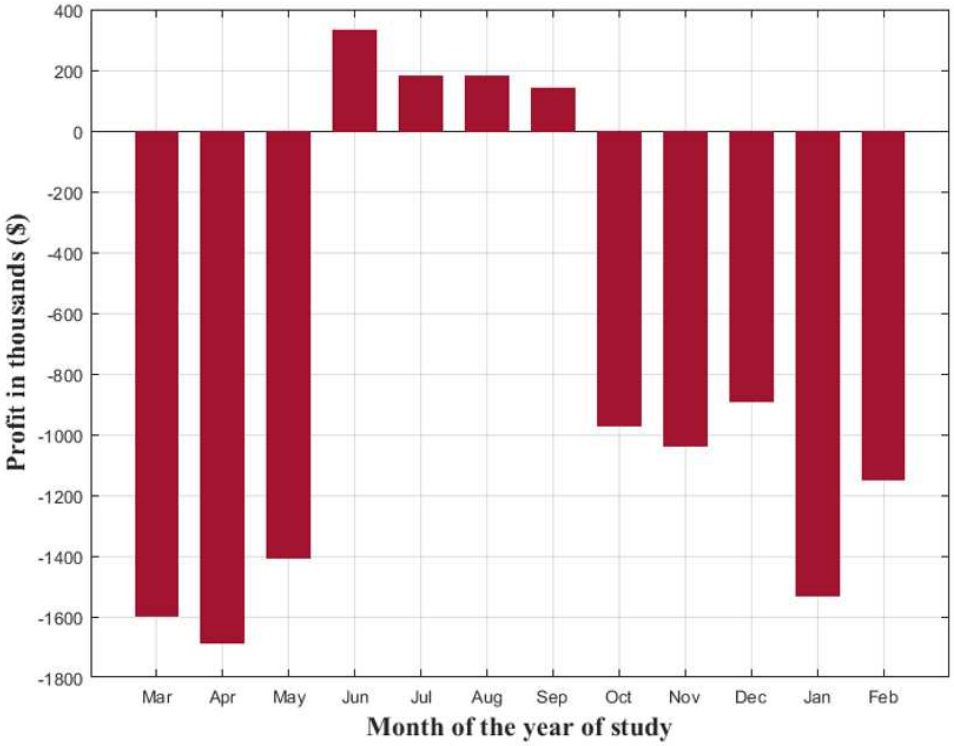

Fig. 4.8 The monthly profit of the utility resulting from the current residential TOU considering the increase of PEVs as of 2018

4.6 Conclusion

The results of our case study indicate the dire need for a fair pricing mechanism that will benefit both the seller of the electricity (i.e., utility) and the rate payers (i.e., customers). We contend that this mechanism should be a dynamic pricing method (like the TOU) but dedicated for PEVs through separate-metered installations at the residential facilities. Our case study presents the need of a pricing mechanism for increasing the participation of PEV charging by owners in residences during the hours when there is an excess of wind energy via an incentive pricing mechanism. The results show how the profit of the utility from the wind energy-PEV charging coordination will mainly depend on the pricing mechanism used.

CHAPTER 5

A DATA DECOMPOSITION APPROACH TO DESIGN A DYNAMIC PRICING MECHANISM FOR RESIDENCES-BASED PLUG-IN ELECTRIC VEHICLES IN WIND ENERGY-RICH GRIDS[4]

5.1 Introduction

There is lost revenue due to wind power curtailments in wind energy-rich grids due forecasting errors and the negative correlations between the loads and wind power generation. Using bulk-level energy storage system is not yet a cost-effective solution to wind power curtailment problem. The coordinated charging of plug-in electric vehicles (PEVs) with the availability of high wind energy generation provides a potential solution to this problem. However, there are multiple considerations pertaining to this coordination. Our recent study in [7] indicated the need for a fair pricing mechanism dedicated to PEVs for increasing the utilization of the available wind energy in the absence of economically feasible grid-level energy storage. In this work, we use a data-driven approach to design a fair pricing mechanism for charging PEVs that benefits both the utility and the customers. This approach employs a decomposition methodology to extract the dynamic pattern of the data under consideration.

Dynamic rates have yielded multiple benefits for utilities and consumers such as avoiding expensive resources for utilities and reduced electricity bills for consumers. However, achieving these benefits needs a precise and well-informed rate design. The many advantages of dynamic rates over flat rate tariff include the following: a) avoiding or deferring resources cost, b) reducing wholesale prices of electricity, c) price-fairness to both the consumers and the utility, d) reducing consumer electricity bills, and e) benefiting the environment. There are several types of dynamic pricing methods considering the trade-off between the incentive (i.e., discount from the flat rate tariff) and the risk (i.e., variation in price).

[4] This chapter is a verbatim reproduction of the manuscript under review in a peer reviewed journal at the time of the writing of this dissertation

Some examples include time of use (TOU), real time pricing (RTP), critical peak pricing (CPP), and peak time rebate (PTR) [76]. For a detailed description of these types, refer to [76], [77].

The time-varying pricing design differs based on the objective of the design. However, there are design criteria that we should consider to ensure the effectiveness of the rate design. These considerations include the following: a) short peak period to ease consumer participation, b) strong price difference to allow meaningful consumer savings, c) justified rates for system cost, d) simple design to facilitate the response of consumers, and e) accounting for risk to ensure the profitability of the utility. After the appropriate rate and mechanism are designed, pilot studies are employed to draw statistics and important conclusions [76].

5.1.1 Motivation

There is a projected increase of PEVs sales in the US and it is expected that the annual sales to reach 2.5 millions PEVs by 2020 [50]. The ERCOT system has the highest installed capacity of wind energy resources. Also, the total number of PEVs in ERCOT is expected to reach 835,000 by 2030 [61]. This rapid increase in adoption of PEVs will lead to an increase in the electricity demand that will need management through coordinated charging with the availability of a renewable energy resource (i.e., wind energy). This is expected to be advantageous to the power provider, customers, and the environment. Designing a time-varying price is important to incentivize charging during the times with there is wind energy available (reduce the utility price) and disincentivize the charging during the times when wind energy is not available.

5.1.2 Related Work

Controlling the charging of PEVs has yielded multiple publications considering maximizing the profit of private charging stations and parking decks, [78], [79], shifting the transformer load profile [80], using an automated demand response for a fleet to generate charging schedule [81], and using coordinated distribution power flow [82]. The coordination of PEVs charging with the availability wind energy is presented in [9], [15], [54], [56]. Although some of these references ([9], [15], [54], [56]) consider using already existing dynamic pricing mechanisms (e.g., TOU), their efforts lack in designing a dynamic pricing exclusive to PEVs for utilizing the excess of wind energy.

Some utilities realized the need for a dedicated dynamic pricing for PEVs charging because of the different power requirements, availability times, and consumption duration than other residential appliances. Designing incentivized pricing mechanisms to encourage PEV owners to charge at the best time for both the utility (i.e., off-peak) and the customers (i.e., availability of cheaper price) is important to maximize the profit and achieve customer savings [83]. Dynamic pricing, such as TOU, has the potential to shift the load to off-peak hours. Also, simulation studies such as [78] indicated that responding to TOU rates can significantly improve the profit of charging stations.

Some utilities have implemented pilot studies to investigate the benefits of developing dynamic pricing exclusively for PEVs. Currently, Pacific Gas and Electric (PG&E) offers two TOU-based pricing plans; the first option is a universal TOU for all loads in the residential premises including PEVs and the second option is a dedicated TOU for PEVs through a separate meter for PEVs. Both options use TOU with peak, partial-peak, and off-peak hours [52], [53]. A Dallas-based utility offered a promotion program called "free nights" for charging PEVs at no cost to the owners. This program attempts to utilize the high wind energy production during nighttime in Texas by incentivizing PEV owners. However, free electricity may not be an efficient way from a market efficiency perspective [57].

5.1.3 Contribution

Here, we use a data-driven approach based on data decomposition to design a dynamic pricing mechanism exclusively for PEVs in wind energy-rich grids. The design will not only depend on the load, but also will depend on the excess of wind energy in the area. We use real data to support the design process that will lead to a customer incentive price for PEVs owners (CIP-PEV) and we coendure that this should lead to increase the revenue of the utility.

The rest of the paper is organized as follows. Section 5.2 provides an explanation of the data decomposition method used in this work. Section 5.3 describes the data used in designing the dynamic pricing mechanism and further analyzes the excess of wind energy data to illustrate the seasons and the hours of the day with potential to incentivize/disincentivize the price. Section 5.4 explains the details of our

performed case study and presents the results of the dedicated dynamic pricing for PEVs in Austin, TX. Section 5.5 concludes the paper.

5.2 Dynamic Mode Decomposition

In data-driven applications, data or measurements are the only available input, and the underlying mathematical model for describing the source of the data is unknown. Dynamic mode decomposition (DMD) accomplishes this by selecting only the relevant dynamics from a time sequential data. A time-discrete linear mapping then works as a low-ranked best linear approximation (i.e., minimum least square) [84]. Representing the nonlinear process as linear discrete sampling maps is the basic concept of applying DMD to solve nonlinear complex data-driven engineering computations [84], [85].

5.2.1 The DMD Algorithm

DMD is a data decomposition algorithm to extract the spatio-temporal structure of a dataset with a fixed time step Δt (i.e., one fixed frequency). DMD extracts a structure that reveals the data type and its spatio-temporal dynamics. We assume a time series data vector V_i with N snapshots as in (5.1)

$$V_i^N = \{v_1, v_2, \dots, v_N\}, \tag{5.1}$$

with Δt as the time step between v_i and v_{i+1}. To move from one snapshot to the next, we use the linear approximation mapping matrix, A as in (5.2) and (5.3)

$$\{v_2, v_3, \dots, v_N\} = A\,\{v_1, v_2, \dots, v_{N-1}\} \approx \{v_1, v_2, \dots, v_{N-1}\}\,A_c \tag{5.2}$$

or

$$V_2^N = A\ V_1^{N-1} \approx V_1^{N-1}\,A_c, \tag{5.3}$$

where A_c is the companion matrix that shifts the snapshots 1 through $N-1$. The main aim of using A_c is to represent the most recent observation by the linear approximation of the previous observation. A_c is a lower ranked matrix from A, whose eigenvalues provide the coefficients of the linear approximation. The best approximation is achieved by finding the least square of the difference between the actual observation matrix and the linear approximation as in (5.4)

$$\min\left\|v_N - V_1^{N-1}\, a_c\right\| \tag{5.4}$$

where a_c is the last column of the companion matrix, A_c

$$A_c = \begin{bmatrix} 0 & 0 & \dots & 0 & -a_0 \\ 1 & 0 & 0 & 0 & -a_1 \\ \vdots & \ddots & \ddots & \vdots & \vdots \\ 0 & 0 & 1 & 0 & -a_{N-2} \\ 0 & 0 & 0 & 1 & -a_{N-1} \end{bmatrix} \tag{5.5}$$

The eigenvalues of the companion matrix, A_c, provides the dynamic behavior of the sequential dataset, ΔP in our case. The algorithm of performing the DMD modes is:

1. Compute the singular value decomposition (SVD) of the observation matrix V_1^{N-1} as, $V_1^{N-1} = U\Sigma Q^H$ where $U \in C^{N\times K}$, $\Sigma \in C^{K\times K}$, $Q \in C^{M\times K}$, K is the rank of the reduced matrix by SVD and U, and Q are unitary matrices. Q^H is the Hermitian (i.e., conjugate) transpose.
2. From (5.3), compute the companion matrix A_c, $A_c = Q\,\Sigma^{+}U^H\,V_N$, where Σ^{+} is the pseudo-inverse of Σ.
3. Compute pseudo-invert left sequence of A_c, $\widetilde{A_c} = U^H\,V_N\,Q\,\Sigma^{-1}$
4. Find the eigenvalues and eigenvectors decomposition of $\widetilde{A_c}$ to be $\widetilde{A_c} = W\Omega W^{+}$, where Ω is a diagonal matrix with the eigenvalues of $\widetilde{A_c}$.
5. Compute the dynamic mode matrix, $\Phi = \mathrm{UW} = \mathrm{V_N}\,Q\Sigma^{+}\,W$, where the columns of Φ are the dynamic modes (ϕ_i).

5.2.2 Dynamic Mode Decomposition Applications in Electric Power Engineering

DMD has been applied to data processing applications in multiple fields such as fluid mechanics [84], computations [85] and dynamic adaptive control models [86]. There are very few data-driven studies using DMD in electric power engineering research, especially as applied to dynamic pattern extraction and forecasting. Reference [87] employs DMD to characterize the demand data and forecast for future demand. In [87], the ability of DMD to capture the spatio-temporal dynamics of the data is effective as it compares to other benchmark forecasting methods. Reference [88] used DMD to estimate the amplitude of the frequency components in a power system by employing the stable dynamic modes. DMD showed a comparable performance to other signal processing techniques such as discrete Fourier transform and zero-

crossing. Reference [89] uses DMD to analyze the switching harmonics generated by the inverters of distributed generators. Reference [90] employs DMD to design a measurement-driven interactive tool to identify oscillation frequency and damping ratio of system's dynamic behavior.

5.3 Data and Analysis

In this study, we use datasets to design the dynamic pricing mechanism dedicated to PEVs in a wind energy-rich grid. We employ data from ERCOT and datasets for a chosen Texan city (i.e., Austin). We start by arranging the data to find the change in price based on the excess of wind energy near Austin and expected PEVs profile. Also, we analyze the excess of wind energy data and illustrate it using box plots.

5.3.1 Data Collection and Arrangement

To use the data decomposition approach, we collect and arrange real data for Austin, TX. In the ERCOT system, Austin lies in the south Houston aggregation, which along with the north west aggregation, is considered one of the two wind energy-rich areas [27]. These datasets include the enhanced hourly wind power forecast (WPF) from our previous work in [4]. This data includes wind power forecast for a year (March 2013-March 2014), electric utility prices (flat rates) for a utility company in Austin [59], and the hourly load data from ERCOT for the same year [58]. The steps of arranging the needed data include: i) finding the locations of the closest urban or suburban cities in the two wind energy-rich areas and identify its ZIP code to locate the closest wind farm; ii) finding a city with high adoption rate of PEVs (we chose Austin, TX); iii) finding a substation within the service area from the synthetic grid model in [32], [35], [72]; and iv) finding an example of a utility flat price in Austin as provided in Table 5-1 . Finally, we used two approaches, that lead to similar profiles, to create realistic expected PEVs profiles for level-I and level-II charging using datasets from national household travel survey (NHTS) and the available meters-validated data from the National Renewable Energy Laboratory (NREL) [60], [71] . We generalized these profiles (i.e., kW/PEV) to use them with the number of PEVs in Austin and generate an expected PEVs power profile. Although we have the wind power and load data for the year of (March 2013-March 2014), we used

the number of PEVs in residence of Austin (20,000 as of 2018) because the PEVs adoption rate is rapidly increasing in Austin [7].

Table 5-1 The flat rate used by a utility in Austin, TX from [59]

Max usage (kWh)	**Non-summer price ($/kWh)**	**Summer price ($/kWh)**
500	0.018	0.033
1000	0.056	0.08
1500	0.072	0.091

We start the data preparation by ensembling the aggregated time series of the enhanced WPF of the south Houston aggregation and scale it down to the farm level similar to our previous work [4], [5]. We use the information from [75] to find the largest wind farm and largest substation closest to Austin, TX from the synthetic model from [32], [35] to create the profiles as shown in (5.6) and (5.7) similar to chapter 4 [7].

$$P_{wf}\,(t) = \frac{P_{wfc}}{P_{TWC}}\,P_W\,(t) \tag{5.6}$$

where $P_{wf}\,(t)$ is the time series of the electric power output from the wind farm wf at hour t, P_{wfc} is the installed capacity of the wind farm wf, P_{TWC} is the total installed capacity of wind energy in the system, and $P_W(t)$ is the hourly wind power output from the enhanced forecast, all in MW.

$$P_s\,(t) = \frac{P_s}{P_{SC}}\,P_{SC}(t) \tag{5.7}$$

where $P_s(t)$ is the time series load of the substation s at hour t, P_s is the rated load of the substation s, P_{SC} is the rated load of the south center area, and $P_{SC}\,(t)$ is the hourly load of the south center area obtained from ERCOT all in MW [58]. It is worth mentioning that south center area is one of the eight areas that constitutes the ERCOT system. The load data available in [58] includes the hourly data of the eight areas.

Now, we have the wind power profile, as generated by (5.6), the load profile (excluding PEVs) as generated by (5.7), and the expected power profile available from [60], [71]. Then, we calculate the hourly variable load, $Var_{load}(t)$, and the excess of wind power, $Ex_{wind}(t)$, in the area of study (i.e., Austin, TX), similar to chapter 4, as shown in (5.8) and (5.9) respectively.

$$Var_{load}\,(t) \;=\; L(t) \;-\; L_B \tag{5.8}$$

$$Ex_{wind}\,(t) \;=\; WPF(t) \;-\; Var_{load}(t) \tag{5.9}$$

where $L(t)$ is the total hourly load, L_B is the monthly base load, and $WPF(t)$ is the hourly enhanced wind power forecast for the farm.

Our objective is to modify (increase/decrease) the PEVs profile to match the $Ex_{wind}(t)$. However, this matching process must be limited to the maximum possible PEVs per hour in the area considering the availability of vehicles in residences as extracted from the NHTS data [60]. This means, if the excess of wind energy at hour t is at a certain value, but the availability of PEVs cannot match all of it, we have to match as much as possible of it. The percentage of vehicles available at residential facilities at different times of the day is shown in Fig. 5.1. We denote the expected PEVs power profile as initial quantity (q_0) in MW, and the desired PEVs power profile final quantity (q_1) in MW. Then, we use the numerator of the price elasticity of demand, ε, (5.10), to find the ratio of the hourly change in quantity, ΔQ (5.11). Reference [74] compared around 100 pilot studies of time-varying pricing and concluded that the ratio of peak to off-peak prices should be around 8:1 to achieve a 15% reduction in demand. This implies a price elasticity of demand, ε, of -0.04 [74]. We then calculate the ratio of hourly price change, ΔP as in (5.10).

$$\varepsilon = \Delta Q / \Delta P \tag{5.10}$$

$$\Delta Q = \frac{\Delta q}{q} = \frac{(q_1 - q_0)}{q_0} \tag{5.11}$$

The ratio of hourly price change, ΔP, represents our input to the DMD model to extract the coherent dynamic structure of the change in price based on the availability of excess of wind energy. The DMD model extracts the dynamic features of the change in price and introduces a change in the current flat rates. In this study, we propose different dynamic rates for different charging levels (level-I and level-II) because these levels are expected to reach different maximum monthly usages (in kWh) as shown in Table 2. Based on the range of energy usage in Table 5-2, it is suitable to use the corresponding initial price for level-I as the price for 1000 kWh and level-II for 1500 kWh from Table 5-1.

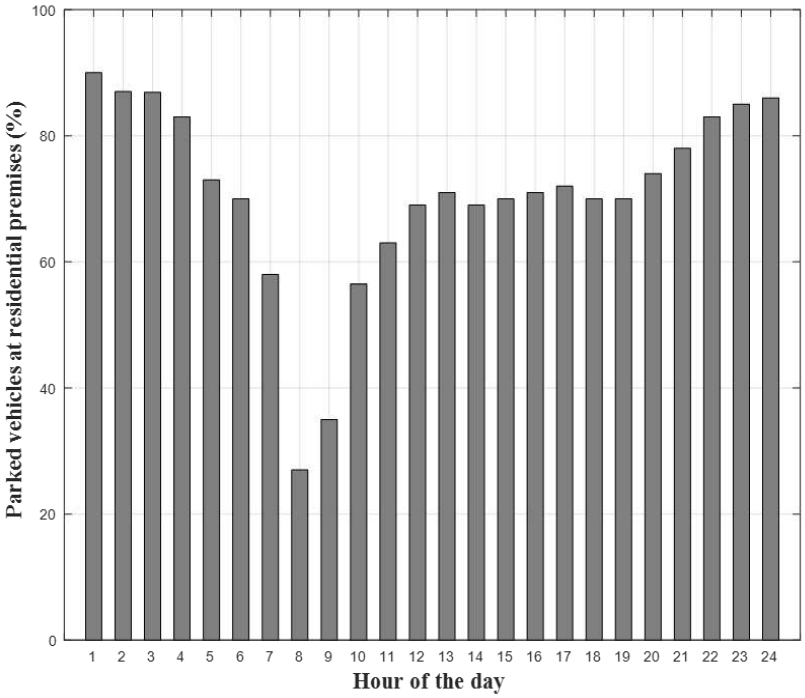

Fig. 5.1 The percentage of the available vehicles in the residential facilities based on the analysis of the NHTS data [31]

Table 5-2 The information of the residential charging levels, their percentage in Austin and usage

Charging level	**Power (kW)**	**Charging duration (hours)**	**Charging points (%)**	**Usage Range (kWh)**
Level-I	1.6–2	8–20	18%	480–1200
Level-II	3.5–6.5	4–8	82%	720–1560

5.3.2 Analysis of the Excess of Wind Energy

In the wind energy-rich area of study (i.e., Austin, TX), we further analyze and illustrate the excess of wind power as calculated in (5.9). Box plots are used to visualize the statistical summary of the excess of wind energy for the area of study. Fig. 5.2 shows the statistical summary of the seasonal excess of wind power for Austin. It shows that summer season has the least excess of wind energy. This is expected as most of Texan cities have summer peaks due to hot and humid weather. We classify the data of each season by the hour to visualize the statistics of excess of wind power in each hour of each season.

Figures 5.3-5.6 show the box plots of the hourly statistics of the excess of wind energy in each season. Although the plots show similar trends in the hour to hour variations, the magnitude of the excess of wind energy significantly differs especially in the summer and the fall months, as shown in Figures 5.4 and 5.5. They show that the excess of wind energy during the afternoon and evening times (12pm-10pm) is very minimal, indicating no potential for wind energy-PEVs charging coordination. On the other hand, in the early morning hours (midnight-8am), there is a potential of charging PEVs as there is an excess of wind energy. As an example, Fig. 5.4 suggests using a summer TOU exclusively for PEVs with a peak period in the afternoon and evening hours.

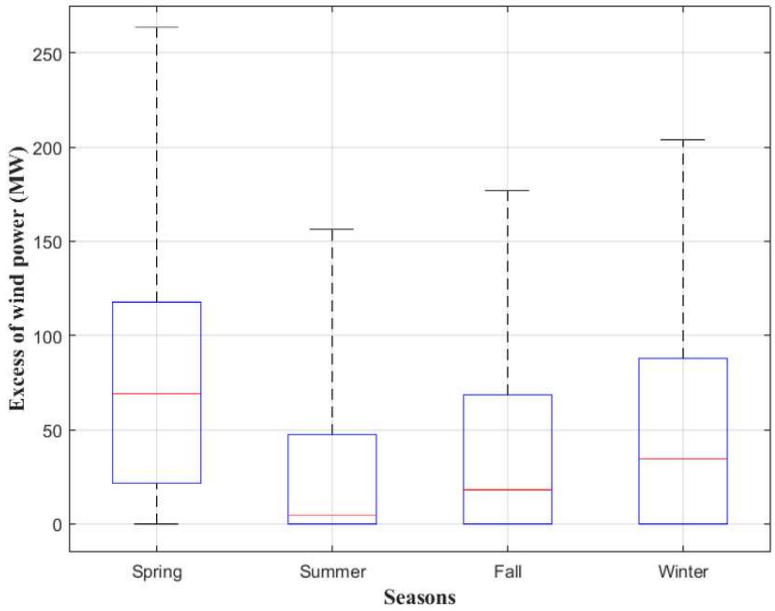

Fig. 5.2 Box plot presents the statistical visualization of the excess of wind power in all seasons in Austin for the year of (March 2013-March 2014)

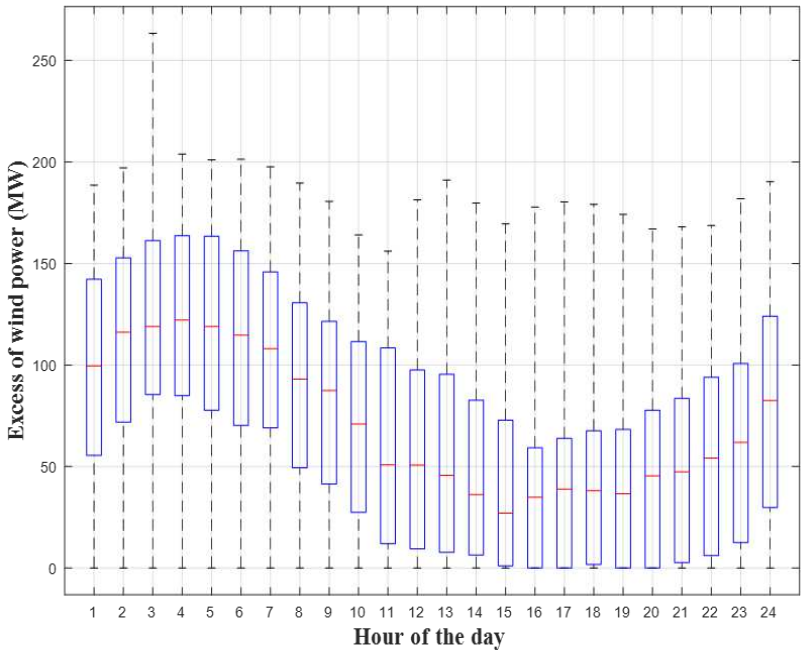

Fig. 5.3 Box plot presents the hourly statistical visualization of the excess of wind power from spring for the year of (March 2013-March 2014)

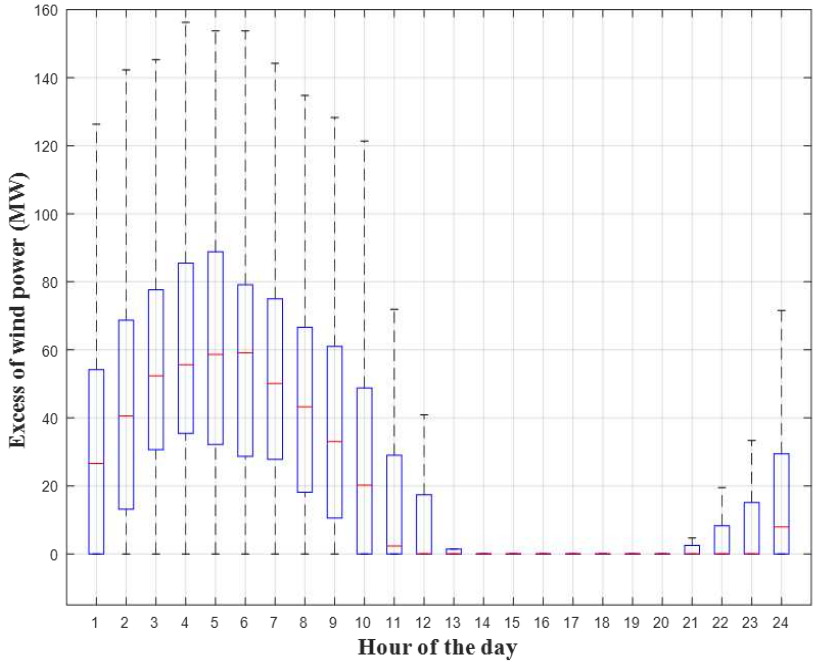

Fig. 5.4 Box plot presents the hourly statistical visualization of the excess of wind power from summer for the year of (March 2013-March 2014)

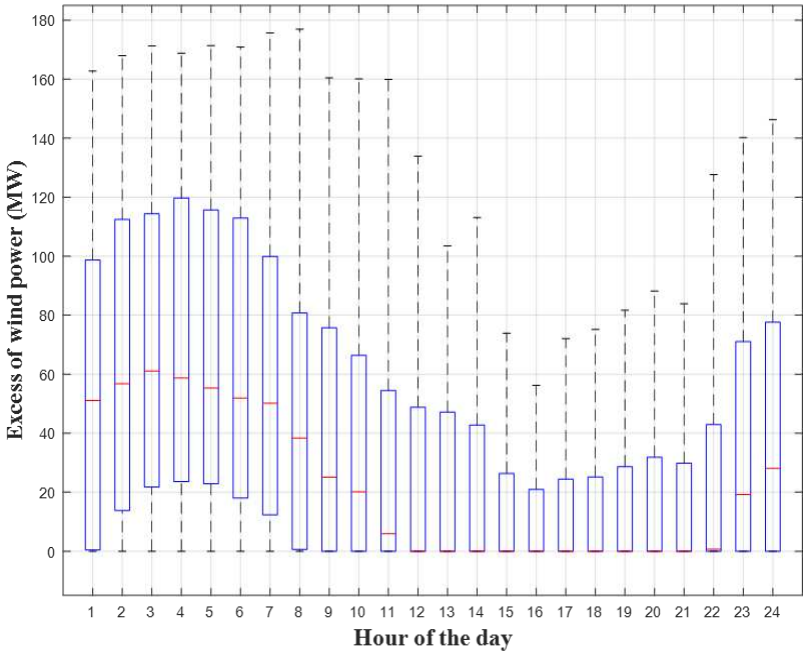

Fig. 5.5 Box plot presents the hourly statistical visualization of the excess of wind power from fall for the year of (March 2013-March 2014)

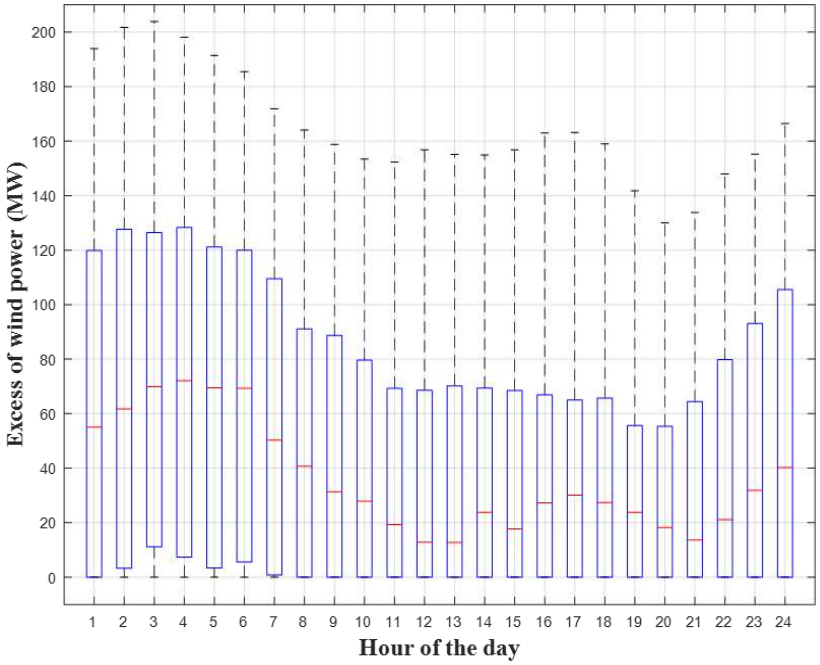

Fig. 5.6 Box plot presents the hourly statistical visualization of the excess of wind power from winter for the year of (March 2013-March 2014)

After we obtained the hourly change in price (ΔP) from (5.6)-(5.11), we classify the data into three groups, namely, monthly, seasonal, and, summer and non-summer. Then, we employ DMD to capture the

trend of change in price to be incorporated with the current flat rate tariff presented in Table 5-1. In the subsequent sections, we describe how we apply DMD for TOU design.

5.4 Case Study and Results

We obtain the ratio of change of price, ΔP, as explained in the section 5.3.1. The annual dataset includes 365 daily snapshots (N), with each snapshot possessing 24 data points of the hourly change in price (ΔP). Then, we divide the dataset into the following groups: months; seasons; and summer and non-summer times of the year. That means, N may take different values based on the division option (e.g., for the monthly division, N = 28, 30, or 31). Although some of the utilities in Texas offer different prices for weekdays and weekends,[59], we found no significant difference to be considered as an option here. That is expected because the excess of wind energy does not depend on the load profile. We use the DMD to determine the modes of price change. That will identify the peak and off-peak periods of the TOU. Then, we determine the average change in price (ΔP) in both periods.

5.4.1 The Process of Implementing the DMD Algorithm

Fig. 5.7 shows the flowchart for the DMD algorithm used here. As a first step, we group data based on the seasons appropriate to Austin, TX as winter (Jan, Feb), spring (Mar-May), summer (Jun–Sep) and fall (Oct–Dec). We arrange the data so that each column of the ΔP matrix represents the change in price values for a day as shown in (5.12),

$$\Delta P = \begin{bmatrix} \Delta p_{11} & \cdots & \Delta p_{1n} \\ \vdots & \ddots & \vdots \\ \Delta p_{m1} & \cdots & \Delta p_{mn} \end{bmatrix}, \tag{5.12}$$

where m is the number of hours in a day ($m = 1,\ldots,24$) and n is the number of the days in the division (e.g., month or season).

These matrices are formed by grouping the appropriate seasonal months. The ΔP matrix values are normalized in the feature range $(-1,1)$ as the data has both positive and negative values representing the increase and decrease in the price, respectively, as shown in (5.13),

$$\Delta p_{ij-Normalized} = 2\left[\frac{\Delta p_{ij} - \Delta P_{min}}{\Delta P_{max} - \Delta P_{min}}\right] - 1, \tag{5.13}$$

where $i = 1 \ldots n$, and $j = 1 \ldots m$.

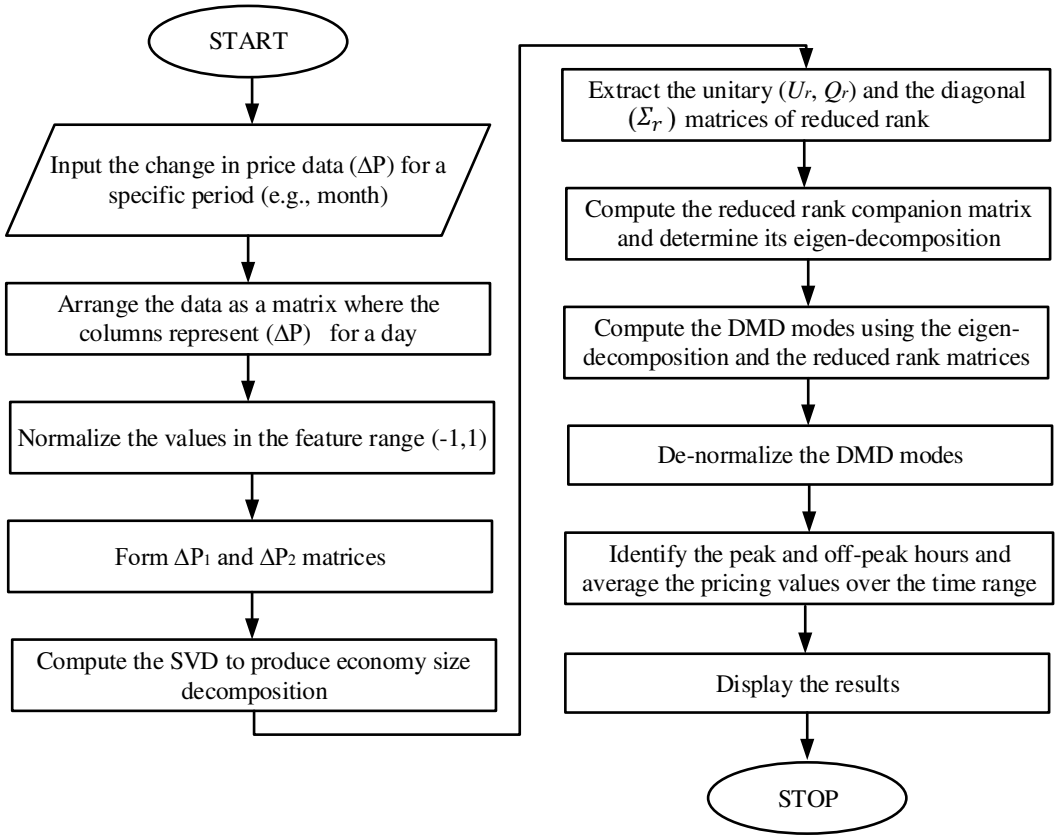

Fig. 5.7 The flowchart of the DMD algorithm implemented in this study

ΔP_1 and ΔP_2 are subsets of ΔP consisting of change in price values $(1 \ldots (n-1))$ days and $(2 \ldots n)$ days respectively.

The SVD version of ΔP is obtained as an economy size decomposition. For instance, economy SVD on ΔP which is of size 24×30, generates U (24×24), Σ (24×30), and $Q^+(30 \times 30)$. The primary objective of this work is to identify the trend in the input dataset (ΔP). Then, we decide the peak and off-

peak hours with the corresponding change in price. This reveals that a single DMD mode will suffice to accomplish the objective.

Hence, the reduced rank matrix, $\tilde{A}_c$, sharing the same non-zero eigenvalues of the time dependent operator matrix *A,* is given by by (5.14),

$$\tilde{A}_c = U_r^T(\Delta P_2)\, Q_r \Sigma_r^{-1}, \tag{5.14}$$

The DMD mode represented as Φ, that reveals the spatial and temporal dynamics in the change in price dataset, is computed by (5.15),

$$\Phi = (\Delta P_2)\, Q_r \Sigma_r^{-1} W, \tag{5.15}$$

where W represents the eigenvector matrix of $\tilde{A}_c$. Then, we de-normalized Φ is given by (5.16),

$$\Phi\hat{} = \left[\left(\frac{\Phi + 1}{2}\right)(\Delta p_{max} - \Delta p_{min})\right] + \Delta p_{min} \tag{5.16}$$

The process of obtaining the de-normalized DMD modes is repeated for the seasonal datasets [87].

5.4.2 Results and Observations

We initially present the colormap of the seasonal data to draw some expectations of the DMD modes (i.e., trends of variations). For the hourly ΔP data for the year of study (March 2013-March 2014), we present the seasonal results. Fig. 5.8 and 5.9 show the colormap of the spring dataset and the DMD modes along with the ΔP change presented as TOU, respectively.

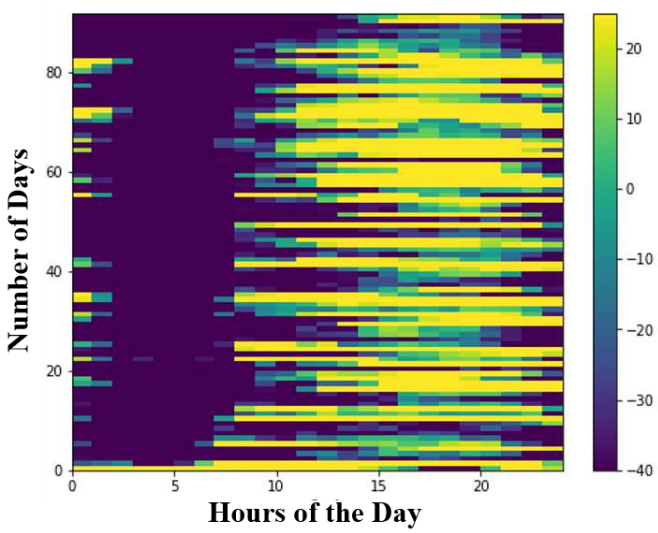

Fig. 5.8 Colormap for the spring dataset

Fig. 5.8 shows the distribution of the spring dataset that includes the change in price data for the months of March – May using a colormap. It is clear that the ΔP values are predominantly lower in the first half of the day and gradually increases on the second half during the spring season. This trend is captured by DMD shown Fig.5.9. Mode represents the SVD mode obtained using the higher dimension linear approximation time dependent operator matrix A as shown in Fig. 5.9 (a). DMD Mode represents the Φ obtained using the reduced rank matrix $\tilde{A}_c$ as shown in Fig 5.9 (b). Once the DMD modes are obtained, we inspect to identify the peak and off-peak hours. The TOU shown in Fig 5.9 (c). Once the peak and off-peak hours are identified, the corresponding values in the Φ matrix are averaged to fix the ΔP values during the intervals resulting in a TOU for the specific dataset. We also can notice the difference between the off-peak to peak ΔP is 9. This is an important parameter in the TOU design.

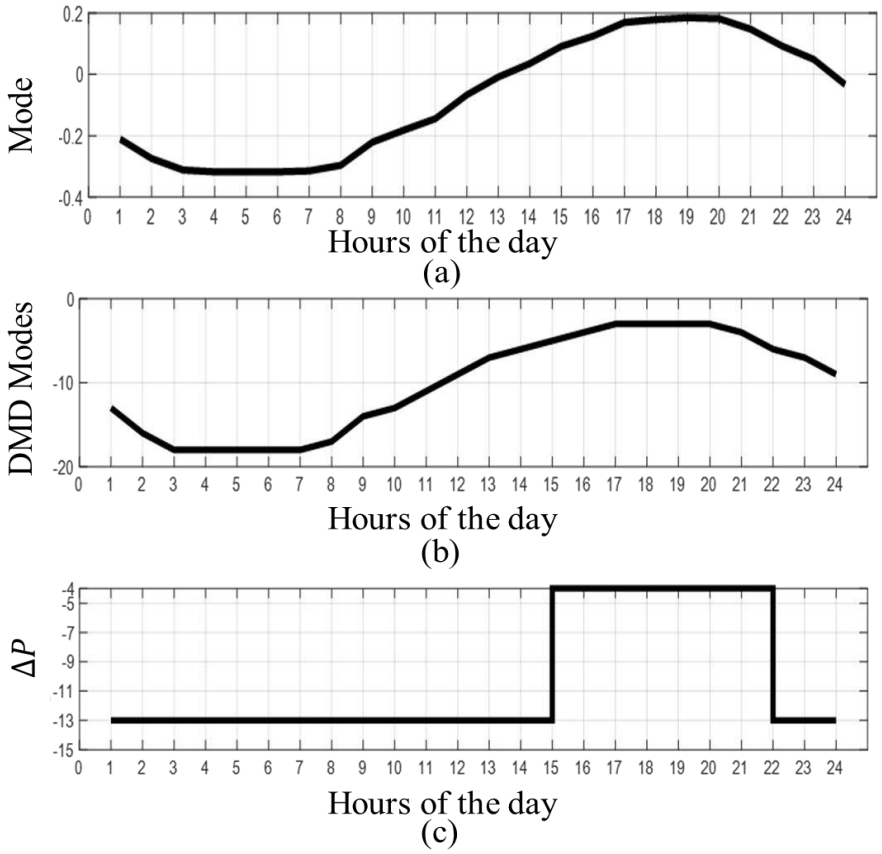

Fig. 5.9 DMD Results for spring dataset. The mode obtained from SVD, (b) the mode obtained from the reduced rank DMD, and (c) the TOU design based on (a) and (b)

Similarly, Fig.5.10 shows the distribution of summer season dataset using a colormap. This reveals the fact that the ΔP values are predominantly higher (higher than the spring data) on the second half of the day and lower on the first half over the summer season because of the high load due to the air conditioning system in the hot humid summer in Texas. This is expected, and it appears in the DMD results as shown in Fig 5.11. We also can notice the difference between the off-peak to peak ΔP is 7. We should also notice that the starting time and the ending time of the peak period of both summer and spring tend to be the same (following the same trend of variation).

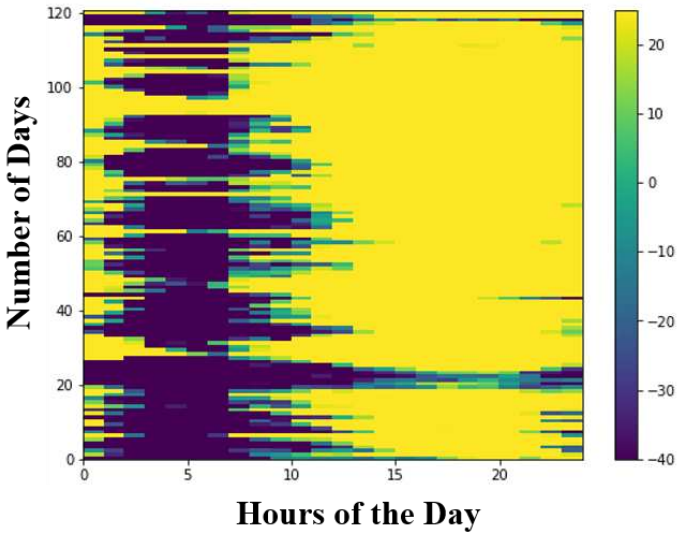

Fig. 5.10 Colormap for the summer dataset

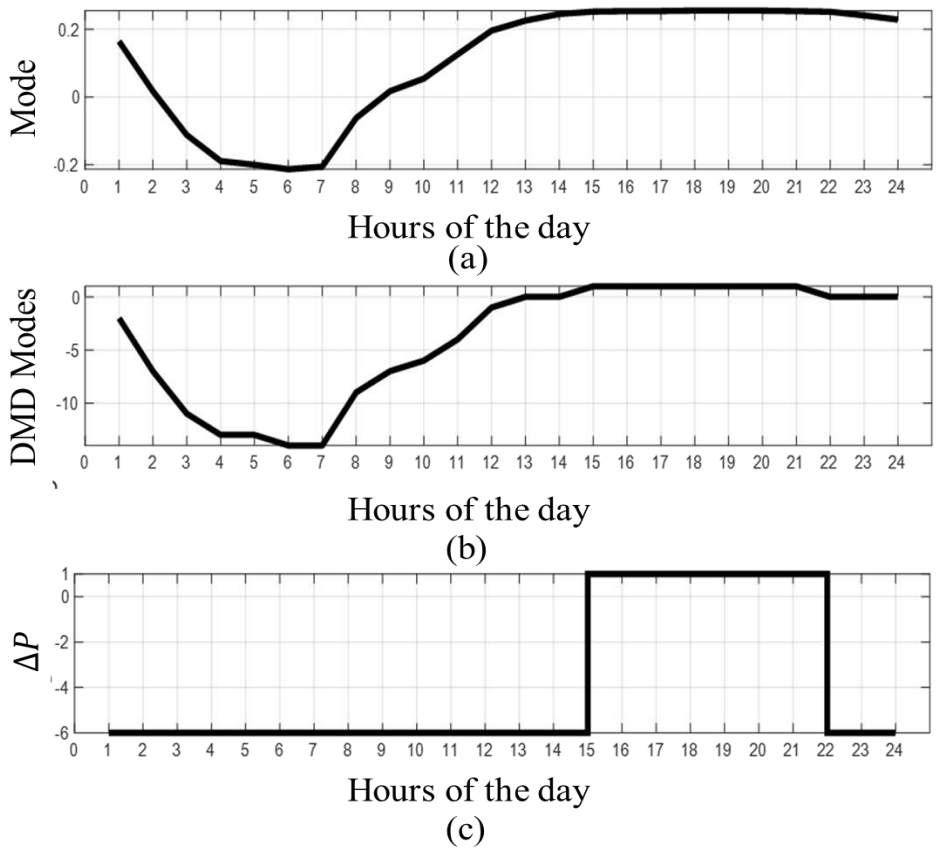

Fig. 5.11 DMD Results for summer dataset. (a) The mode obtained from SVD, (b) The mode obtained from the reduced rank DMD, and (c) The TOU design based on (a) and (b)

The inclination of ΔP for both summer and spring seasons is the same in terms of the time intervals for peaks and off-peaks. This indicates a single TOU for both the summer and spring seasons. Whereas there are significant variations in the ΔP values between the two seasons for both peaks and off-peaks. In order to augment this difference, we apply DMD to the spring and summer datasets together expecting a reasonable ΔP for the peak and off-peak hours. Fig 5.12 shows the results of the DMD for the summer and spring datasets taken together. The DMD modes are not impacted by the drift of ΔP of the actual datasets from Figs 5.8 and 5.10. This leads to the decision of averaging the ΔP values in the peak and off-peak hours of summer and spring datasets obtained individually to design of the TOU for PEVs for March-September, as shown in Fig 5.13.

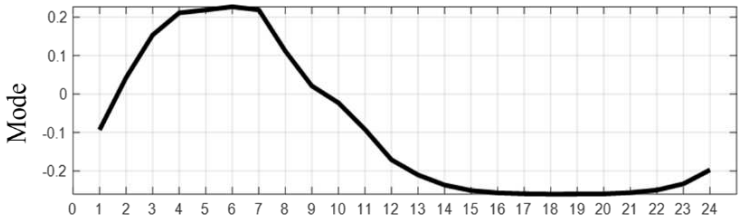

(a)

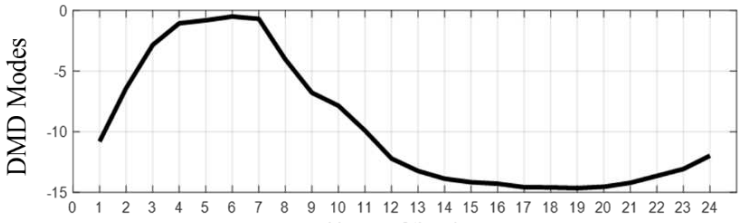

(b)

Fig. 5.12 DMD Results for the combined spring and summer dataset. (a) The mode obtained from SVD and (b) The mode obtained from the reduced rank DMD

For winter and fall seasons, the DMD modes and the colormaps of the data indicate that there are not dominating trends of variation in the price, as shown in Figs 5.14-5.17.

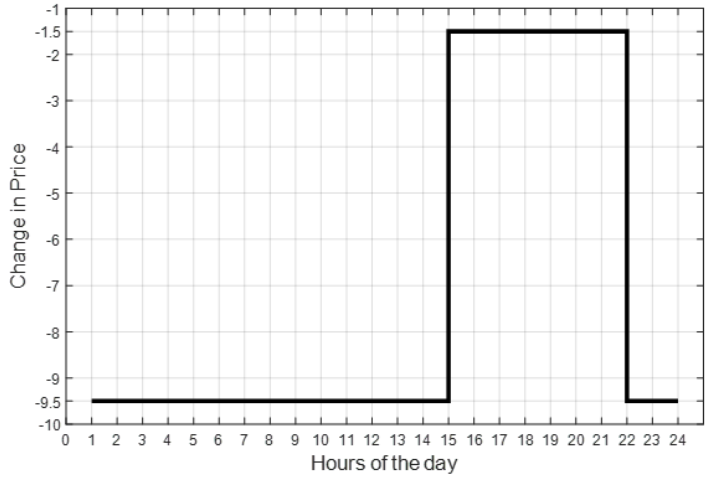

Fig. 5.13 TOU for March-September (spring and summer)

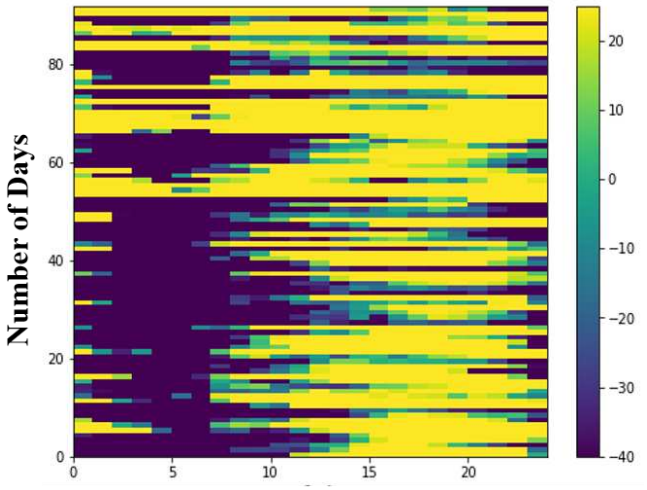

Fig. 5.14 Colormap for the fall dataset

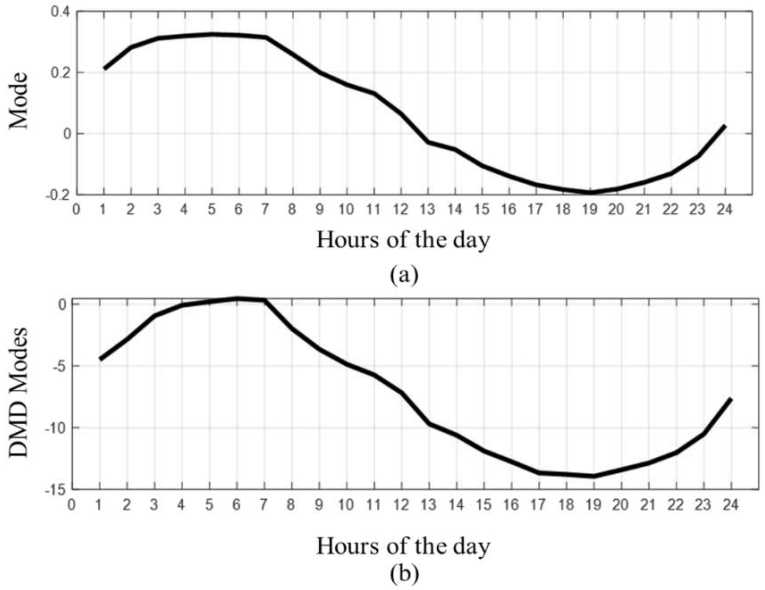

Fig. 5.15 DMD Results for fall dataset. (a) The mode obtained from SVD and (b) The mode obtained from the reduced rank DMD

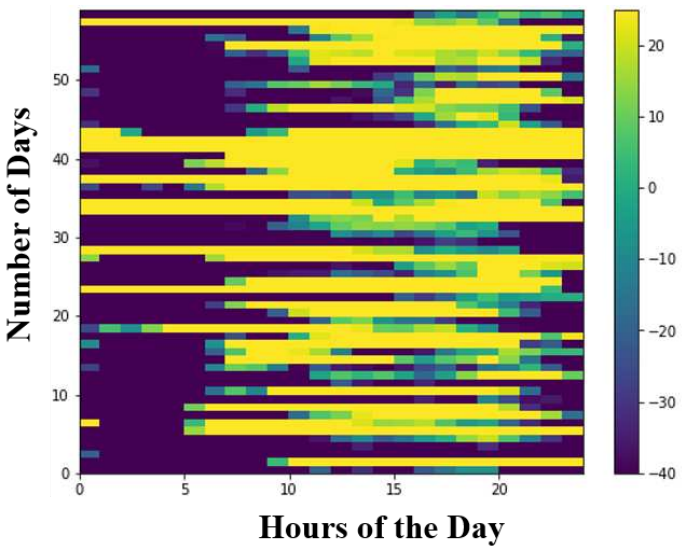

Fig. 5.16 Colormap for the winter dataset

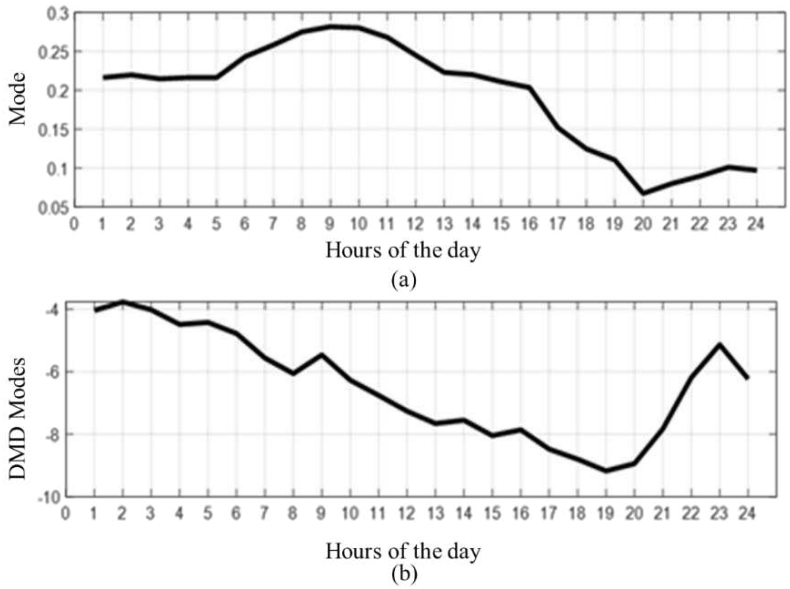

Fig. 5.17 DMD results for winter dataset. (a) The mode obtained from SVD and (b) The mode obtained from the reduced rank DMD

Finally, the DMD model for October through February indicates that some months have certain trends (October, November and February) while the others do not have a trend of variation (December and January). However, the former group does not conform to a common trend. After analyzing the DMD results with the original data spread for both the fall and the winter seasons, as well as the individual months, we conclude that a flat rate TOU be offered for the PEV customers for both fall and winter seasons.

Lastly, we must consider that the reduction in price in either the TOU design or a reduced flat rate tariff to incentivize the PEV owners must have a lower bound. That is because it is neither realistic nor fair for the utility to offer that zero or negative utility price. That will lead to loss and not efficient when it comes to the market prospective. Based on other TOU designs available for that area [59], we propose that the minimum price bound to be the average wholesale market or average locational marginal price (LMP) of that node. Table 3 summarizes the results for all the seasons and Table 4 shows the results for levels-I and II charging for the two time periods of the year (March-September and October-February). It is worth mentioning that we define the difference in price between the off-peak ΔP and peak ΔP as:

$\delta = \Delta P_{peak} - \Delta P_{off-peak}$.

Table 5-3 The summary of results of change in price in the two different times of the year

	March-September	**October-February**
Peak period ΔP (ΔP_{peak})	-1.5	–
Off-peak period ΔP ($\Delta P_{off-peak}$)	-9.5	–
Difference in price between peak and off-peak (δ)	8	–
Average flat rate change in price (ΔP)	–	-8

As the change in price might lead to negative or zero prices, we set our lowest price equal to the average wholesale price of the two periods of consideration and add $\Delta\delta$ to find the peak price. After we obtain the new price for level-I, we use the same ratio of the original pricing of level-II to level-I used in the flat rate from the considered utility [59].

Table 5-4 Final results of the dedicated pricing mechanism for PEVs in Austin

Level of charging	Original flat rate ($/kWh)		Proposed rates ($/kWh)		
	Summer	Non-summer	March-September		October-February
			peak price (3pm-10pm)	Off-peak price (10pm-3pm)	
Level-I	0.08	0.056	0.35	0.04*	0.03*
Level-II	0.091	0.072	0.39	0.045	0.035

* The average locational marginal price (LMP) for the closest node to Austin as obtained from ERCOT

5.5 Conclusion

In wind energy-rich grids, there is a potential for the coordinated charging to manage the excess of wind energy. However, there is a dire need to design a pricing mechanism that will incentivize the PEV owners to charge during times of high-wind energy output. The dynamic price design must be fair for the utility and the consumers to benefit both of them. In this work, we employed a data-decomposition approach to find the trend in the dataset of change in price. The results of our study indicated that it is suitable to use TOU in the spring and summer months (March-September) and a reduced flat rate tariff for the rest of the year (October-February) for the system and data considered (ERCOT, PEV projections and representative utility rates for Austin, TX). Our study also indicated that summer TOU must have a strong price signal (peak/off-peak ratio, 8.66 in our example) to drive the change in charging patterns. We assume that using multi-year data could result to a more precise design. The future step of any dynamic pricing design is to have a pilot study and collect some statistics of the charging profile.

CHAPTER 6

CONCLUSIONS AND FUTURE WORK

6.1 Conclusions

Wind energy is growing globally. In the wind energy-rich grids, there is a dire need to utilize energy generated from wind because of its cost-effectiveness and its environment-friendliness. To better utilize the wind energy generation, this dissertation provided: (i) a model and implementing a time series forecasting method to improve WPF; (ii) a set of realistic metrics through risk-adjusted cost ratios for assessing the improvement to WPF, and (iii) a design of a dynamic pricing mechanism for coordinated charging of PEVs based on the availability of excess of wind power.

First, the WPF method showed an improvement in the WPF initially represented as L_p norm that is explained in chapter 2 [4]. The results of the ARIMA process on the WPF show improvements for all cases presented (L_1, L_2, and L_∞ norms). Second, with the increased attention of improving the forecast of renewable resources, especially wind power, there is a need to use realistic metrics that will quantify the improvements and its impact on grid operations. Using risk-adjusted financial metrics is believed to better represent the improvement of WPF [5]. It is also believed that these metrics can be applied to evaluate other forecasting techniques to choose the option with the lower expected cost per unit of deviation. Third, the results of the case study, presented in chapter 4 [7], show how the profit of the utility from the wind energy-PEV charging coordination will mainly depend on the pricing mechanism used. Finally, this dissertation used data-decomposition technique to design a time-varying pricing mechanism based on the availability of excess of wind power in a wind energy-rich grid.

6.2 Future Work

The future of this research can be carried out to further improve the utilization of wind energy using other methodologies and techniques. This includes combining time series statistical models with other forecasting techniques (e.g., machine learning and neural networks) and examine if that will lead to further

WPF improvement. Also, as a continuation of the dynamic pricing design, conducting simulation and pilot studies to examine the impact of dynamic pricing on shifting the PEVs charging to reduced price "incentivized" times is deemed important. Also, there is a need to further examine the price elasticity of demand in the areas rich of wind energy. The simulation and pilot studies will need real data, PEVs meters, and other costs.

REFERENCES

[1] U. S. DOE Office of Energy Efficiency and Renewable Energy. 20% wind energy by 2030.

[2] T. R. Ayodele, A. Jimoh, J. L. Munda, and A. J. Tehile, "Challenges of grid integration of wind power on power system grid integrity: A Review," International Journal of Renewable Energy Research (IJRER), vol. 2, pp. 618-626, 2012.

[3] Wind Energy and Storage, American Wind Energy Association (AWEA) [Online]. Available: https://goo.gl/YZtvGA (accessed on: 11/25/2017).

[4] F.A. Eldali, T.M. Hansen, S. Suryanarayanan, and E.K.P. Chong, "Employing ARIMA models to improve wind power forecasts: A case study in ERCOT", in Proc. 2016 *North American Power Symposium* (NAPS), Denver, CO, Oct. 2016, pp. 1-6.

[5] F. Eldali, M. Samper, and S. Suryanarayanan, "Risk-adjusted cost ratios for quantifying improvements in wind power forecasting," *accepted to appear in 2019 IEEE PES PowerTech*.

[6] M. Samper, F. Eldali, and S. Suryanarayanan, "Risk assessment in planning high penetrations of solar photovoltaic installations in distribution systems," *Electrical Power and Energy Systems*, vol. 104, pp. 724-733, Jan 2019.

[7] F. Eldali, and S. Suryanarayanan, "A data-driven justification for dedicated dynamic pricing for residences based plug-in electric vehicles in wind energy-rich electricity grids," *submitted* to *IEEE Power and Energy Technology Systems*, 2019.

[8] M.-S. Lu, C.-L. Chang, W.-J. Lee, and L. Wang, "Combining the wind power generation system with energy storage equipments," *in Industry Applications Society Annual Meeting*, 2008. IAS'08. IEEE, 2008, pp. 1-6.

[9] C. X. Wu, C. Y. Chung, F. S. Wen and D. Y. Du, "Reliability/cost evaluation with PEV and wind generation system," in *IEEE Transactions on Sustainable Energy*, vol. 5, no. 1, pp. 273-281, Jan. 2014.

[10] M. E. Khodayar, L. Wu, and M. Shahidehpour, "Hourly coordination of electric vehicle operation and volatile wind power generation in SCUC," *Smart Grid, IEEE Transactions on*, vol. 3, pp. 1271-1279, 2012.

[11] J. G. Vlachogiannis, "Probabilistic constrained load flow considering integration of wind power generation and electric vehicles," *Power Systems, IEEE Transactions on*, vol. 24, pp. 1808-1817, 2009.

[12] A. Y. Saber and G. K. Venayagamoorthy, "Plug-in vehicles and renewable energy sources for cost and emission reductions," *Industrial Electronics, IEEE Transactions on*, vol. 58, pp. 1229-1238, 2011

[13] Z. Li, H. Sun, Q. Guo, Y. Wang, and B. Zhang, "Study on wind-EV complementation in transmission grid side," *in Power and Energy Society General Meeting*, 2011 IEEE, 2011, pp. 1-12.

[14] C. Shao, X. Wang, C. Du, C. Dang, and S. Liu, "Cooperative dispatch of wind generation and electric vehicles with battery storage capacity constraints in SCUC," 2014.

[15] M. G. Vayá and G. Andersson, "Integrating renewable energy forecast uncertainty in smart-charging approaches for plug-in electric vehicles," in PowerTech (POWERTECH), *2013 IEEE Grenoble*, 2013, pp. 1-6.

[16] M. E. Khodayar, L. Wu, and Z. Li, "Electric vehicle mobility in transmission-constrained hourly power generation scheduling," *Smart Grid, IEEE Transactions* on, vol. 4, pp. 779-788, 2013.

[17] T.N. Rollinger and S.T. Hoffman, “Sortino: A ‘Sharper’ ratio”, Red Rock Capital, Newport Beach, CA, USA, Feb. 2014.

[18] K. Orwig, et al., “Economic evaluation of short-term wind power forecasts in ERCOT: Preliminary results,” *in Proc: 11th Intl Workshop Large-Scale Integration Wind Power into Power Systems*, 5 pp., Nov. 2012.

[19] D. Ruppert, Statistics and Data Analysis for Financial Engineering. New York: Springer, 2011.

[20] R. C. Garcia, J. Contreras, M. van Akkeren, and J. B. C. Garcia, “A GARCH forecasting model to predict day-ahead electricity prices,” *IEEE Trans. Power Syst*., vol. 20, no. 2, pp. 867–874, May 2005.

[21] Y. Zhang, M. Beaudin, H. Zareipour, and D. Wood, “Forecasting solar photovoltaic power production at the aggregated system level,” *North American Power Symposium (NAPS), 2014*, Pullman, WA, 6 pp., 2014.

[22] X. Jin, Y. Dong, J. Wu, and J. Wang, “An improved combined forecasting method for electric power load based on autoregressive integrated moving average model,” *International Conf. Information Science and Management Engineering*, vol. 2, pp. 476-480, 2010.

[23] Z. Guo, Y. Dong, J. Wang, and H. Lu, “The forecasting procedure for long-term wind speed in the Zhangye Area,” *Mathematical Problems in Engineering*, vol. 2010, 17 pp., 2010.

[24] R. G. Kavasseri and K. Seetharaman, “Day-ahead wind speed forecasting using f-ARIMA models,” *Renew. Energy*, vol. 34, no. 5, pp. 1388–1393, May 2009.

[25] S. Murugesan, J. Zhang, and V. Vittal, “Finite state Markov chain model for wind generation forecast: a data-driven spatio-temporal approach”, *IEEE PES Innovative Smart Grid Technol*., 8 pp., 2012.

[26] A. Botterud, J. Wang, V. Miranda and R. J. Bessa, “Wind power forecasting in U.S. electricity markets,” Electr. J., vol. 23, pp. 71-82, 2010.

[27] (2015, July). Potomac Economics, LTD. 2014 State of the market report for the ERCOT wholesale electricity markets [Online]. Available: https://goo.gl/gwgWZJ (accessed on: 5/30/2016).

[28] S. S. Soman, H. Zareipour, O. Malik and P. Mandal, "A review of wind power and wind speed forecasting methods with different time horizons," *North American Power Symposium 2010, Arlington*, TX, 2010, pp. 1-8.

[29] J. Zhang, A. Florita, B.-M. Hodge, S. Lu, H. Hamann, V. Banunarayanan, A. M. Brockway, “A suite of metrics for assessing the performance of solar power forecasting”, *Solar Energy* vol. 111, pp. 157-175, Jan. 2015.

[30] M. A. Ortega-Vazquez and D. S. Kirschen, "Estimating the spinning reserve requirements in systems with significant wind power generation penetration," *in IEEE Transactions on Power Systems*, vol. 24, no. 1, pp. 114-124, Feb. 2009.

[31] N. Rajbhandari, Weifeng Li, Pengwei Du, S. Sharma and B. Blevins, "Analysis of net-load forecast error and new methodology to determine Non-Spin Reserve Service requirement," *2016 IEEE Power and Energy Society General Meeting (PESGM),* Boston, MA, 2016, pp. 1-5.

[32] A.B. Birchfield, K.M. Gegner, T. Xu, K.S. Shetye, and T.J. Overbye, "Statistical considerations in the creation of realistic synthetic power grids for geomagnetic disturbance studies", *IEEE Trans. Power Syst.*, in press.

[33] 2016 Long-term System Assessments [Online]. Available: http://www.ercot.com/content/wcm/lists/89476/2016_Long_Term_System_Assessment_for_the_ERCOT_Region.pdf (accessed on: 5/12/2017).

[34] T. Xu, A.B. Birchfield, K.M. Gegner, K.S. Shetye, and T.J. Overbye, "Application of large-scale synthetic power system models for energy economic studies", in Proc. *50th Hawaii International Conference on System Sciences (HICSS-50)*, Waikoloa, Hawaii, Jan. 2017.

[35] Illinois Center for a Smarter Electric Grid (ICSEG) [Online]. Available: http://icseg.iti.illinois.edu/synthetic-power-cases/texas2000-june2016/ (accessed on: 5/12/2017).

[36] W.E. Sharpe, "Mutual fund performance", Journal of Business, vol. 39, no. 1, pp. 119-138, Jan 1966.

[37] F. Sortino, L. Price, "Performance measurement in a downside risk framework," *J. Invest*., vol. 3, no. 3, pp. 59–64, 1994.

[38] T. Rollinger, S. Hoffman, "Sortino ratio: a better measure of risk", Risk Management - FUTURES, Feb 2013.

[39] R. Brealey, S. Myers, F. Allen, "Principles of corporate finance", 8th ed., New York: McGraw-Hill, 2006.

[40] J. Moody, L. Wu, "Optimization of trading systems and portfolios", *In Proceedings of the IEEE IAFE Computational Intelligence for Financial Engineering (CIFEr)*, 1997.

[41] F. Gökgöz, M.E. Atmaca, "Financial portfolio optimization in electricity markets: evaluation via Sharpe ratio", World Academy of Science, Engineering and Technology, vol. 10, no. 11, 2016.

[42] F. Cucchiella, I. D'Adamo, M. Gastaldi, "Optimizing plant size in the planning of renewable energy portfolios", Springer, Letters in Spatial and Resource Sciences, vol. 9, no. 2, pp 169-187, Jul 2016.

[43] J.N. Rauch, "Price and risk reduction opportunities in the new England electricity generation portfolio", ELSEVIER , *The Electricity Journal*, vol. 27, no. 8, pp. 27-36, Oct 2014.

[44] V. Mohan, J.G. Singh, and W. Ongsakul, "Sortino ratio based portfolio optimization considering EVs and renewable energy in microgrid power market", *IEEE Trans. Sustain. Energy*, v. 8, no. 1, pp. 219-229, Jan. 2017.

[45] M. Samper, A. Vargas, "Investment decisions in distribution networks under uncertainty with distributed generation - Part I: model formulation", IEEE Transactions on Power Systems, vol. 28, no. 3, pp. 2331-2340, Aug 2013.

[46] V.N. Coelho, et al., "Multi-objective energy storage power dispatching using plug-in vehicles in a smart-microgrid", ELSEVIER, *Renewable Energy*, vol. 89, pp. 730-742, Apr 2016.

[47] G.A. Blanco, et al., "Transmission expansion planning under uncertainty - The role of FACTS in providing strategic flexibility", *2009 IEEE Bucharest Power Tech Conference*, Romania.

[48] J.I. Muñoz, et al., "Optimal investment portfolio in renewable energy: The Spanish case", ELSEVIER *Energy Policy*, vol. 37, no. 12, pp. 5273-5284, Dec 2009.

[49] K. Fell, K. Huber, B. Zink, R. Kalisch, D. Forfia, D. Hazelwood, N. Dang, D. Gionet, M. Musto, and Johnson, "Assessment of plug-in electric vehicle integration with ISO/RTO systems," Tech. Rep., 2010, (Date last accessed on Mar. 19, 2019). [Online]. Available: https://bit.ly/2SQzskg

[50] "Electric vehicle charging long range plan for the greater Houston area," (Date last accessed on Mar. 10, 2019). [Online]. Available: https://bit.ly/2SQAGfm

[51] "Texas river cities plug-in electric vehicle initiative: Regional plan and final report," (Date last accessed on Mar. 10, 2019). [Online]. Available: https://bit.ly/2H9hSqm

[52] "PG&E launches new program to accelerate electric vehicle adoption in northern and central California," Pacific Gas and Electric Company (PG&E), Jan 2018, (Date last accessed on Mar. 10, 2019). [Online]. Available: https://bit.ly/2ONoISb

[53] "Electric vehicle (EV) rate plans: Making sense of the rates," Pacific Gas and Electric Company (PG&E), Dec 2018, (Date last accessed on Mar. 10, 2019). [Online]. Available: https://bit.ly/2inPcga

[54] Z. Li, Q. Guo, H. Sun, Y. Wang, and S. Xin, "Emission-concerned wind- EV coordination on the transmission grid side with network constraints: Concept and case study," *IEEE Transactions on Smart Grid*, vol. 4, no. 3, pp. 1692–1704, 2013.

[55] M. G. Vaya´ and G. Andersson, "Integrating renewable energy forecast uncertainty in smart-charging approaches for plug-in electric vehicles," *in 2013 IEEE Grenoble Conference*. IEEE, 2013, pp. 1–6.

[56] M. G. Vaya´, G. Andersson, "Self-scheduling of plug-in electric vehicle aggregator to provide balancing services for wind power," *IEEE Transactions on Sustainable Energy*, vol. 7, no. 2, pp. 886–899, 2016.

[57] Z. McDonald, "Texas energy provider gives free power at night to electric car owners," Plugin Cars, July 2013, (Date last accessed on Mar. 10, 2019). [Online]. Available: https://bit.ly/2UsRQkH

[58] "Hourly load data archives," (Date last accessed on Mar. 10, 2019). [Online]. Available: http://www.ercot.com/gridinfo/load/load hist/

[59] "Openei: U.S. utility rate database," (Date last accessed on Mar. 10, 2019). [Online]. Available: https://openei.org/apps/USURDB/

[60] "U.S. department of transportation, federal highway administration, 2017 National Household Travel Survey," 2017. [Online]. Available: https://nhts.ornl.gov/

[61] E. W. Wood, C. L. Rames, M. Muratori,S. Srinivasa Raghavan, and M. W. Melaina, "National plug-in electric vehicle infrastructure analysis," National Renewable Energy Laboratory (NREL), Golden, CO (United States), Tech. Rep., 2017, (Date last accessed on Mar. 16, 2019). [Online]. Available: https://bit.ly/2F6jfTc

[62] "(2017) U.S. energy information administration (EIA)," 2017, (Date last accessed on Mar. 10, 2019). [Online]. Available: https://bit.ly/2A0sD7W

[63] "(2017, January) fleetcarma. Electric vehicle sales in the United States: 2016 final update," 2017, (Date last accessed on Mar. 10, 2019). [Online]. Available: https://bit.ly/2XNbxG8

[64] “Texas emissions reduction plan (TERP),” Texas commission on environmental quality, Tech. Rep., 2019. [Online]. Available: https://www.tceq.texas.gov

[65] “2016 Texas registered vehicle report by fuel type,” Texas department of motor vehicles, Tech. Rep., 2016, (Date last accessed on Mar. 10, 2019). [Online]. Available: https://bit.ly/2TueEnE

[66] “Auto alliance with data provided by Hedges & Co,” auto alliance driving innovation, Tech. Rep., 2017, (Date last accessed on Mar. 10, 2019). [Online]. Available: https://bit.ly/2u7G2cl

[67] “Electricity data browser: wind, all sectors 2018,” U.S. Energy Information Administration (EIA), Tech. Rep., 2018, (Date last accessed on Mar. 6, 2019). [Online]. Available: https://bit.ly/2NLbAO0

[68] “Dallas-Fort Worth clean cities.” [Online]. Available: https://www.dfwcleancities.org/evnt

[69] “Wholesale electricity and natural gas market data,” 2019, (Date last accessed on Mar. 10, 2019). [Online]. Available: https://bit.ly/2XP4f4t

[70] “LMP contour map: Day-ahead market - settlement point pricing and real-time market - locational marginal pricing.” [Online]. Available: http://www.ercot.com/content/cdr/contours/rtmLmp.html

[71] M. Muratori, “Impact of uncoordinated plug-in electric vehicle charging on residential power demand-supplementary data,” National Renewable Energy Laboratory-Data (NREL-DATA), Golden, CO (USA), Tech. Rep., 2017. [Online]. Available: https://data.nrel.gov/submissions/69

[72] “Electric grid test case repository,” (Date last accessed on Mar. 13, 2019). [Online]. Available: https://is.gd/UHi2gq

[73] “Texas plugs in Houston and San Antonio residents expectations of and purchase intentions for plug-in electric vehicles,” Electric Power Research Institute (EPRI), Tech. Rep., Sep 2012.

[74] A. Faruqui, R. M. Hledik, A. Levy, and A. L. Madian, “Will smart prices induce smart charging of electric vehicles?” Available at SSRN 1915658, 2011.

[75] “Wind projects map: installed wind projects,” WTWH Media, LLC, Tech. Rep., 2019, (Date last accessed on Mar. 10, 2019). [Online]. Available: https://bit.ly/2SUGKDt

[76] A. Faruqui, R. Hledik, J. Palmer, “Time-varying and dynamic rate design”, *The Brattle Group and RAP Global Power Best Practice Series*. RAP 2012

[77] T. M. Hansen, R. Roche, S. Suryanarayanan, A. A. Maciejewski, H. J. Siegel, and E. K. Chong, "Customer modeling and pricing-mechanisms for demand response in smart electric distribution grids," *Cyber-Physical-Social Systems and Constructs in Electric Power Engineering*, vol. 2, p. 135, 2016.

[78] Z. Xu, Z. Hu, Y. Song, Z. Luo, K. Zhan, and J. Wu, "Coordinated charging strategy for pevs charging stations," in *2012 IEEE Power and Energy Society General Meeting*. IEEE, 2012, pp. 1–8.

[79] Y. Guo, X. Liu, Y. Yan, N. Zhang, and W. Su, "Economic analysis of plug-in electric vehicle parking deck with dynamic pricing," in *2014 IEEE PES General Meeting— Conference & Exposition*. IEEE, 2014, pp. 1–5.

[80] B. Geng, J. K. Mills, and D. Sun, "Two-stage charging strategy for plug-in electric vehicles at the residential transformer level," *IEEE Transactions on Smart Grid*, vol. 4, no. 3, pp. 1442–1452, 2013.

[81] N. Taheri, R. Entriken, and Y. Ye, "A dynamic algorithm for facilitated charging of plug-in electric vehicles," *IEEE Transactions on Smart Grid*, vol. 4, no. 4, pp. 1772–1779, 2013.

[82] I. Sharma, C. Canizares, and K. Bhattacharya, "Smart charging of PEVs penetrating into residential distribution systems," *IEEE Transactions on Smart Grid*, vol. 5, no. 3, pp. 1196–1209, 2014.

[83] T. M. Hansen, R. Roche, S. Suryanarayanan, A. A. Maciejewski, and H. J. Siegel, "Heuristic optimization for an aggregator-based resource allocation in the smart grid," *IEEE Transactions on Smart Grid*, vol. 6, no. 4, pp. 1785–1794, 2015.

[84] P. J. Schmid, "Application of the dynamic mode decomposition to experimental data," *Experiments in fluids*, vol. 50, no. 4, pp. 1123–1130, 2011.

[85] M. Jovanovic, P. Schmid, and J. Nichols, "Low-rank and sparse dynamic mode decomposition," *Center for Turbulence Research Annual Research Briefs*, vol. 2012, pp. 139–152, 2012.

[86] J. L. Proctor, S. L. Brunton, and J. N. Kutz, "Dynamic mode de- composition with control," *SIAM Journal on Applied Dynamical Systems*, vol. 15, no. 1, pp. 142–161, 2016.

[87] N. Mohan, K. Soman, and S. S. Kumar, "A data-driven strategy for short-term electric load forecasting using dynamic mode decomposition model," *Applied energy*, vol. 232, pp. 229–244, 2018.

[88] N. Mohan, K. P. Soman, and K. S. Sachin, "A data-driven approach for estimating power system frequency and amplitude using dynamic mode decomposition," in *2018 International Conference and Utility Exhibition on Green Energy for Sustainable Development (ICUE)*, Oct 2018, pp. 1–9.

[89] A. Saldañ a, E. Barocio, A. Messina, J. Ramos, R. J. Segundo, and G. Tinajero, "Monitoring harmonic distortion in microgrids using dynamic mode decomposition," in *2017 IEEE Power & Energy Society General Meeting*. IEEE, 2017, pp. 1–5.

[90] S. Mohapatra and T. J. Overbye, "An interactive tool for measurement-driven modal analysis of large-scale power sys- tems," in *2015 IEEE Power and Energy Conference at Illinois (PECI)*, Feb 2015, pp. 1–8.

[91] J. Eyer and G. Corey, "Energy storage for the electricity grid: Benefits and market potential assessment guide," Sandia National Laboratory, SAND2010-0815, 2010.

[92] M. Molina, "Emerging advanced energy storage systems: Dynamic modeling, control and simulation," Nova Science Publishers Inc., New York, USA, 1st Ed., 2013.

[93] P. Lyons, N. Wade, T. Jiang, et al., "Design and analysis of electrical energy storage demonstration projects on UK distribution networks," ELSEVIER, *Applied Energy*, vol. 137, no. 1, pp. 677-691, Jan 2015.

[94] M. Kraning, Y. Wang, E. Akuiyibo, and S. Boyd, "Operation and configuration of a storage portfolio via convex optimization," *in Proc. of the IFAC World Congress*, pp. 487-492, 2010.

[95] J. Mitra, "Reliability-based sizing of backup storage," *IEEE Trans. Power Syst*., vol. 25, no. 2, pp. 1198-1199, Jun 2010.

[96] M. Nick, R. Cherkaoui, and M. Paolone, "Optimal allocation of dispersed energy storage systems in active distribution networks for energy balance and grid support," *IEEE Trans. Power Syst*., vol. 29, no. 5, pp. 2300-2310, Feb 2014.

[97] A. F. Crossland, D. Jones, and N. S. Wade, "Planning the location and rating of distributed energy storage in LV networks using a genetic algorithm with simulated annealing," *Int. J. Elect. Power Energy Syst*., vol. 59, pp. 103–110, Jul. 2014.

[98] O. Ekren, B. Y. Ekren and B. Ozerdem, “Break-even analysis and size optimization of a PV/wind hybrid energy conversion system with battery storage - A case study,” ELSEVIER, *Applied Energy*, vol. 86, no. 7-8, pp. 1043-1054, Aug. 2009.

[99] S. X. Chen, H. B. Gooi and M. Q. Wang, “Sizing of energy storage for microgrids,” *IEEE Trans. Smart Grid,* vol. 3, no. 1, pp. 0142-0151, Mar. 2012.

[100] J. Tant, F. Geth, D. Six, P. Tant and J. Driesen, “Multiobjective battery storage to improve PV integration in residential distribution grids,” *IEEE Trans. Sustain. Energy*, vol. 4, no. 1, pp. 182-191, Jan. 2013.

[101] G. Carpinelli, G. Celli, S. Mocci, F. Mottola, F. Pilo and D. Proto, “Optimal integration of distributed energy storage devices in smart grids,” *IEEE Trans. Smart Grid*, vol. 4, no. 2, pp. 985-995, Jun. 2013.

[102] E. Reihani, S. Sepasi, L. R. Roose, M. Matsuura, "Energy management at the distribution grid using a battery energy storage system (BESS)", *Int. J. Elect. Power Energy Syst.*, vol. 77, pp. 337-344, May 2016.M.

[103] M. Farrokhifar, "Optimal operation of energy storage devices with RESs to improve efficiency of distribution grids; technical and economical assessment", *Int. J. Electr. Power Energy Syst*., vol. 74, pp. 153-161, Jan. 2016.

[104] R.-C. Leou, "An economic analysis model for the energy storage system applied to a distribution substation", *Int. J. Elect. Power Energy Syst*., vol. 34, no. 1, pp. 132-137, Jan. 2012.

[105] M. Samper, A. Vargas, F. Eldali, and S. Suryanarayanan, “Assessments of battery storage options for distribution expansion planning using an OpenDSS®-based framework,” in Proc. 2017 *IEEE PES PowerTech Conf.,* Manchester, UK, Jun. 2017, 6 pp.

[106] V. Miranda, H. Keko, and A. Jaramillo, “EPSO: evolutionary particle swarms,” Eds. Springer, *Advances in Evolutionary Computing for System Design*, vol. 66, pp. 139-167, 2007.

[107] R. Dugan, J. Taylor, and D. Montenegro, “Energy storage modeling for distribution planning,” *IEEE Trans. Industry Appl*., vol. 53, no. 2, pp. 954-962, Mar.-Apr. 2017.

[108] R. Dugan, "Reference guide: The open distribution system simulator (OpenDSS®)," Electric Power Research Institute, Inc. (EPRI), Mar. 2016.

[109] R. Weron, "Modeling and forecasting electricity loads and prices, A statistical approach," John Wiley & Sons Ltd., England, 2006.

[110] "Planificacion quinquenal de crecimiento del sistema electrico provincial 2016-2020," (technical report in Spanish) Energia San Juan, Argentina, Nov. 2014.

[111] "Mapa eolico y solar de la provincia de San Juan," (technical report in Spanish) EPSE (Ente Provincial Sociedad del Estado), Argentina, 2015.

[112] F. Morán, M. Facchini, D. Pontoriero, V. Doña, and A. Galvan, "Balance energetico del comportamiento de un sistema fotovoltaico instalado en una vivienda residencial conectado a la red electrica de distribucion," (*periodical paper in Spanish*) Energias Renovables y Medio Ambiente – ERMA, Asociación Argentina de Energia Solar (ASADES), vol. 32, pp. 37-44, 2013.

[113] "DOE/EPRI Electricity Storage Handbook," SANDIA REPORT, 2015.

[114] "Battery storage for renewables: market status and technology outlook," *IRENA (International Renewable Energy Agency)*, Jan 2015.

[115] N. Li, and K. Hedman, "Economic assessment of energy storage in systems with high levels of renewable resources," *IEEE Trans. Sustain. Energy*, vol. 6, no. 3, pp. 1103-1111, Aug. 2014.

[116] A. Subburaj, B. Pushpakaran, and S. Bayne, "Overview of grid connected renewable energy based battery projects in USA," ELSEVIER, *Renewable and Sustainable Energy Reviews*, vol. 45, pp. 219–234, May. 2015.

[117] B. Zakeri, and S. Syri, "Electrical energy storage systems: A comparative life cycle cost analysis," ELSEVIER, *Renewable and Sustainable Energy Reviews*, vol. 42, pp. 569–596, Feb 2015

APPENDIX A

RISK ASSESSMENT IN PLANNING HIGH PENETRATIONS OF SOLAR PHOTOVOLTAIC INSTALLATIONS IN DISTRIBUTION SYSTEMS

I. Introduction

Battery energy storage systems (BESS) are integrated with distribution networks to help buffer the stochastic energy generated by renewable energy resources (RER) such as solar photovoltaics (PV). The combination of RER and BESS holds the potential for deferring capital investment on electricity grid assets by performing peak-shaving, peak-shifting, and minimizing the financial risk that limits investments in delivery networks expansion [91]-[93].

There is a correlation between the selections of the size and the location of ESS. In the literature, some studies focused on finding the optimal choice of energy storage technologies and their dispatch profiles in order to improve supply reliability or to shave and shift the peak demand [94]-[96]. The work in [97] presents a heuristic planning tool using genetic algorithm (GA) to make the decision of sizing and allocating ESS in the distribution network. This should help the distribution system operator (DSO) to solve the problem of operating voltage rise due to high penetration of solar PV systems. The study shows that single-phase residential distributed energy storage might be more financially viable than the three-phase aggregated energy storage at the head of the feeder or at the substation.

Reference [98] proposes an optimal sizing of a hybrid energy system technique with RER independent of BESS. It calculates the net present value (NPV) to compare against the transmission line extension plans to ensure cost-effectiveness. The paper uses response surface methodology to optimize and ensure breakeven of the hybrid system and its location in comparison with transmission line extension. It is worth mentioning that the paper considers the stochasticity of the input variables when solving the optimization problem.

Reference [99] presents a methodology to optimally size BESS on a microgrid system that has a variety of RER by including BESS in the unit-commitment formulation. The optimization is based on cost benefit analysis. The paper builds a mathematical model for each microgrid mode of operation (i.e., the grid-connected and the islanded modes) and uses mixed linear integer programing (MLIP) to minimize the total cost.

In [100] and [101], the papers attempt to examine the potential of using BESS in the low-voltage

side of the distribution grid to defer upgrades needed to increase the penetration of PV. In [100], a multi-objective function is proposed to combine three objectives. These include the combination of maintaining voltage level, shaving peak demand, and minimizing the total cost. The work in [101] attempts to find the optimal sizing and location of distributed BESS. The aim of the optimization technique is to minimize the total cost considering price arbitrage and adopting different tariffs. GA is used to find the solution of the optimization problem.

From the literature, several goals are targeted by employing BESS such as peak shaving [96], [102], minimizing the total cost [99], [101] , minimizing power losses in the distribution grid [103], and differing investment [103].The main objective of this work is the assessment of risk in deferring capital-intensive investments in distribution grid assets in lieu of investments in BESS technologies, considering the stochasticity associated with the solar PV generation and the load growth. The expected flexibility of BESS options enables the system to closely follow the growths in demand and PV integration.

In capital asset management and investment portfolios, some risk-adjusted ratios (RARs) such as Sharpe and Sortino ratios are usually used for assessing returns of an investment per unit risk [17]. Hence, the objective in investment studies is to find the highest value of these ratios. In this work, we attempt to target the lowest total cost per unit of risk for distribution grid planning using modifications to such RARs.

The contributions of this work are: i) a risk-based optimization framework for distribution expansion planning; ii) two modified RARs for investment risk assessment; iii) the analysis of investing in BESS on a real distribution network in Latin America along with high PV penetrations; considering actual data of solar-weather conditions and associated load data, cost values, and projected growth rates. This work builds on the initial results of the authors from [103] and [5]. In [103], the authors proposed an initial study of investing in BESS for supporting high penetration of PVs, without considering uncertainties. In [5], the authors quantified improvements in wind power forecasts by deferring ancillary services using newly developed metrics for RARs. In this paper, the authors further modify the new metrics from [5] to fit the application, and consider uncertainties along with the original framework from [103] to provide a

comprehensive approach to assessing risk in distribution planning.

The rest of the paper is organized as follows. Section II explains the proposed framework of the optimization problem. Section III applies the optimization framework to a case study on a typical Argentinian distribution network. Finally, Section IV gives the conclusions of the work.

II. Optimization Problem Formulation

The proposed optimization framework is based on stochastic Monte Carlo simulations (MCS) to take into consideration the uncertainties of the input variables in the distribution planning problem. The original (unmodified) sharp ratio (SR) considers the expected return (profit), E[R], and the risk, σ[R], associated with an investment portfolio as shown in (1) [38]. Further, the SR considers a risk-free rate, rf, which is usually represented by the minimum acceptable rate (MAR) of return on the investments. Note that the values of E[R] and σ[R] correspond to the mean and the standard deviation of the returns, respectively. This is under the assumption that the returns are nearly normally distributed, implying the skewness of the probability distribution of the returns is close to zero.

$$\mathrm{SR} = \frac{\mathrm{E[R]} - \mathrm{r_f}}{\sigma} \tag{1}$$

If the skewness of the returns distribution is non-negligible, the use of the downside deviation is better than the standard deviation for risk. In this sense, the original Sortino ratio (SOR) considers those returns falling below a specified target value as the MAR that could be set to *rf* or zero. Then, the risk in an investment portfolio is evaluated as the target downside deviation (TDD) or semi-variance, as shown in (2) [17].

$$\mathrm{SOR} = \frac{\mathrm{E[R]} - \mathrm{MAR}}{\mathrm{TDD}} \tag{2}$$

where, TDD is the root mean square of the deviations of the underperforming returns from the target return (i.e., the MAR), which is mathematically computed as in (3).

$$TDD = \sqrt{\frac{1}{N}\sum_{\mathrm{i}=1}^{\mathrm{N}}\left(\mathrm{Min}(0, \mathrm{X_i} - \mathrm{T})\right)^2} \quad (3)$$

where, R_i is the i^{th} return, and N is the total number of returns.

In this work, both a modified Sharp cost ratio (MSCR) and a modified Sortino cost ratio (MSOR), which are presented in (4) and (5) respectively, are proposed to assess risk in distribution expansion investments. The proposed modifications pertain to considering only the present value of the total costs (C_{Pre}) of—but neglecting the incomes from—the investments in BESS and distribution grid assets, that means for each expansion alternative assessed ($\bar{u}$). Further, it does not consider the *rf* in (4), as it does not pertain to this analysis, and the target MAR in (5) is set to zero. The *minus* signs in (4) and (5) indicate the consideration of the above assumptions. C_{Pre} is computed in (6) using the following: investment cost for each expansion alternative ($\bar{u}$), C_{Inv}; the cost of energy losses, C_{Loss}; the penalty cost of energy supplied with poor quality (i.e., by violating voltage limits), C_{PQEN}; the penalty cost of violating the ratings of feeders and distribution power transformers by over load energy, C_{OEN}; the discount rate, r; and, the planning horizon, T. In (6) also is considered the total number of MCS, M. The variables t and i correspond to the indexes of the planning horizon and MCS, respectively.

$$MSCR = \frac{E[-C_{Pre}(\bar{u})]}{\sigma[-C_{Pre}(\bar{u})]} \quad (4)$$

$$MSOR = \frac{E[-C_{Pre}(\bar{u})]}{-TDD[C_{Pre}(\bar{u})]} \quad (5)$$

$$C_{Pre}(\bar{u}) = \sum_{t=1}^{T}\sum_{i=1}^{M}\frac{(C_{inv(\bar{u})} + C_{Loss(\bar{u})} + C_{PQEN(\bar{u})} + C_{OEN(\bar{u})})_{i,t}}{(1+r)^t} \quad (6)$$

Either the MSCR or the MSOR could be minimized as the objective function of the optimization problem. Based on a simply analysis performed in the previous work [103], in this work the objective function of the optimization method is to minimize the MSOR (5) by considering constraints vis-à-vis load flow, as shown in (7), and later the MSCR is just calculated for the best solutions found (corresponding to

the expansion plan).

$$\underset{Min\ MSOR}{Min} \left\{ \frac{E[-C_{Pre}(\bar{u})]}{-TDD[C_{Pre}(\bar{u})]} \right\} \tag{7}$$

$$\text{S.t.} \quad IL_{j,t} = IL_{\max j,t} + \Delta\, IL_{EXCE\ j,t} \tag{8}$$

$$IT_{DS\,t} = IT_{\max\ t} + \Delta\, IT_{EXCE\ t} \tag{9}$$

$$P_{load\,t} + P_{loss\ t} + P_{DER\ t} \tag{10}$$

The constraints (8)-(10) represent the line capacity constraint, the DS capacity constraint, and the power balance constraint, respectively. Where, the current that exceeds the capacity of a line (j), ΔIL_{EXCE}, is then used to compute the overload energy, OEN; the maximum capacity of the power distribution substation (DS), IT_{MAX}, is determined by the power rating of the transformers, and the current that exceeds the DS capacity, ΔIT_{EXCE}, is also used to compute the OEN. In turn, with the power losses, P_{LOSS}, the energy losses are calculated; and the nodes with high voltage drops are considered to evaluate the energy supplied with poor quality, PQEN. The power of distributed energy resources (DER) that considers the power injection of both the solar PV distributed generators and the BESS is presented in (10), as well as the possibility of BESS consuming electric energy as a load; along with the power load demand, P_{LOAD}, and the P_{LOSS}, assuming the DS as the slack node.

Each expansion alternative ($\bar{u}$) considers the decision variables of the optimization problem, including both conventional reinforcements of networks (such as upgrading feeders, installing capacitor banks, and expanding the DS) and the installation of BESS. Because the decision variables include integer, binary, real, and complex types, we can justify using heuristic optimization techniques for finding near-optimal solutions. Particularly, the Evolutionary Particle Swarm Optimization (EPSO) algorithm is applied to solve the expansion problem. It is well used in several complex power system problems, presenting appropriate qualities such as mainly self-adaptation of the algorithm parameters, robustness, and fast convergence [103],[106]. Moreover, the OpenDSS® software is used for running power flow simulations

and computing the energy losses, the energy supplied with poor quality (PQEN) and the over load energy (OEN). OpenDSS® is an open-source tool developed by Electrical Power Research Institute (EPRI) to model and simulate the electrical behavior of distribution grids [107], [108]. This paper does not commercialize the OpenDSS® software nor does it support its exclusive use for such studies; rather, the authors present it as one of the freely available software options for conducting such distribution studies.

Fig. 1 depicts the proposed risk-based optimization problem, where the input includes deterministic parameters such as the network data to be analyzed, demand characteristics (types of customers, and typical load curves), costs of conventional reinforcements, and discount rate as well as stochastic variables such as the load growth, the PV penetration, the solar-weather conditions (temperature and irradiance), and the cost of BESS. After running the expansion optimization, the best-compromise expansion plan is obtained as a solution.

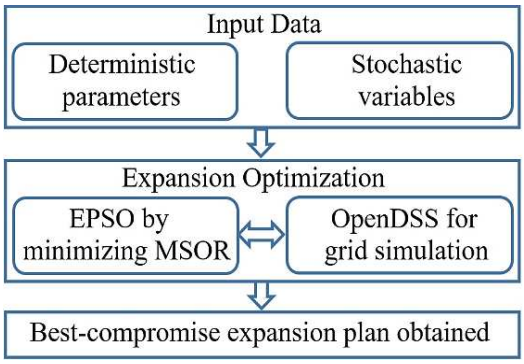

Fig. 1. General flowchart of the risk-based optimization framework

In brief, the near-optimal solution of the proposed optimization framework is mathematically equivalent to finding the investment decision option (or expansion plan) that minimizes the expected present value of the total costs, i.e., investment and operational costs, per unit of cost deviation (or risk). In this sense, the framework considers the installation of new equipment—feeders, capacitors, transformers, or BESS—to supply the expected load requirements on time and with acceptable power quality. Particularly, when the installation of BESS is optimized, the size and allocation of BESS are also optimized considering the time of their investment (i.e., the "timing"). In this last sense, Fig. 2 shows the

computational encoding done of the relationship between the optimization algorithm (the EPSO) and the OpenDSS® environment when the BESS are taken into consideration as an expansion plan, where:

- the dimension or total number of elements of the particles of EPSO is equal to the number of the suggested locations for installing BESS in the network under study; and,
- each element of a particle of EPSO is represented by a two-digit integer, where the first digit represents the timing at which the BESS investment is made, e.g., 0 is not installed, 1 represents the first year, 2 denotes the second year, and so on; and the second digit indicates the sizing of BESS (i.e., the power capacity) to be installed, e.g., 1 is 250 kW, 2 is 500 kW, and 9 is 2.250 MW.

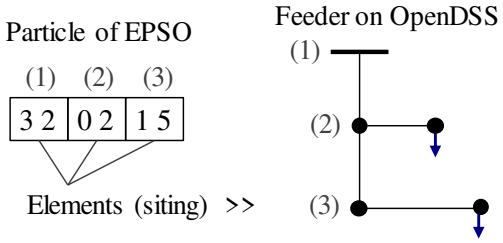

Fig. 2. Encoding of BESS as expansion plans into the optimization problem

Based on the encoding example in Fig. 2, the first element of the particle represents an option for installing a BESS unit in the first node of the feeder, in the third year, at a rating of 500 kW. Note that to reduce the computational time resulting from the combinatorial explosion of this large optimization problem, distributed or parallel computing may be easily used.

III. Case Study and Results

A. Data of the Test System

In this study, a typical Latin American distribution network is used [103]. It is a 13.2 kV three-phase balanced network with four feeders and 20 MW of peak load demand (not coincident), as described in Table I, where residential loads constitute 44% and 74% of the total load composition of feeders F1 and F4, respectively. Figure 3 depicts the one-line diagram of such distribution network. For this test system, actual data of load, temperature, and irradiance for the San Juan province in Argentina (30.87° S 68.98° W)

are mapped [107]-[109]. Figures 4 and 5 represent the typical load curves of a weekday for the residential, commercial, and industrial customers in summer and winter, respectively. Note that in the San Juan province, the average of 60% of the days per year are mostly considered summer-days and the remaining 40% as winter-days.

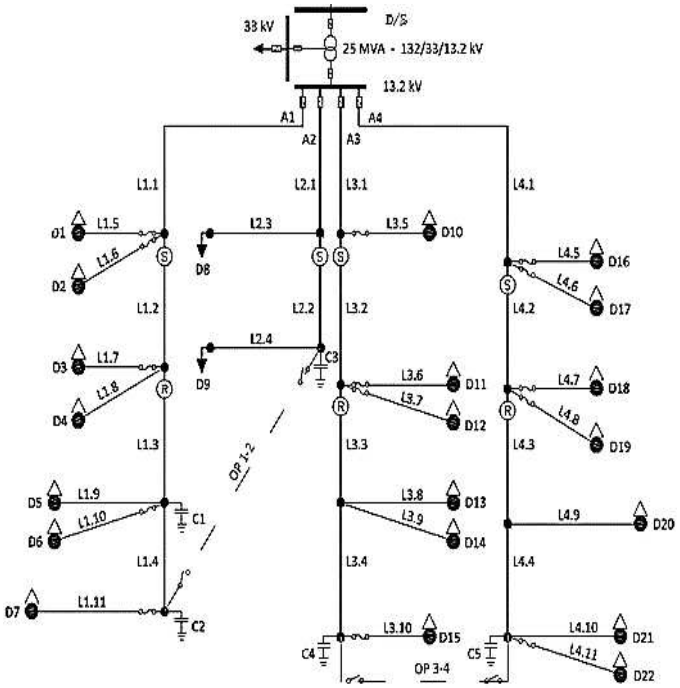

Fig. 3. One-line diagram of the distribution network under study [103].

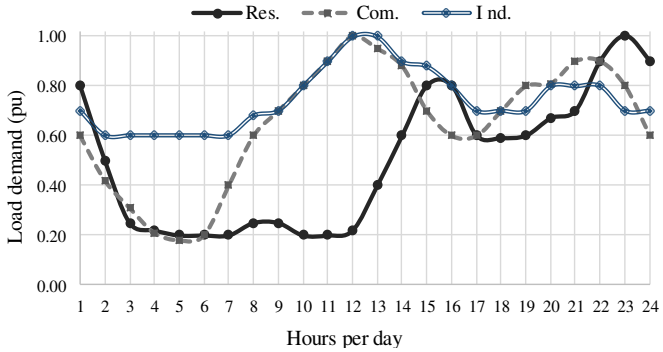

Fig. 4. Typical curves of load demand of a weekday in summer

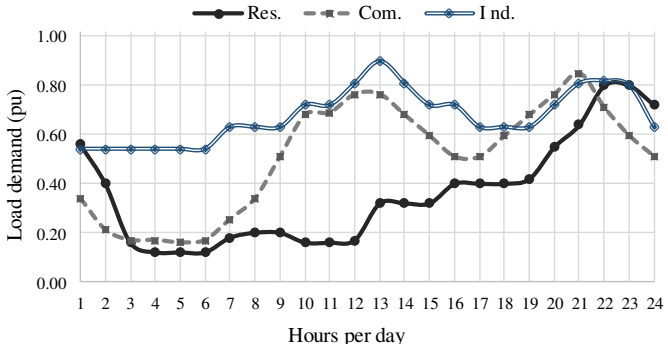

Fig. 5. Typical curves of load demand of a weekday in winter

TABLE I. CHARACTERISTICS OF INDIVIDUAL DEMAND BY CUSTOMER TYPE

Customer type	Peak load		Distribution of load per feeder (%)				Power factor (cos φ)	Annual growth rate (%)
	(MW)	(%)	F1	F2	F3	F4		
Residential	8.50	42.5	44	0	34	74	0.80	6
Commercial	4.50	22.5	25	0	31	26	0.85	3
Industrial	7.00	35.0	31	100	35	0	0.90	2
∑	20.00	100	100	100	100	100		

For a ten-year analysis period within the expansion planning horizon, the following parameters are assumed, in US Dollars ($), which represent typical values in Argentina:

- Cost of energy to evaluate energy losses: 100 $/MWh in year 1, growing with a constant annual rate of 5 $/MWh
- Cost of PQEN for ± 5% voltage variations: 300 $/MWh
- Cost of OEN for power rating violations: 1500 $/MWh
- Annual discount rate, r: 10%

Stochastic Input Data

1) Load Growth

When performing MCS, the load demand growth is assumed to be governed by a geometric Brownian motion (GBM) [106]. For a time-interval, Δt, the variation of a GBM satisfies the stochastic differential equation (11).

$$\Delta Dp_{i,t} = \Delta Dp_{i,t-1} \cdot \left(\mu \cdot \Delta t + \sigma \cdot \varepsilon \cdot \sqrt{\Delta t}\right) \qquad (11)$$

where Dp is the peak power demand per node, μ is the drift or growth rate, σ is the standard deviation or volatility, ε is a normally distributed random variable such that $N(0,1)$, i is the MCS index, and t is a period of time.

Based on typical load growth data in Argentina described in [103] and [110], the drift values (μ) are the same annual growth rate values shown in Table I for each type of costumer, and the volatility values, σ, are assumed as 5% for residential customers, 4% for commercial, and 3% for industrial customers. Figure 6 shows an example of the load growth for a residential customer of 1 MW, by running 100 MCS.

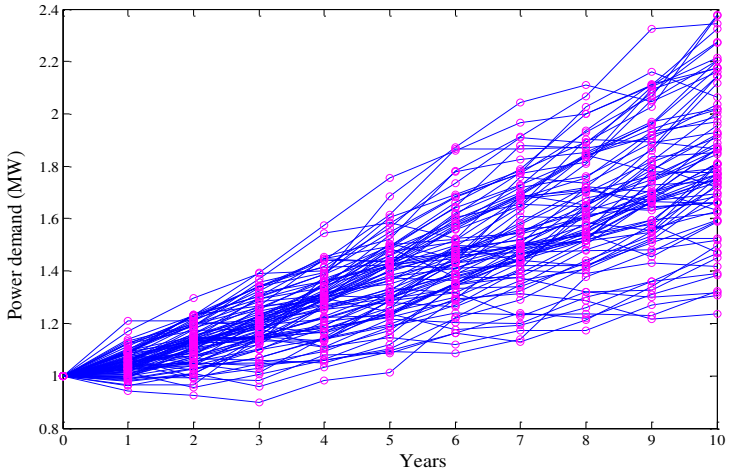

Fig. 6. Load growth for a residential customer by running 100 simulations

2) Solar-Weather Conditions

Two years of solar-weather data for the San Juan province were collected and analyzed to model the distributed PV generation installed by residential customers [111]. Based on that, we performed a statistical study of the data to find the probability distribution functions (PDFs) for typical-weather summer and winter days.

With the PDFs obtained, we run MCS to take into consideration the uncertainties from the temperature and the irradiance into the PV model in OpenDSS®. Also, the parameters of efficiency of the PV model were adjusted based on current PV generators installed on the roof of some houses and buildings

in San Juan province[112]. Tables II and III summarize the PDFs and their statistical parameters obtained for the summer and winter seasons, respectively, where the main characteristic of the distribution functions are the rate or inverse scale parameter for the exponential function (λ), the scale parameter (a) and the shape parameter (b) for Weibull distribution, and the mean (μ) and the standard deviation (σ) for the normal function.

TABLE II. SOLAR-WEATHER STATISTICAL DATA FOR SUMMER

Hours	Irradiance (kW/m^2)			Temperature (°C)		
	Function	Parameters		Function	Parameters	
06-09	Exponential (λ)	0.1004		Weibull (a, b)	22.8565	7.4829
09-11	Weibull (a, b)	0.5303	3.4459	Weibull (a, b)	24.5887	7.5287
11-13	Weibull (a, b)	0.8993	7.7747	Normal (μ, σ)	25.5081	3.6973
13-15	Weibull (a, b)	1.0462	13.249	Normal (μ, σ)	27.8122	3.8533
15-17	Weibull (a, b)	0.9362	7.0707	Normal (μ, σ)	29.6591	3.9675
17-19	Weibull (a, b)	0.5775	3.2155	Weibull (a, b)	32.3325	9.0031
19-21	Exponential (λ)	0.1316		Weibull (a, b)	32.0183	9.0414

TABLE III. SOLAR-WEATHER STATISTICAL DATA FOR WINTER

Hours	Irradiance (kW/m^2)			Temperature (°C)		
	Function	Parameters		Function		Parameters
08-11	Exponential (λ)	.1231		Normal (μ, σ)	.7485	4.1497
11-13	Weibull (a, b)	.4330	.9398	Normal (μ, σ)	1.7648	4.4413
13-15	Weibull (a, b)	.5713	.0784	Weibull (a, b)	6.2582	3.3538
15-17	Weibull (a, b)	.4799	.7126	Weibull (a, b)	8.3536	3.9711
17-19	Exponential (λ)	.1857		Weibull (a, b)	8.8866	4.1604

Based on the statistical data of Tables II and III, Figs. 7 and 8 show the modeled PV generation of 100 kW by running 100 stochastic simulations for summer and winter, respectively.

3) PV Penetration

In this planning study, varying levels of PV penetration between 10% and 60% are considered to account for expected growth, using uniform probability distribution. For instance, Figure 9 presents the expected coincident power flow profile at the head of the feeder F4, which has the highest residential load demand composition (see Table I), considering different levels of PV penetration installed by residential

loads for a summer day. Similarly, Figure 10 shows the voltage profile at the end-node of the feeder F4.

Based on the previous analysis, the BESS are set for a daily load peak-shaving operation, storing energy produced by PV generators during off-peak demand periods (between the 9th and the 12th hours) and injecting it later at peak hours (between the 21st and the 24th hours).

4) Cost of BESS

BESS technologies include a variety of materials such as the classic and well-known lead-acid (LA) batteries, modern redox (reduction-oxidation) flow batteries, advanced-LA and new alkaline batteries such as with nickel chemistry and sodium chemistry (sodium-sulfur NaS or sodium-salt NaNiCl or ZEBRA)[92], [112]-[117]. The main technical characteristics of BESS are the nominal power, in kW, the maximum energy stored, in kWh, which reflects the maximum time to store energy at the nominal power rate, their efficiency of charging and discharging, and the idling losses.

LA batteries are the most commercially mature rechargeable battery technology. Advanced-LA technologies, comprising the absorbent glass mat (AGM), have improved their efficiency and life-time cycles. NaS batteries are a commercial technology finding applications in electric utility distribution grid support, because of its long discharge period (about 6 hours). ZEBRA batteries have been commercially available since 1990's for mobile applications and now are seeing deployment in the size range of 50-1000 kW. Table IV summarizes the main characteristics of these key three kinds of batteries [114], [117].

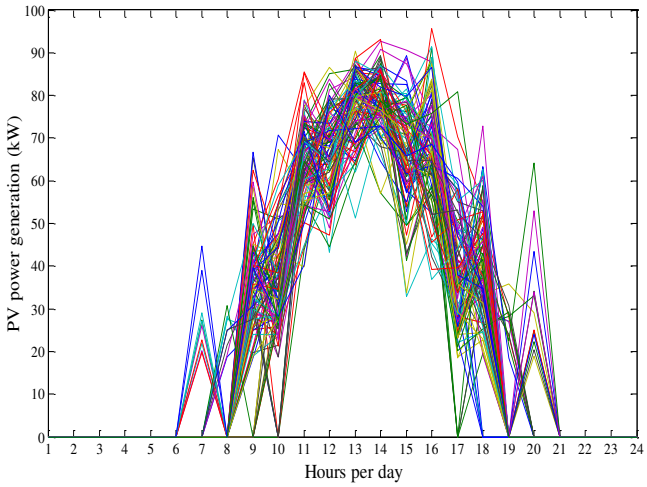

Fig. 7. PV generation in summer by running 100 stochastic simulations

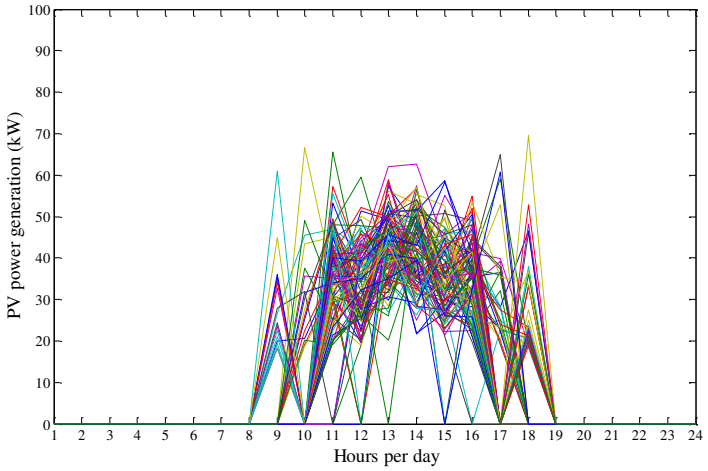

Fig. 8. PV generation in winter by running 100 stochastic simulations

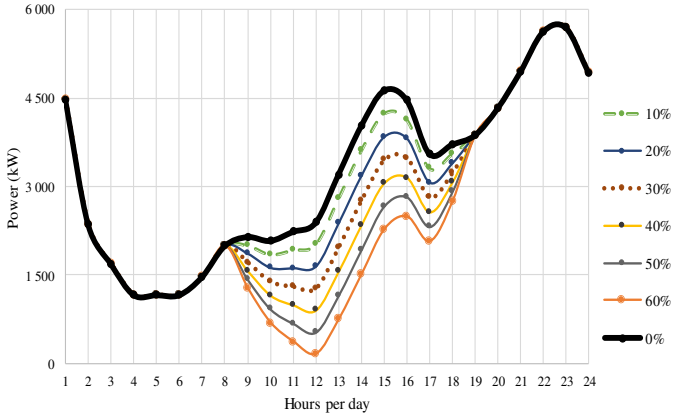

Fig. 9. Expected coincident power at the head of the feeder F4 by different levels of PV penetrations in summer

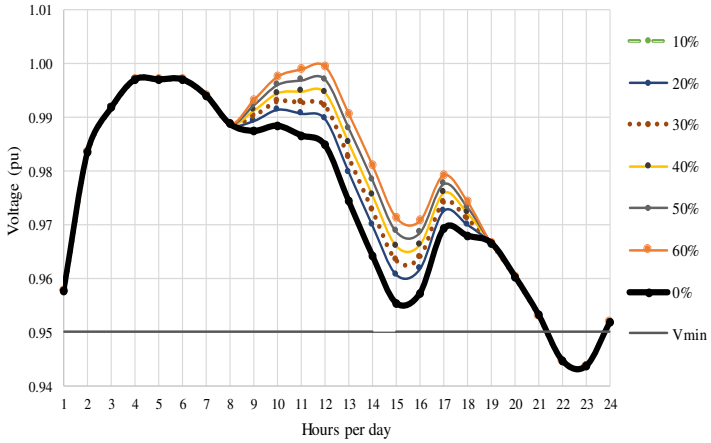

Fig. 10. Expected voltage at end-node of the feeder F4 by different levels of PV penetrations in summer

TABLE IV. CHARACTERISTICS OF THREE MAIN BESS

BESS	Efficiency	Life Cycles	Investment Cost	Energy Capital Cost
Advanced-LA	75-90 %	3000-4500 (8-12 yr)	1000-2500 $/kW	350-750 $/kWh
NaS	75-90 %	2500-4500 (7-12 yr)	1500-2500 $/kW	400-600 $/kWh
ZEBRA	85-90 %	2500-3000 (7-8 yr)	1500-4000 $/kW	400-950 $/kWh

Then, advanced-LA batteries are considered for this study, assuming the following considerations: a range investment cost between 1200 $/kW and 1800 $/kW (that means between 400 $/kWh and 600 $/kWh, respectively, considering up to three hours of energy storage at maximum power); a lifetime about 4000 cycles of charging and discharging, i.e., 10 years approximately for a daily operation; and an efficiency of 10% for charging and 10% for discharging. For varying levels of this investment cost of BESS, uniform probability distribution is used.

C. Results

We run the proposed risk-based optimization framework for analyzing the following three cases in the distribution network under study at first considering 1000 MCS, *M*, for a ten-year planning horizon, *T*, and later the best-compromise expansion plans obtained in each were checked by running 5000 MS:

1. base case is the expansion planning taking into account traditional reinforcements, such as expanding the power capacity of the main distribution substation (DS), feeders, and installing fixed capacitor banks.
2. BESS option is the distribution planning for siting and sizing batteries as expansion options, by avoiding capital-intensive reinforcements such as an expansion of the main DS.
3. flexible plan considers the installation of BESS as a flexible expansion option by deferring some large network reinforcement, by closely following the growth demand and the PV integration.

Table V and Figure 11 summarize the results obtained for the three expansion planning cases, by running the EPSO algorithm for 50 iterations of 10 particles each, where:

- in the base case, the major investment is installing a new power transformer of 25 MVA at the main substation (DS) in the third year, with a cost of $ 3M (which its present value is $2.25 M). The expected total cost of this plan is $3.09 M, with a significant deviation of $0.67 M (21.8%) and a MSOR equal to 0.987.
- the BESS option considers the installation of 2.0 MW in BESS, which includes installing 0.50 MW in the second year at the point of common coupling (PCC) of line L.4.4, 0.75 MW in the third year at the PCC of line L.4.3, and 0.75 MW in the fourth year at the PCC of line L.1.2.
- the flexible plan proposes to install 1.50 MW of BESS (0.50 MW in the second, third, and fourth years at the same locations, respectively, as the previous second case) by deferring the transformer investment for five years until the eight year. This plan gives a major flexibility to the distribution planner during the first half of the planning period, which could be assessed by taking into account the recovery value of such investments in BESS (through a constant-line depreciation) when the investment in expanding the main DS will be done.

The second option concerns the expected present value of BESS investment of $2.28 M, without considering the large investment in expanding the main substation. In this case, the expected total cost is about 60% higher than the first case, equal to $4.93 M, but with a lower deviation of $0.53 M (10.8%) and a resultant MSOR of 0.985 (that is very close to MSOR of the base case).

The third expansion case involves the expected present value of investment of $3.03 M between both the BESS and the transformer investments, obtaining the expected total cost just about 2.7% higher than the base case, equal to $3.17 M, but with the lowest risk or deviation of $0.26 M (8.2%) and also the lowest MSOR value of 0.976.

Realizing the obtained results and specifically comparing the base case with the flexible plan indicates that their expected total costs are close ($3.09 M and $3.17 M, respectively) but the deviation of the last case is 13.6% lower than the first case, meaning the expansion plan with lower risk should be rationally chosen. In this sense, the values of both MSOR and MSCR are justly the lowest for the flexible

plan.

Finally, contrasting these achieved results regarding the initial results [103], in both works the expansion plans obtained are similar. However, this work considers uncertainties and the proposed risk-adjusted cost ratios (either MSOR or MSCR) point to making near-optimal investments decisions, by choosing the expansion option with the lowest expected total cost per unit cost deviation. Based on [5], note that the MSOR allows for better decisions making to choose the option with the lower expected cost per unit of deviation.

TABLE V. EXPANSION PLANNING RESULTS

Present Value of Costs (M$)	Base case	BESS option	Flexible plan
Feeders and capacitors investments	0.1118	0.1118	0.1118
Power transformer investment at DS	2.2539	0	1.3995
Expected BESS investments	0	2.2803	1.6363
Expected total cost	3.0917	4.9315	3.1753
Standard deviation	0.6738	0.5322	0.2615
MSCR (modified Sharpe cost ratio)	-4.5885	-9.2661	-12.143
Target semi-variance (TDD)	3.1322	5.0055	3.2513
MSOR (modified Sortino ratio)	0.9871	0.9852	0.9766

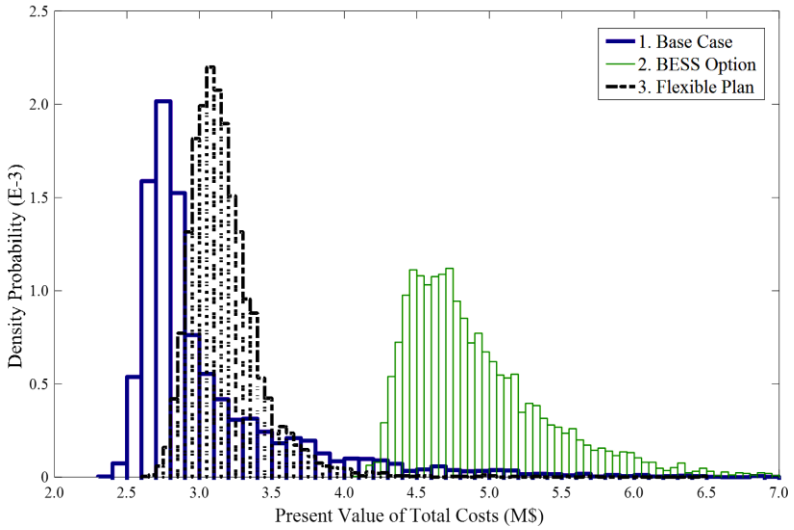

Fig. 11. Results of the risk-based expansion planning framework

IV. Conclusions

A comprehensive framework to assess risk in distribution expansion investments was proposed in this work by using modified risk-adjusted cost ratios. The framework was applied specifically to quantify the benefit of investing in BESS (battery energy storage systems), considering distributed PV generation and uncertainties in the load growth, the PV penetration, the solar-weather conditions, and the cost of BESS. Moreover, the size and allocation of BESS were optimized by considering the timing of their investment.

By application to a typical Argentinian distribution network we showed the main contribution of BESS lies in the flexibility for distribution planning by deferring large capital-intensive reinforcements. This flexibility was mainly given for closely following the uncertain growth demand along with fairly high distributed PV generation penetrations.

APPENDIX B

Thesis / Dissertation Reuse

The IEEE does not require individuals working on a thesis to obtain a formal reuse license, however, you may print out this statement to be used as a permission grant:

Requirements to be followed when using any portion (e.g., figure, graph, table, or textual material) of an IEEE copyrighted paper in a thesis:

1) In the case of textual material (e.g., using short quotes or referring to the work within these papers) users must give full credit to the original source (author, paper, publication) followed by the IEEE copyright line © 2011 IEEE.
2) In the case of illustrations or tabular material, we require that the copyright line © [Year of original publication] IEEE appear prominently with each reprinted figure and/or table.
3) If a substantial portion of the original paper is to be used, and if you are not the senior author, also obtain the senior author's approval.

Requirements to be followed when using an entire IEEE copyrighted paper in a thesis:

1) The following IEEE copyright/ credit notice should be placed prominently in the references: © [year of original publication] IEEE. Reprinted, with permission, from [author names, paper title, IEEE publication title, and month/year of publication]
2) Only the accepted version of an IEEE copyrighted paper can be used when posting the paper or your thesis on-line.
3) In placing the thesis on the author's university website, please display the following message in a prominent place on the website: In reference to IEEE copyrighted material which is used with permission in this thesis, the IEEE does not endorse any of [university/educational entity's name goes here]'s products or services. Internal or personal use of this material is permitted. If interested in reprinting/republishing IEEE copyrighted material for advertising or promotional purposes or for creating new collective works for resale or redistribution, please go to http://www.ieee.org/publications_standards/publications/rights/rights_link.html to learn how to obtain a License from RightsLink.

If applicable, University Microfilms and/or ProQuest Library, or the Archives of Canada may supply single copies of the dissertation.

BACK CLOSE WINDOW

APPENDIX C

RETAINED RIGHTS/TERMS AND CONDITIONS

- Authors/employers retain all proprietary rights in any process, procedure, or article of manufacture described in the Work.
- Authors/employers may reproduce or authorize others to reproduce the Work, material extracted verbatim from the Work, or derivative works for the author's personal use or for company use, provided that the source and the IEEE copyright notice are indicated, the copies are not used in any way that implies IEEE endorsement of a product or service of any employer, and the copies themselves are not offered for sale.
- Although authors are permitted to re-use all or portions of the Work in other works, this does not include granting third-party requests for reprinting, republishing, or other types of re-use.The IEEE Intellectual Property Rights office must handle all such third-party requests.
- Authors whose work was performed under a grant from a government funding agency are free to fulfill any deposit mandates from that funding agency.